Zoological Journal of the Linnean Society, 2021, **193**, 1020–1071. With 23 figures.

Species boundaries and phylogeographic patterns in new species of *Nannoniscus* (Janiroidea: Nannoniscidae) from the equatorial Pacific nodule province inferred from mtDNA and morphology

STEFANIE KAISER[1,2,*], TERUE CRISTINA KIHARA[3,4], SASKIA BRIX[1], INGA MOHRBECK[3], ANNIKA JANSSEN[3], and ROBERT M. JENNINGS[5]

[1]*German Centre for Marine Biodiversity Research (DZMB), Senckenberg am Meer, c/o Center of Natural History (CeNak), Universität Hamburg, Martin-Luther-King-Platz 3, 20146 Hamburg, Germany*
[2]*CeNak, Universität Hamburg, Martin-Luther-King-Platz 3, 20146 Hamburg, Germany*
[3]*German Centre for Marine Biodiversity Research (DZMB), Senckenberg am Meer, Südstrand 44, 26382 Wilhelmshaven, Germany*
[4]*INES Integrated Environmental Solutions UG, Südstrand 44, 26382 Wilhelmshaven, Germany*
[5]*Biology Department, Temple University, 1900 North 12th Street, Philadelphia, PA 19122, USA*

Received 12 March 2020; revised 30 October 2020; accepted for publication 11 November 2020

Spatial patterns of genetic variation (based on *COI* and 16S mtDNA) for morphologically similar species in the isopod genus *Nannoniscus* G.O. Sars. 1870 were examined that occur broadly across the Clarion Clipperton Fracture Zone (CCZ). Samples were obtained from five different licence areas as well as an Area of Particular Environmental Interest (APEI-6) with sites located at various distances (a few to several hundred kilometres) from one another. Applying three different species delimitation (SD) methods (sGMYC, mPTP and ABGD) of the molecular data, we could distinguish between four and 12 different molecular taxonomic operational units (MOTUs). Morphological analyses could confirm five distinct phenotypic clades that represent species new to science and are described here: ***Nannoniscus brenkei* sp. nov.**, ***Nannoniscus hilario* sp. nov.**, ***Nannoniscus magdae* sp. nov.**, ***Nannoniscus menoti* sp. nov.** and ***Nannoniscus pedro* sp. nov.** Despite the assumed limited dispersal capacity of *Nannoniscus* species, we found haplotypes of two species to be geographically widespread (up to > 1400 km apart), as opposed to several divergent clades occurring in close vicinity or even sympatry. Geographic distance appeared to explain the phylogeographic structure of *Nannoniscus* species to some extent, although oceanographic features and level of environmental heterogeneity were probably equally important.

ADDITIONAL KEYWORDS: Abyssal – Abyssline – Clarion Clipperton Fracture Zone – JPI-Oceans– molecular species delimitation – recovery potential – taxonomic key – redescription.

INTRODUCTION

Dispersal and migration of organisms link suitable habitats and are key elements to shape marine assembly biodiversity and distributional patterns across a range of spatial and temporal scales. The level of population connectivity, as such defined as exchange of individuals (i.e. larvae, juveniles or adults) among subpopulations (Cowen & Sponaugle, 2009) allows the persistence of fragmented populations, but, if restricted, also controls population divergence and speciation. Assessing a realized biogeographic range of a species and its potential drivers is important for the evaluation of vulnerability to potential impacts (O'Hara, 2002); that is, wide-ranging species with high genetic connectivity are potentially more robust and have a greater recovery potential following disturbance events than species with a narrow geographic range

*Corresponding author. Current address: University of Lodz, Department of Invertebrate Zoology and Hydrobiology, Banacha St. 12/16, Łódź, 90-237, Poland. E-mail: ssm.kaiser@gmail.com
[Version of record, published online 1 February 2021; http://zoobank.org/ urn:lsid:zoobank.org:pub:A68FDF1F-2825-47D8-B9CE-FEB8432896DF]

and/or limited gene flow among subpopulations (O'Hara, 2002; Sewell & Hoffmann, 2011).

The abyssal seafloor (i.e. areas between 3000 and 6000 m depth) has long been among the most pristine and stable environments on Earth. However, human pressures are currently increasing to exploit its mineral resources [foremost polymetallic nodules, rare earth elements and ytrium (REY) (Ramirez-Llodra *et al.*, 2010; Kato *et al.*, 2011)], which would cause unprecedented impacts for the resident fauna (Vanreusel *et al.*, 2016; Jones *et al.*, 2017; Gollner *et al.*, 2017). For polymetallic nodules, the Clarion Clipperton Fracture Zone (CCZ) represents the economically most viable deposit. The CCZ is located in Areas Beyond National Jurisdiction (ABNJ) spanning more than six million square kilometres in the north-eastern equatorial Pacific. The International Seabed Authority (ISA) is in the process of framing regulations for seafloor exploitation in ABJN (www.isa.org.jm). Concurrently, international agreements are underway to develop legally-binding instruments under the United Nations Convention on the Law of the Sea (UNCLOS) to enhance the protection and preservation of marine biodiversity in ABNJ (e.g. Gjerde *et al.*, 2016; Danovaro *et al.*, 2017). Here, knowledge of biogeographic ranges and connectivity of species provides the necessary background information to enable informed conservation planning and to forecast recovery and recolonization potential following mining impacts. However, still only few faunistic data are available from the CCZ and most of the collected species tend to be new to science (e.g. Malyutina, 2011; Kaiser, 2014; Riehl *et al.*, 2014b; Kaiser *et al.*, 2017, 2018; Kamenskaya *et al.*, 2017; Wilson, 2017; Bonifácio & Menot, 2019; Malyutina *et al.*, 2020; Riehl & De Smet, 2020), which limits the robust evaluation of species ranges and distribution patterns in these remote areas.

Asellotan isopods have been widely used as a model to study trends in deep benthic biogeography and evolution owing to their high diversity and ubiquity in the deep-sea benthos (e.g. Birstein, 1971; Hessler *et al.*, 1979; Svavarsson *et al.*, 1993, Wilson, 1998; Brandt *et al.*, 2007; Kaiser *et al.*, 2007; Brix *et al.*, 2015; Janssen *et al.*, 2015, 2019; Riehl & De Smet, 2020). With the exception of a few parasitic groups, isopods lack planktonic larval stages, but brood their offspring in a ventral brooding pouch. This characteristic has important implications for their dispersal ability, which is governed by mobility of adults or passive drift. Molecular data revealed some putatively widely distributed isopod morphospecies to represent species complexes with each having a restricted range (Raupach *et al.*, 2007; Schnurr *et al.*, 2018). On the contrary, there is also evidence for long-distance dispersal in a number of isopod lineages being separated by hundreds of kilometres of deep seafloor (Riehl & Kaiser, 2012; Brix *et al.*, 2015, 2018; Janssen *et al.*, 2015). The question remains, what the mechanisms and drivers are, affecting faunal connectivity and thus population differentiation or maintenance in abyssal waters.

Here, we examine geographic patterns of genetic variation for morphologically similar, yet previously undescribed species within the isopod genus *Nannoniscus* G.O. Sars, 1870 (family Nannoniscidae Hansen, 1916) that occur broadly across the CCZ. Sampling conducted during five expeditions to the CCZ (BIONOD, MANGAN 13 and 14, ABYSSLINE 2 and JPI-Oceans EcoResponse) enabled assessment of phylogeographic patterns at multiple spatial scales (tens to several hundred kilometres) using two mitochondrial DNA markers (*COI*, 16S). Due to their prevailing reproduction mode alongside the putatively poor swimming abilities of nannoniscids we expected to find strong genetic divergence in relation to geographic distance (see also Wright, 1943; Rousset, 1997). Molecular techniques were coupled with morphological examinations to aid and increase confidence in species identification and unravel the nature and the primary mechanisms of biological variability. Within the Nannoniscidae, *Nannoniscus* represents the most diverse genus so far comprising 30 species, including seven from the Pacific Ocean (Boyko *et al.*, 2008 onwards; Kaiser, 2014), yet species described herein are the first from the CCZ. In this study, we provide a description of these species along with a taxonomic key for species of *Nannoniscus* known to the Pacific, to facilitate identification.

MATERIAL AND METHODS

Sampling and sample processing

Nannoniscus specimens were collected during five expeditions to the CCZ: BIONOD onboard RV L'Atalante in 2012, MANGAN 13 and 14 onboard RV Kilo Moana in 2013 and 2014, respectively, ABYSSLINE 2 onboard RV Thomas G. Thompson in 2015, and JPI-Oceans EcoResponse (SO239) onboard RV Sonne in 2015. Samples were collected at 22 stations in the eastern German (GER), French (FRA), Singapore (Ocean Mineral Singapore Pte. Ltd., OMS), UK-1B (UK Seabed Resources Ltd.) and Belgian (G-TEC Sea Mineral Resources NV, GSR) licence areas as well as one APEI (APEI-6, formerly known as APEI-4) using an epibenthic sledge [EBS *sensu* Brenke (2005)]. Stations were located between 3.2 and 1438 km apart, while depth ranged from 4076 to 5055 m between stations (Table 1; Fig. 1). Within the German licence area, samples were also obtained from prospective mining areas (PA), impact reference zones (IRZ) and preservation reference zones (PRZ, Table 1), where PAs represent potential future mining

Table 1. Station list of CCZ sampling sites across where examined *Nannoniscus* specimens were collected [including gear type, date, position (degrees) and depth (m)]

Voyage	Area	Gear	Station	Date	Start latitude °N	Start longitude °W	End latitude °N	End longitude °W	Depth (m)
AB02	OMS*	EBS	S10	2015-03-14	12°2'17.16"	117°14'12"	12°2'29"	117°13'1"	4097–4094
AB02	OMS	EBS	S11	2015-03-16	12°2'43.08"	117°25'26"	12°3'1.44"	117°24'17"	4223–4235
AB02	APEI-6	EBS	APEI-6#1	2015-03-20	19°27'52"	120°1'31"	19°28'54"	120°0'58"	4099–4076
AB02	OMS	EBS	S5	2015-03-01	12°15'3"	117°19'14"	n.a.	n.a.	4137
AB02	UK	EBS	U7	2015-03-02	12°27'5"	116°37'48"	n.a.	n.a.	4145
JPIO	GER PA	EBS	20	2015-03-21	11°50'9"	117°58'29"	11°50'11"	116°58'0"	4093
JPIO	GER PA	EBS	24	2015-03-22	11°51'19"	117°1'30"	11°51'31"	116°58'0"	4093
JPIO	GSR	EBS	117	2015-04-07	13°52'19"	123°15'27"	13°52'37"	123°14'16"	4498–4521
JPIO	GSR	EBS	133	2015-04-10	13°50'45"	123°15'39"	13°51'8"	123°14'8"	4516–4427
JPIO	FRA	EBS	158	2015-04-15	14°3'25"	130°7'59"	14°3'49"	130°6'29"	4946–4978
JPIO	FRA	EBS	171	2015-04-17	14°2'41"	130°5'57"	14°3'12"	130°4'36"	5024–5017
MA13	GER PA	EBS	07	2013-04-12	11°51'30.18"	117°01'12.30"	11°51'45.36"	117°0'10.26"	4131–4121
MA13	GER PRZ	EBS	90	2013-05-03	11°49'44.52"	117°30'16.68"	111°49'54.36"	117°29'23.7"	4340–4357
MA14	GER IRZ	EBS	20	2014-05-10	11°51'32"	117°01'8"	11°51'43"	117°00'19"	4127–4124
MA14	GER IRZ	EBS	21	2014-05-10	11°49'44.52"	117°00'27.06"	11°49'56.76"	116°59'40.62"	4132–4136
MA14	GER PRZ	EBS	38	2014-05-13	11°47'52"	117°30'31"	11°48'3"	117°29'45"	4363–4373
MA14	GER PRZ	EBS	39	2014-05-13	11°49'37"	117°30'49"	11°49'47"	117°30'5"	4361–4343
BIONOD	GER	EBS	06	2012-04-02	11°46'13"	116°41'8"	11°46'13"	116°41'7"	4259
BIONOD	GER	EBS	33	2012-04-07	11°51'44"	117°3'10"	11°51'54"	117°3'8"	4133
BIONOD	GER	EBS	43	2012-04-09	11°48'12"	117°32'3"	11°48'20"	117°31'57.079"	4358
BIONOD	FRA	EBS	67	2012-04-19	14°3'4"	130°4'36"	14°3'10"	130°4'27"	5021
BIONOD	FRA	EBS	101	2012-04-25	14°4'51"	130° 6'11"	14°5'0"	130°6'11"	5055

*APEI: Area of Particular Environmental Interest; FRA: French licence area; GER: German licence area; GSR: G-TEC Sea Mineral Resources NV; OMS: Ocean Mineral Singapore Pte. Ltd.; UK: UK Seabed Resources Ltd.; IRZ: impact reference zone; PA, prospective mining area; PRZ: preservation reference zone.

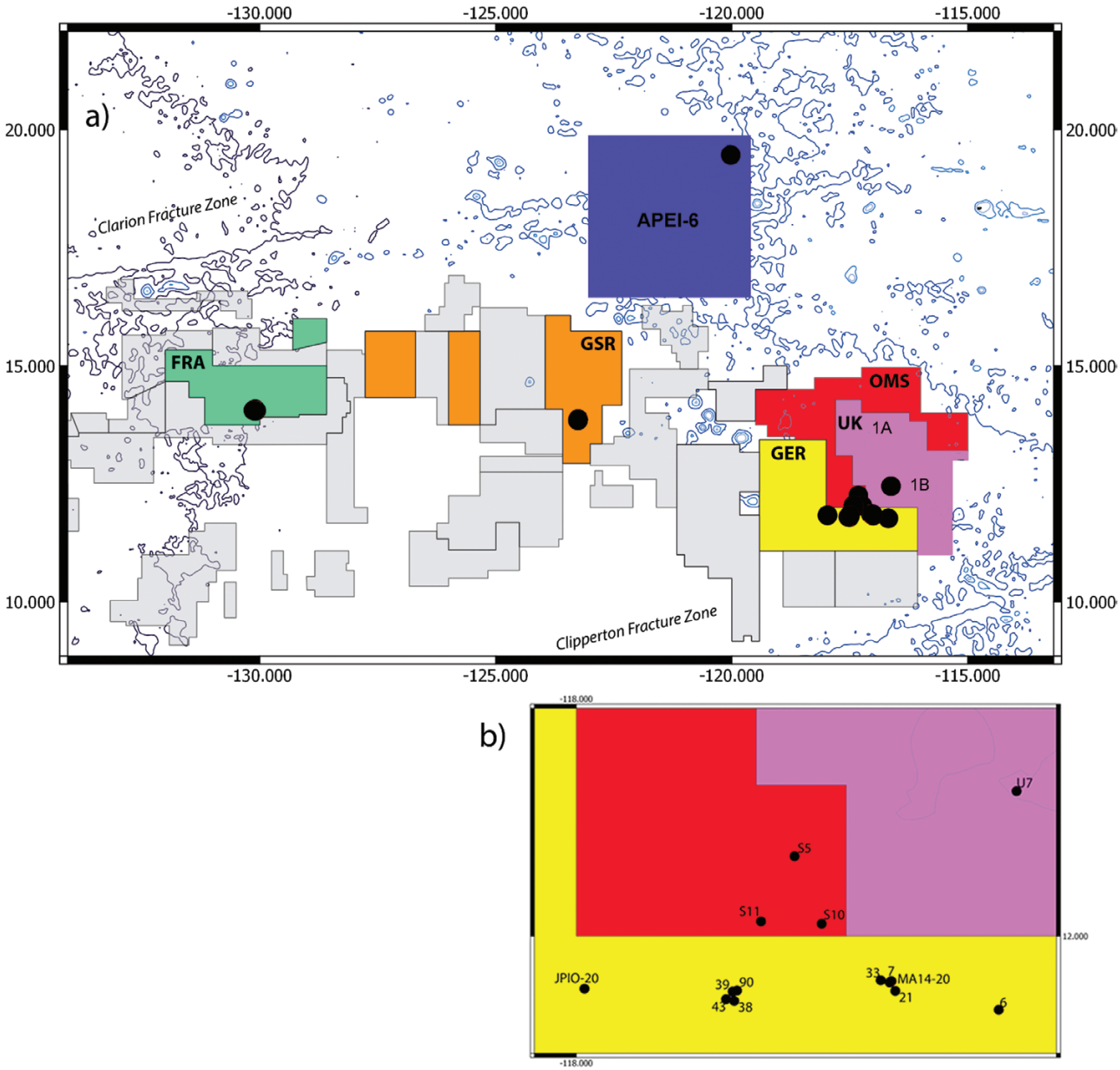

Figure 1. a, the CCZ and distribution of sampling locations across five licence areas and APEI 6; (b) detail: sampling sites in the German, UK and OMS licence area; FRA: French licence area; GSR: G-TEC Sea Mineral Resources NV (Belgium); GER: German licence area; OMS: Ocean Mineral Singapore Pte. Ltd.; UK: UK Seabed Resources Ltd.

areas, IRZs may be affected by mining activities, while PRZs are designated as no-mining areas (www.isa.org.jm). Sample processing on-board included elutriation and sieving through a 300-µm mesh using chilled (+4 °C, except during BIONOD at +11 °C) filtered sea water; samples were then fixed in pre-cooled (-20 °C) 96% undenatured ethanol (EtOH) and stored at -20 °C for at least 48 h. During this time (for the first 12 h) the samples were gently moved every 3 h to ensure thorough fixation and avoid freezing of the samples. After 12–24 h the samples were fixed again with 96% pure EtOH and kept at -20 °C until further sample processing (Riehl *et al.*, 2014a).

Morphological methods

Specimens were first identified to morphospecies level in the laboratories of the German Centre for Marine Biodiversity Research (DZMB, Wilhelmshaven and Hamburg, Germany). Appendages were dissected from

selected specimens and mounted in Congo-red stained glycerine gelatine or Euparal (Roth, pereopods only). For the latter, appendages were stepwise transferred from: (1) 96% denatured EtOH; via (2) Congo-red stained EtOH; (3) 50/50 EtOH/Euparal solution; to (4) 100% Euparal, with each step taking at least 20 mins. Illustrations were made using a Leica DM 2500 microscope with a camera lucida. Measurements of length-width ratios follow Hessler (1970), except body length/width ratio, which is measured against pereonite 1 width. Setal nomenclature follows Wolff (1962), Hessler (1970) and Riehl & Brandt (2010). The type material is deposited at the Zoological Museum of Hamburg (ZMH), while the voucher material of undescribed species is stored at the German Centre for Marine Biodiversity Research (DZMB) (Table 2). For Pacific species in the genus *Nannoniscus* a dichotomous identification key based on the available literature (Birstein, 1963; Menzies & George, 1972; Mezhov, 1986), as well as species described herein was constructed.

Confocal laser scanning microscopy (CLSM)

Five adult specimens (four females, one male) were used for CLSM as indicated in the descriptions below: one preparatory female specimen (voucher no. Na8, ZMH K-55358); one ovigerous female (voucher no. Na27, ZMH K-55354); one adult male (voucher no. Ma14Iso272, ZMH K-55350); one preparatory female (voucher no. Na23, ZMH K-55342); one preparatory female (voucher no. Na26, ZMH K-55375). Before dissection, each specimen was stained with a 1:1 solution of Congo Red and Acid Fuchsin overnight using procedures adapted from Michels & Büntzow (2010). The whole specimen was temporarily mounted onto a slide with glycerine, and self-adhesive plastic reinforcement rings were used to support the coverslip (Kihara & Rocha, 2009; Michels & Büntzow, 2010). The material was examined using a Leica TCS SP5 equipped with a Leica DM5000 B upright microscope and three visible-light lasers (DPSS 10 mW 561 nm; HeNe 10 mW 633 nm; Ar 100 mW 458, 476, 488 and 514 nm), combined with the software LAS AF v.2.2.1. (Leica Application Suite Advanced Fluorescence).

Images were obtained using the objective HCX PL APO CS 10.0 × 0.40 DRY UV and a 561 nm excitation wavelength with an 80% acousto-optic tunable filter (AOTF). Series of stacks were obtained, collecting overlapping optical sections throughout the whole preparation with an optimal number of sections according to the software. The acquisition resolution was 2048 × 2048 pixels, final images were obtained by maximum projection, and CLSM illustrations were composed and adjusted for contrast and brightness using Adobe Photoshop CS4 software.

Molecular-genetic methods

DNA extraction, amplification and sequencing

Total genomic DNA was isolated from either a pereopod for large individuals, or from the whole specimen for small individuals, from 39 specimens using the Chelex extraction method (Walsh *et al.*, 1991). Fragments of the mitochondrial cytochrome *c* oxidase subunit I (*COI*, ~ 650 bp) and ribosomal small subunit (16S, ~450 bp) genes were amplified using LCOI490/HC02198 (Folmer *et al.*, 1994) and SR/SF primers (Tsang *et al.*, 2009), respectively. Separate polymerase chain reactions (PCR) were conducted for *COI* and 16S. For *COI*, the PCR was performed in 25 µL volumes using Illustra PureTaq PCR beads from GE Healthcare Life Science (Buckinghamshire, UK). PCRs contained 20 µL sterile molecular grade H_2O, 0.5 µL of each primer (10 pmol/µL) and 4 µL of DNA template. Amplification was conducted using an Eppendorf Mastercycler pro S thermocycler (Hamburg, Germany) with the following parameters: initial denaturation at 94 °C for 5 min followed by 38 cycles repeating the sequence of 94 °C for 45 s (denaturation), 42 °C for 45 s (annealing) and 72 °C for 80 s (elongation). Final extension was performed at 72 °C for 7 min. For 16S, the PCR temperature profile comprised the following parameters: initial denaturation at 95 °C for 10 min followed by 36 cycles repeating the sequence of 95 °C for 30 s (denaturation), 48 °C for 30 s (annealing) and 72 °C for 45 s (elongation). Final extension was performed at 72 °C for 5 min (see Riehl *et al.*, 2014a for more details). PCR products were confirmed by size with electrophoresis on a 1% agarose gel with GelRed (Biotium, Hayward, USA) using commercial DNA size standards. PCR product which produced light bands after electrophoresis were outsourced for purification and Sanger sequencing to a contract sequencing facility (MacroGen Europe Laboratory, Amsterdam, Netherlands) using primer sets as for PCR. Alignments of DNA sequences of *COI* and 16S were performed using the Clustal X algorithm [*COI* (Larkin *et al.*, 2007)] and MAFFT [16S (Katoh *et al.*, 2002)]. Published *COI* sequences of eight *Nannoniscus* specimens (NB12_Iso020, NB12_Iso445, NB12_Iso098, NB12_Iso068, NB12_Iso290, NB12_Iso330, NB12_Iso070 and NB12_Iso099) were extracted from GenBank (Janssen *et al.*, 2015; Table 2). Furthermore, sequences of three species of *Ketosoma* Kaiser & Brix, 2018 and one undescribed *Nannoniscus* species (including NB12_Iso303, NB12_Iso310, NB12_Iso307; Table 2) were retrieved from GenBank (Janssen *et al.*, 2015; Kaiser *et al.*, 2018; Table 2) and included in alignment and trimming steps as an outgroup. For 16S, sequence data from one *Ketosoma* species were included (Table 2). All new sequences generated in this work were deposited in GenBank (see Table 2).

Table 2. List of voucher specimens used for molecular-genetic analyses. All type specimens are located at the CeNak, Universität Hamburg (ZMH catalogue), while voucher specimens of undescribed species are located at the DZMB, Hamburg

Voucher ID #	Voyage	Area	Station	Species	Marker	GenBank accession #	Collection #	Sex
Na43	AB02	OMS*	S11	*Nannoniscus* sp.	16S	MT259290	DZMB-69115	F
Na37	AB02	OMS	S11	*Nannoniscus* sp.	16S	MT259291	DZMB-69116	F
Na39	AB02	OMS	S11	*Nannoniscus* sp.	16S	MT259292	DZMB-69117	F
AB2ISO431	AB02	OMS	S5	*Nannoniscus* sp.	*COI*	MT256412	DZMB-69118	F
AB2ISO442	AB02	UK	U7	*Nannoniscus* sp.	*COI*	MT256413	DZMB-69119	M
Na41	AB02	OMS	S10	*Nannoniscus* sp.	*COI*	MT256414	DZMB-69120	F
NB12_Iso020	BIONOD	GER	06	*N. hilario*	*COI*	KJ736105	ZMH K-55341	F
Na25	JPIO	GER PA	24	*N. hilario*	*COI*,	MT256415	ZMH K-55381	F
					16S	MT259293		
Na23	JPIO	GER PA	24	*N. hilario*	*COI*	MT256416	ZMH K-55342	F
NB12_Iso445	BIONOD	FRA	101	*Nannoniscus* sp.	*COI*	KJ736107	DZMB-69121	F
Na14	JPIO	FRA	158	*Nannoniscus* sp.	*COI*	MT256417	DZMB-69124	F
NB12_Iso098	BIONOD	FRA	67	*Nannoniscus* sp.	*COI*	KJ736106	DZMB-69122	F
Na16	JPIO	FRA	158	*Nannoniscus* sp.	*COI*	MT256418	DZMB-69125	M
Na20	JPIO	GSR	133	*Nannoniscus* sp.	*COI*,	MT256419	DZMB-69126	F
					16S	MT259294		
MA13_Iso453	MA13	GER PRZ	90	*N. menoti*	*COI*	MT256420	ZMH K-55348	F
Iso1005/Na40	AB02	OMS	S11	*N. menoti*	*COI*	MT256421	ZMH K-55349	F
MA14_Iso272	MA14	GER PRZ	38	*N. menoti*	*COI*	MT256422	ZMH K-55350	M
MA14_Iso352	MA14	GER PRZ	39	*N. menoti*	*COI*	MT256423	ZMH K-55351	F
Na06	JPIO	GSR	117	*N. menoti*	*COI*	MT256424	ZMH K-55352	F
NB12_Iso068	BIONOD	GER	33	*N. menoti*	*COI*	KJ736104	ZMH K-55353	F
Na27	JPIO	FRA	171	*N. menoti*	*COI*,	MT256425	ZMH K-55354	F
					16S	MT259295		
Iso1120/Na42	AB02	APEI-6	APEI-6#1	*N. menoti*	*COI*	MT256426	ZMH K-55355	F
Na18	JPIO	GER PA	20	*N. menoti*	*COI*	MT256427	ZMH K-55356	F
MA13_Iso049	MA13	GER PA	07	*N. pedro*	*COI*	MT256428	ZMH K-55357	F
Na08	JPIO	GSR	133	*N. pedro*	*COI*,	MT256429	ZMH K-55358	F
					16S	MT259296		
MA13_Iso593	MA13	GER PRZ	90	*N. pedro*	*COI*	MT256430	ZMH K-55359	F
NB12_Iso290	BIONOD	GER	43	*N. pedro*	*COI*	KJ736102	ZMH K-55360	F
Na04	JPIO	GER PA	20	*N. pedro*	*COI*,	MT256431	ZMH K-55361	F
					16S	MT259297		
Na11	JPIO	FRA	171	*N. pedro*	*COI*	MT256432	ZMH K-55362	F
Na22	JPIO	GER PA	24	*N. pedro*	*COI*	MT256433	ZMH K-55363	F
NB12_Iso330	BIONOD	GER	43	*N. pedro*	*COI*	KJ736103	ZMH K-55364	F

Table 2. Continued

Voucher ID #	Voyage	Area	Station	Species	Marker	GenBank accession #	Collection #	Sex
Na05	JPIO	GER PA	20	*N. pedro*	*COI*, 16S	MT256434 MT259298	ZMH K-55365	F
MA14_Iso242	MA14	GER PRZ	39	*N. pedro*	*COI*	MT256435	ZMH K-55366	M
MA14_Iso319	MA14	GER PRZ	39	*N. pedro*	*COI*	MT256436	ZMH K-55367	F
MA14_Iso258	MA14	GER IRZ	21	*N. brenkei*	*COI*	MT256437	ZMH K-55368	M?
Na03	JPIO	GER PA	20	*N. brenkei*	*COI*, 16S	MT256438 MT259299	ZMH K-55369	F
NB12_Iso070	BIONOD	GER	33	*N. brenkei*	*COI*	KJ736101	ZMH K-55370	F
Na24	JPIO	GER PA	24	*N. brenkei*	*COI*	MT256439	ZMH K-55371	F
Na21	JPIO	GER PA	24	*Nannoniscus* sp.	*COI*	MT256440	DZMB-69129	F
NB12_Iso099	BIONOD	FRA	67	*N. magdae*	*COI*	KJ736099	ZMH K-55373	F
Na12	JPIO	FRA	171	*N. magdae*	*COI*	MT256441	ZMH K-55374	F
Na26	JPIO	FRA	171	*N. magdae*	*COI*, 16S	MT256442 MT259300	ZMH K-55375	F
Na28	JPIO	FRA	171	*N. magdae*	*COI*	MT256443	ZMH K-55376	F
Na49	JPIO	FRA	171	*N. magdae*	*COI*	MT256444	ZMH K-55377	M
Na19	JPIO	GER PA	20	*Nannoniscus* sp.	16S	MT271781	DZMB-69130	M
Na33	JPIO	FRA	158	*Nannoniscus* sp.	16S	MT259301	DZMB-69131	F
Na17	JPIO	FRA	158	*Nannoniscus* sp.	16S	MT259302	DZMB-69132	F
NB12_Iso303	BIONOD	GER	43	*Nannoniscus* sp. 4	*COI*	KJ736054	DZMB-69133	
NB12_Iso310	BIONOD	GER	43	*Nannoniscus* sp. 4	*COI*	KJ736055	DZMB-69134	
NB12_Iso307	BIONOD	GER	43	*Nannoniscus* sp. 4	*COI*	KJ736053	DZMB-69135	
VTDesm013	VEMA	NEA	2–6	*Ketosoma vemae*	*COI*	MF040892	ZMH K-46140	M
D3D060	DIVA3	ARG	534	*Ketosoma werneri*	*COI*	MF040893	ZMH K-46142	F
NBIso337	BIONOD	GER	43	*Ketosoma ruehlemanni*	*COI*	KJ736158	ZMH K-46139	M

*APEI: Area of Particular Environmental Interest, FRA: French licence area; GER: German licence area, GSR: G-TEC Sea Mineral Resources NV; OMS: Ocean Mineral Singapore Pte. Ltd.; UK: UK Seabed Resources Ltd.; IRZ: impact reference zone; PA, prospective mining area; PRZ: preservation reference zone; NEA: North-East Atlantic; Argentine basin; M: male, F: female.

Molecular species delimitation analyses

Three species delimitation methods were employed, encompassing a range of speciation models and analysis types. The Automatic Barcode Gap Detection [ABGD (Puillandre *et al.*, 2011)] algorithm was performed on alignments of *COI* and 16S online (https://bioinfo.mnhn.fr/abi/public/abgd/abgdweb.html) using pairwise K2P distances to determine the barcode gap. The General Mixed Yule Coalescent [GMYC (Pons *et al.*, 2006)] and multiple Poisson Tree Process [mPTP (Kapli *et al.*, 2017)] algorithms require ultrametric trees as inputs; these were made using the BEAUTi/BEAST v. 2.6.0 package (Bouckaert *et al.*, 2019) with the following options: for *COI*, the HKY mutational model was chosen based on its simplicity and prior support for related taxa (e.g. Brix *et al.*, 2018; Jennings *et al.*, 2018; Kaiser *et al.*, 2018), and for 16S the GTR model was chosen. Both markers were given a four-category gamma-distributed model of rate variation with default mutational gamma priors replaced with default log-normal priors; both trees were estimated with Yule tree priors and strict clocks on the branches. Final trees were computed with TreeAnnotator, discarding the first 10% of trees in the run as indicated by Tracer v.1.6 (Rambaut *et al.*, 2014). The GMYC analysis was conducted in R using the single threshold criterion [see Fujisawa & Barraclough (2013); called herein sGMYC]. The mPTP analysis was conducted using command-line software, with three replicate runs of 100 million MCMC steps, discarding the first million as burn-in.

Haplotype networks and phylogeographic inferences

Haplotype networks were made separately for each locus in PopART (http://popart.otago.ac.nz) using the TCS algorithm (Clement *et al.*, 2002). Networks were edited by hand in PopART for clarity and finalized by adding species boundaries in Adobe Illustrator (CS6).

Because the number of sampled individuals per delimited species was low (and even lower when divided by sampling area and station; see *Results*), few statistical analyses were suitable to investigate relationships between genetic and geographic distances (e.g. isolation-by-distance, IBD). This problem was addressed by computing these distances across all pairs of individuals, rather than across all pairs of stations. Another problem is that ordinary least-squares (OLS) regression is not applicable, because the data points are not independent, since they are calculated across all pairs of specimens. Therefore, several approaches were employed that address dependence of data points and uncertainty: major axis (MA) regression, reduced major axis (RMA) regression, and the Mantel test, a matrix-based regression approach typically used on pairwise measures of genetic and geographic distance between sampling stations. Genetic distances were calculated as p-distance (y variable), and geographic great-circle distances were calculated using the Haversine formula (x variable). Three datasets were analysed: linear p-distance against linear physical distances, linear p-distance against log-transformed physical distances, and log-transformed p-distances against log-transformed physical distances. The OLS, MA and RMA regressions were performed using the R package 'lmodel2' and the 'rma' script written by Philip Bergmann at Clark University; Mantel tests were performed in Arlequin v.3.5 using user-specified matrices. Scatterplots were made in linear space to visualize the relationships.

As a complement to these analyses, sampling area was treated as a discrete trait and estimated along the phylogenetic trees in BEAST, to assess the historical locations of taxa within the study boundaries, and the historical patterns of connectivity among sampling areas.

Comparative material

For comparison, the following type material was examined from the CeNak [formerly Zoological Museum Hamburg (ZMH)], Universität Hamburg, the Zoological Museum of Moscow University (ZMMU), Natural History Museum, Berlin, Germany (ZMB) and the United States National Museum of Natural History, Washington, USA (USNM):

Nannoniscus australis Vanhöffen, 1914, unspecified 'types', ZMB 17687–688.

Nannoniscus bidens Vanhöffen, 1914, unspecified 'type', ZMB 17689.

Nannoniscus bidens sensu Brandt, 1992, ZMH K-40956.

Nannoniscus coalescus (Menzies & George, 1972), holotype, male, USNM 120964.

Nannoniscus menziesi Mezhov, 1986, holotype, female, ZMMU 6143.

Nannoniscus meteori (Brandt, 2002), paratype, ZMH K-40107.

Nannoniscus ovatus Menzies & George, 1972, holotype, male, USNM 121022; allotype female (Vema.U-15–69), under the same accession number as holotype.

Nannoniscus perunis Menzies & George, 1972, holotype, female, USNM 121017–121018.

Nannoniscus teres Siebenaller & Hessler, 1981, holotype female, USNM 344192.

Abbreviations

In the taxonomic descriptions and figure legends the following abbreviations were used: AI—antennula,

AII—antenna, lMd—left mandible, rMd—right mandible, MxI—maxillula, MxII—maxilla, Mxp—maxilliped, Op–operculum, PI–PVII—pereopods I–VII, PlpI–V—pleopods I–V, Plt—pleotelson.

RESULTS

Species delimitation analyses

Initial morphological examination of differences in apparent external features without dissection of specimens revealed three distinct phenotypes based on the presence or absence of robust spines on the anterolateral tergites of pereonite 2 and biramous or uniramous uropods. The molecular distinctiveness of these phenotypes was confirmed by our SD analysis for *COI*; however, further species may be present, with mPTP delimiting 12 species, sGMYC delimiting 11 species and ABGD four species (excluding outgroup E, Fig. 2). An ABGD barcode gap of 3.8–5.7% (uncorrected p-distance) separated intra- vs. interspecific distances. Full morphological investigation of all species delimited with *COI* is beyond the scope of the present work. However, five of these species were robustly separated from neighbouring taxa and have clear morphological differences warranting confirmation as valid species and thus naming and description (see below).

The amplification success for 16S was low (28%), thus we did not receive sufficient sequence data to allow a meaningful comparison between both mitochondrial markers employed. In janiroidean isopods, including the Nannoniscidae, amplification and sequencing of the 16S marker has been shown to be more reliable than *COI* (e.g. Riehl *et al.*, 2014a; Schnurr *et al.*, 2018). As we used standard PCR protocols and 16S primers that have been successfully tested for isopods, and

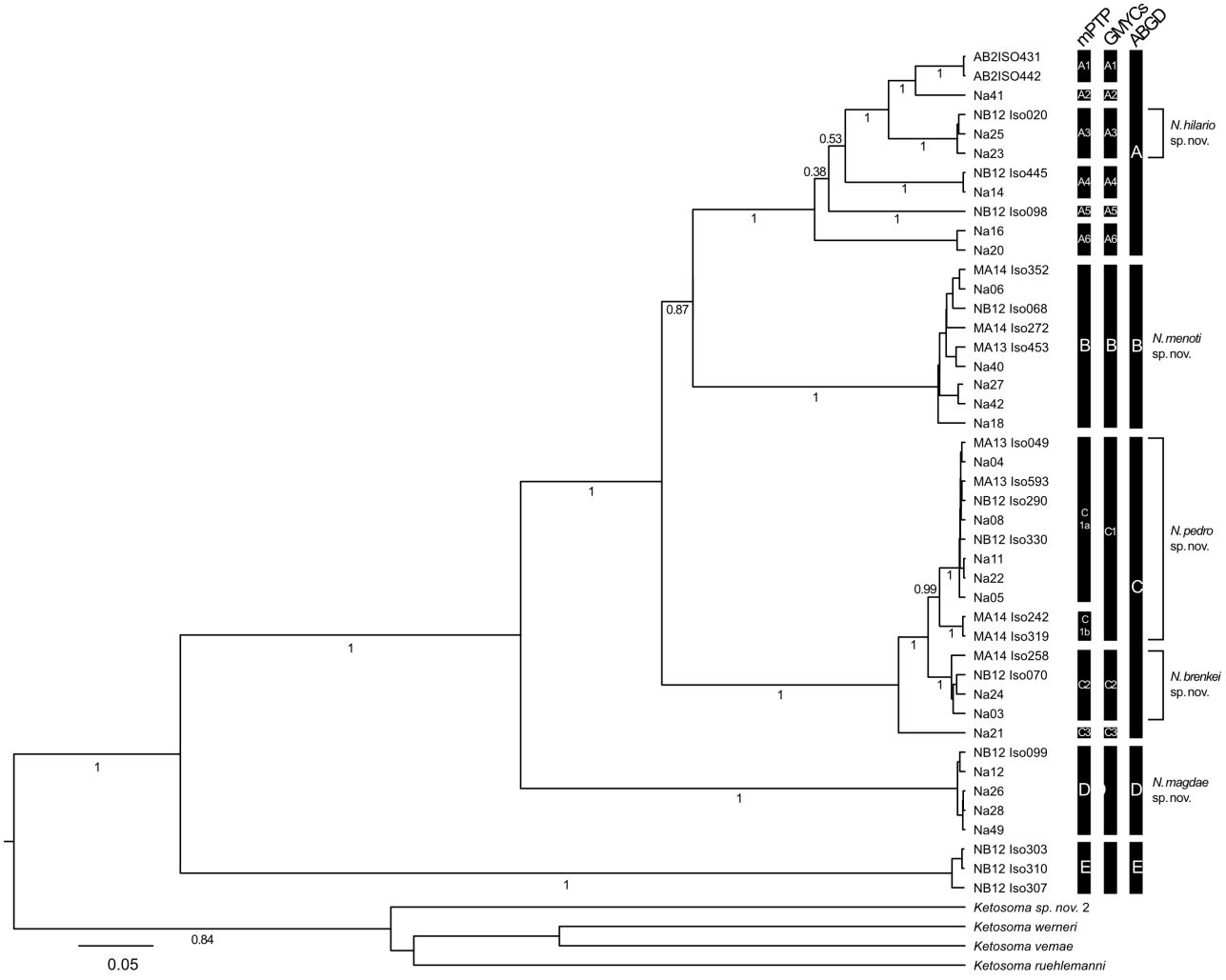

Figure 2. Bayesian phylogenetic tree of *Nannoniscus* lineages based on *COI*, with molecular species delimitations shown as black bars.

furthermore received good results for other nannoniscid specimens treated in the same PCR run (first author, pers. obs.), reasons for the low amplification rate remain unclear. Furthermore, the results of the SD analysis for the 16S data did not match the *COI*-based species delimitation nor the morphological distinction, and the relative magnitudes of pairwise genetic distances did not correlate in a sensible manner with morphological identification; these conflicts suggest that an error occurred in the sequence metadata record-keeping, resulting in specimen names being mapped incorrectly to 16S sequences. We therefore excluded the 16S data from the analysis in order to avoid misinterpretation of the results as well as species classification.

Haplotype networks

The haplotype network for *COI* (Fig. 3) exhibited a long central "spine" with numerous side branches representing delimited species; the distances between these delimited species was usually much larger than the those within a particular species (e.g. 35 steps between the new species *Nannoniscus pedro* and *Nannoniscus menoti*). Haplotype diversity was low within each single species (maximum of five for *N. menoti*), reflecting the overall low numbers of specimens per species. Neither the entire network nor the single-species sub-networks showed the star-like pattern indicative of recent growth from a large ancestral haplotype.

Phylogeographic analyses

The plot of genetic vs. geographic distance for the new species *N. menoti* (Fig. 4) showed a scattered relationship. However, regression analysis indicated a significant positive relationship for all methods except the Mantel tests when both variables were log-transformed (Supporting Information, Table S3). Ordinary least squares also produced a significant positive relationship when only geographic distance was log-transformed. In contrast, the plot for the new species *N. pedro* (Supporting Information, Fig. S1) shows two separated clusters of pairwise distances regardless of geographic distance; comparisons between clade C1b and the others generated large values, whereas comparisons within C subclades generated small values. None of the regression methods detected a significant correlation of transformed or untransformed variables.

Within the study region, discrete character reconstruction of historical geographic locations of genetic lineages indicated a fairly high degree of movement (Fig. 5). This analysis suggested that most lineages have persisted longest in the German licence area [posterior probability (PP) 0.5882] or the French licence area (PP 0.3740). Four of the five species newly described herein also likely persisted longest in GER (*Nannoniscus hilario* PP 0.9989, *N. menoti* PP 0.7514, *N. pedro* and *Nannoniscus brenkei* both PP 1.0), whereas *Nannoniscus magdae* was historically strongly associated with the French area (PP 1.0) and was only sampled there in the present material. Although quantitative connectivity estimates were not possible from this analysis, it appeared that *N. menoti* was found at more licence areas (five of six) and out of fewer extant lineages (nine) compared to *N. pedro* (three areas out of 11 extant lineages).

TAXONOMY

SUBORDER ASELLOTA LATREILLE, 1803

SUPRAFAMILY JANIROIDEA SARS, 1897

FAMILY NANNONISCIDAE HANSEN, 1916

Desmosomidae Sars, 1899: 118; Vanhöffen, 1914: 549; Nannoniscini Hansen, 1916: 83; Nannoniscidae Siebenaller & Hessler, 1977: 17–43.

Type genus: Nannoniscus Sars, 1870.

Genus: Nannoniscus Sars, 1870.

Nannoniscus Sars, 1870: 164; Hansen, 1916: 87–89; Gurjanova, 1932: 51; Menzies, 1962b: 133; Birstein, 1963: 78; Siebenaller & Hessler, 1981: 241; Kussakin, 1999: 68; Wilson, 2008: 13; *Saetoniscus* Brandt, 2002: 11.

Type species: Nannoniscus oblongus Hansen, 1916.

Species included (see also Table 3): Nannoniscus acanthurus Birstein, 1963, *Nannoniscus aequiremus* Hansen, 1916, *Nannoniscus affinis* Hansen, 1916, *Nannoniscus analis* Hansen, 1916, *Nannoniscus antennaspinis* Brandt, 2002, *Nannoniscus arcticus* Hansen, 1916, *Nannoniscus arctoabyssalis* Just, 1980, *Nannoniscus australis* Vanhöffen, 1914, *Nannoniscus bidens* Vanhöffen, 1914, *Nannoniscus bidens sensu* Brandt, 1992, *Nannoniscus brenkei* Kaiser, Brix & Jennings sp. nov., *Nannoniscus camayae* Menzies, 1962, *Nannoniscus caspius* Sars, 1899, *Nannoniscus cristatus* Mezhov, 1986, *Nannoniscus detrimentus* Menzies & George, 1972, *Nannoniscus hilario* Kaiser & Kihara sp. nov., *Nannoniscus inermis* Hansen, 1916, *Nannoniscus laevis* Menzies, 1962, *Nannoniscus laticeps* Hansen, 1916, *Nannoniscus magdae* Kaiser, Brix & Jennings sp. nov., *Nannoniscus menoti* Kaiser, Janssen & Mohrbeck sp. nov., *Nannoniscus menziesi* Mezhov, 1986, *Nannoniscus meteori* (Brandt, 2002), *Nannoniscus minutus* Hansen, 1916, *Nannoniscus muscarius* Menzies & George, 1972, *Nannoniscus*

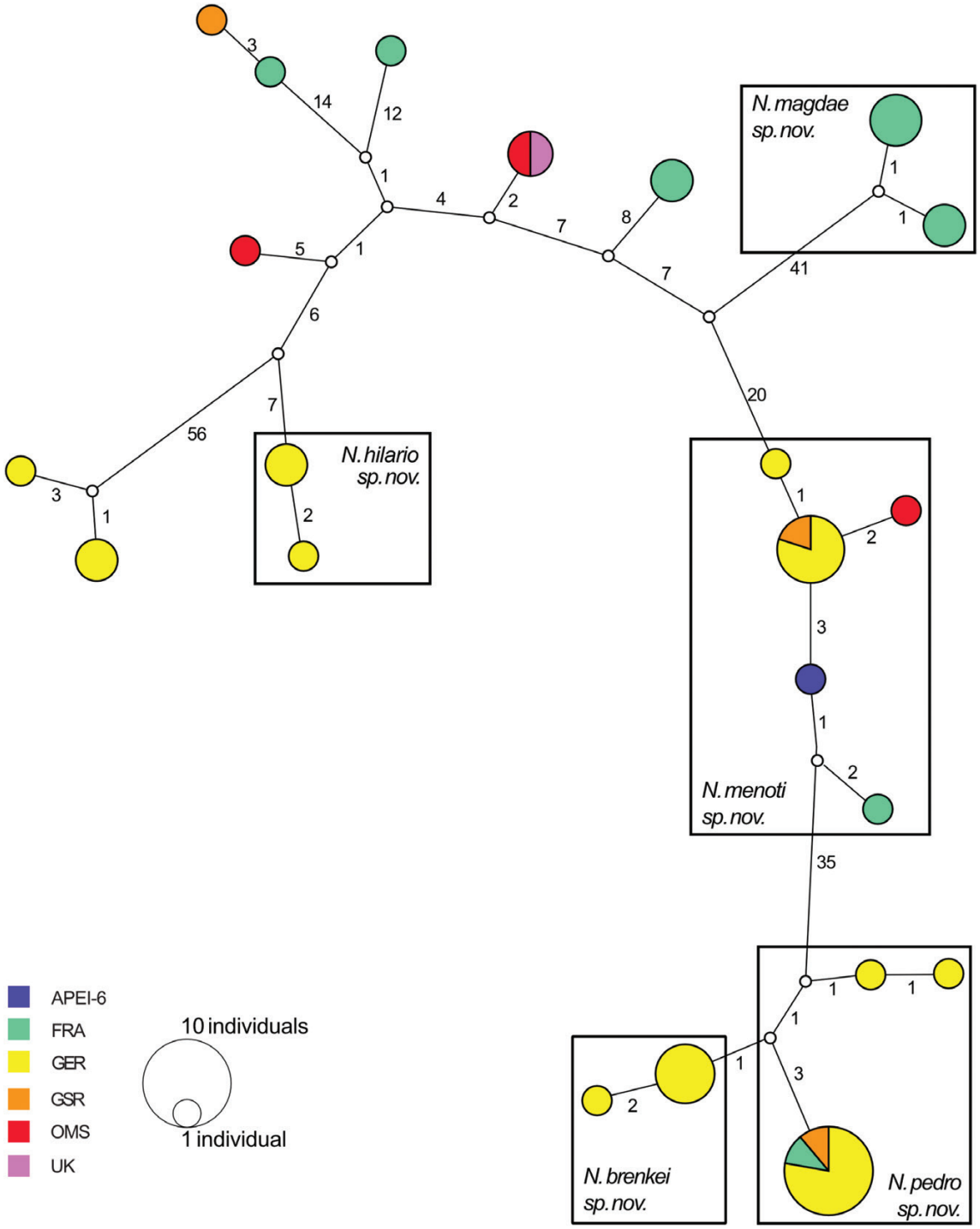

Figure 3. Haplotype network for *COI*. Sampled haplotypes are shown as solid circles with circle area proportional to the number of individuals possessing that haplotype; open circles represent unsampled haplotypes required to connect the network. The number of mutational steps between haplotypes are shown along connecting lines. The colours represent sampling locations as indicated in the legend. Species described herein are indicated with bounding boxes.

oblongus Sars, 1870, *Nannoniscus ovatus* Menzies & George, 1972, *Nannoniscus pedro* Kaiser, Brix & Kihara sp. nov., *Nannoniscus perunis* Menzies & George, 1972, *Nannoniscus plebejus* Hansen, 1916, *Nannoniscus profundus* Svavarsson, 1982, *Nannoniscus reticulatus* Hansen, 1916, *Nannoniscus simplex* Hansen, 1916,

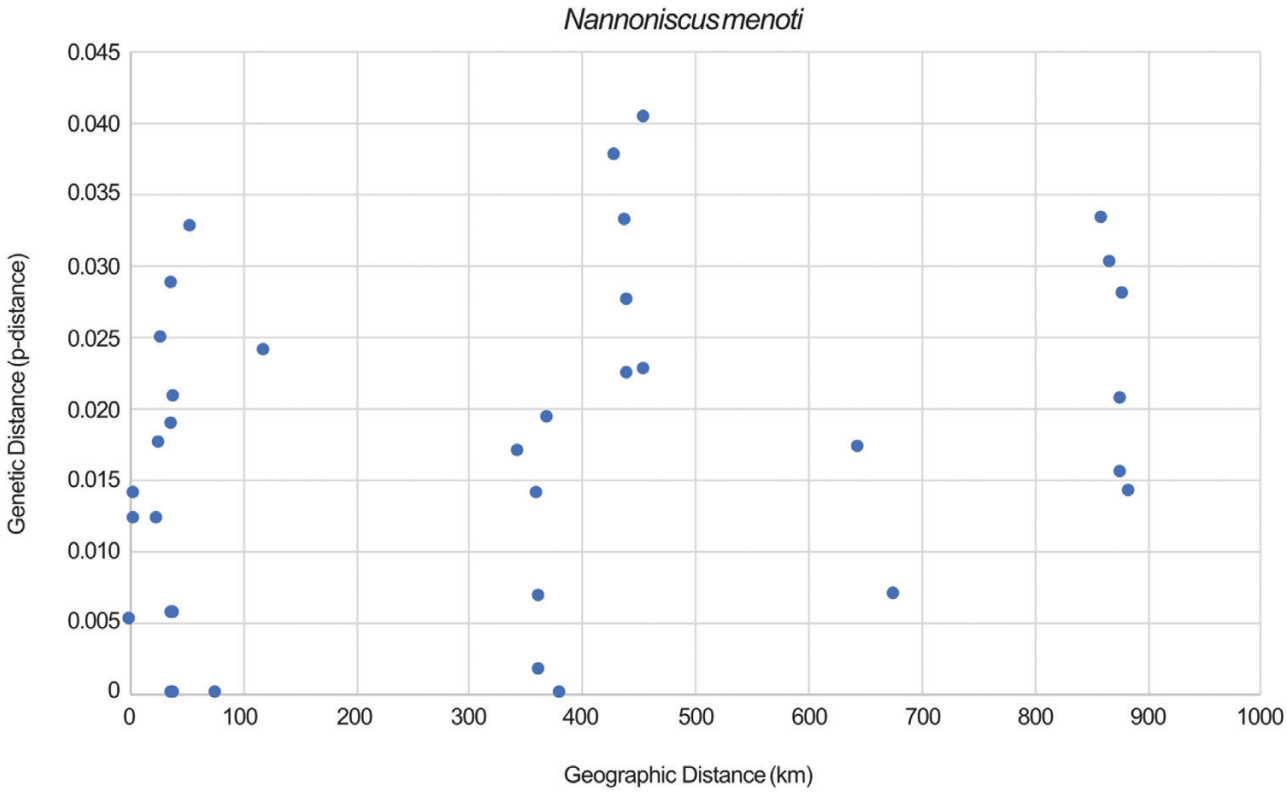

Figure 4. Genetic divergence (p-distance) in relation to geographic distance in kilometres for *N. menoti*.

Nannoniscus spinicornis Hansen, 1916, *Nannoniscus teres* Siebenaller & Hessler, 1981.

Diagnosis (modified from Siebenaller & Hessler, 1981: 241; Wilson, 2008: 14): Pereonal tergites projecting laterally from pereopodal coxae; pereonites 6–7 dorsal articulation absent medially. Pleotelson distinctly shorter than pereonites 5–7 combined. Antennula with 5 segments, distal article bulbous, article 4 distal margin with ventromedial angular projection. Mandible with 3-segmented palp. Pereopods I–II equally robust. Uropods biramous or rarely uniramous.

Distribution: Known records from the Arctic, Atlantic, Pacific and Southern oceans and the Caspian Sea, although likely to be globally distributed. Although few *Nannoniscus* species are described from the continental shelf (≥ 75 m), they occur mainly at slope and abyssal depth, with two species recorded from the hadal Zone (*N. ovatus* Menzies & George, 1972 and *N. perunis* Menzies & George, 1972; Table 3).

Remarks: Species described herein were assigned to *Nannoniscus* due to the following characters: antennula article 4 distal margin with ventromedial angular projection, antennula terminal article 5 bulbous, pereopods 1 and 2 equally robust, lack of ventral articulation between pereonites 6 and 7. However, the genus *Nannoniscus*, thus far, is largely defined by a combination of plesiomorphic characters, such as uropods inserting posteroventrally close to the anus (Wilson, 2008), defining the family Nannoniscidae, as well as synapomorphic characters, such as a bulbous terminal article of the antennula, a specialized antennula article 4 and fusion of pereonites 6 and 7 that characterize a cluster of nannoniscid genera containing *Nannoniscus*, *Nannonisconus* Schultz, 1966, *Nymphodora* Kaiser, 2009, *Rapaniscus* Siebenaller & Hessler, 1981 and *Regabellator* Siebenaller & Hessler, 1981. Wilson (2008) states that the broad body form with laterally projecting pereonite tergites is present in all *Nannoniscus* species. While this is true for some species (e.g. the type species *N. oblongus*), others have a slender body (body length > 4.5 times pereonite 1 width) with lateral tergites that extend only slightly, if at all (e.g. *N. ovatus*, *N. perunis*, *N. menziesi*, *N. meteori* and species described herein). Overall, the genus comprises species with diverse morphologies mostly referring to the shape of the pleotelson and the presence of a ventral spine on the female operculum and/or pereonite 7. While *N. oblongus* possesses a ventral opercular spine, there are several species, where a spine is overall absent (e.g. *N. aequiremis*,

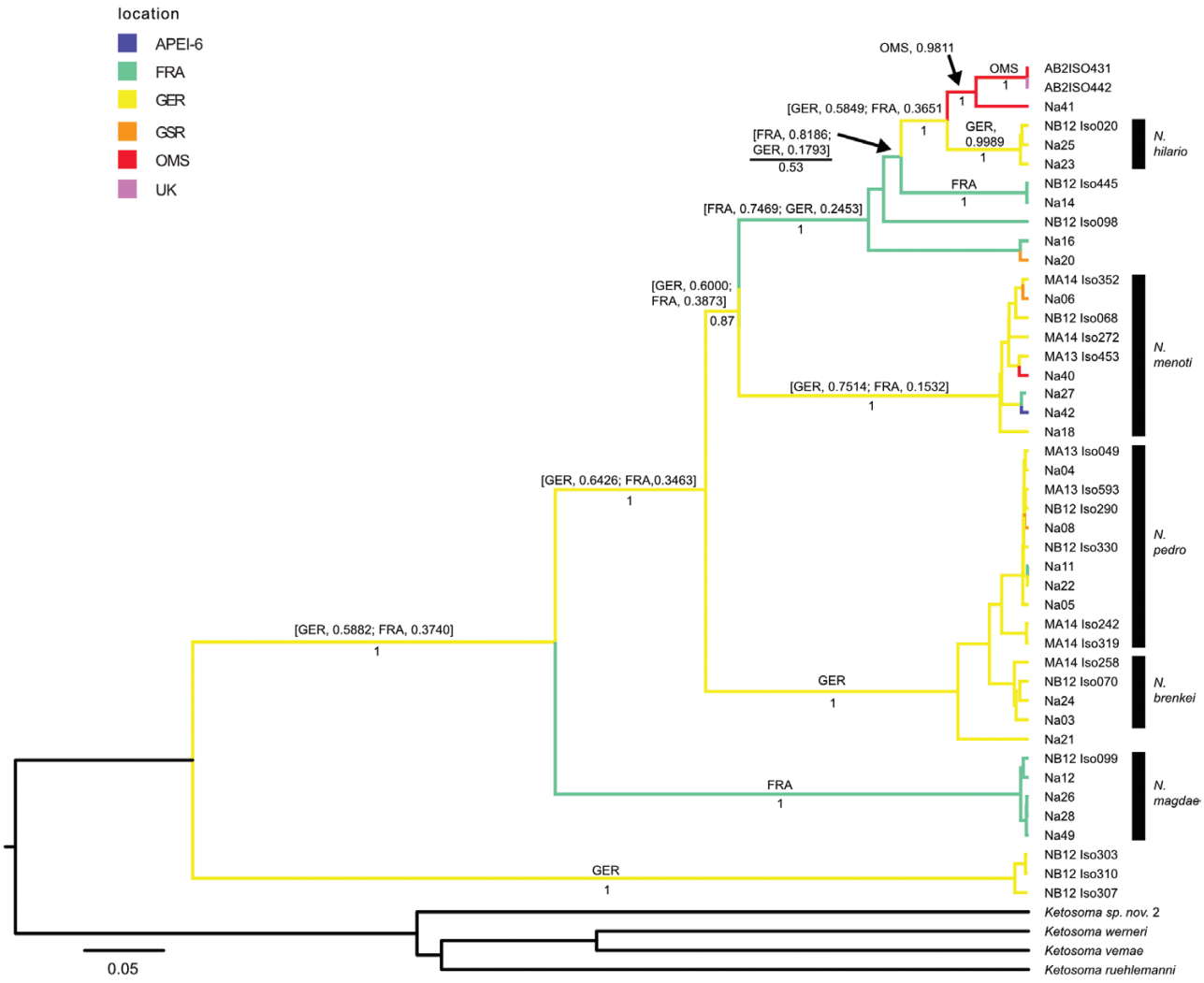

Figure 5. Bayesian reconstruction of geographic location of ancestral lineages of *Nannoniscus*, based on sampling area of extant lineages. Brackets above and below branches list potential locations and their 95% highest posterior distributions, respectively.

N. arctoabyssalis, *N. cristatus*, *N. inermis*), or one occurring on the seventh pereonite (*N. australis*, *N. minutus*, *N. muscarius*, *N. spinicornis*, *N. reticulatus*, *N. plebejus*, *N. affinis*, *N. profundus*, *N. caspius*). In *N. reticulatus*, ventral spines are present both on the female operculum and the seventh pereonite. The presence or absence of a ventral opercular spine has been found a useful character to separate the nannoniscid genera *Ketosoma* and *Thaumastosoma* Hessler, 1970 (Kaiser *et al.*, 2018). Equally, the position of ventral spines on pereonites 6 and 7 represents an apomorphy of *Regabellator*. In contrast, in *Rapaniscus* species, similar to *Nannoniscus*, the position of the ventral spines is variable, present on either pereonite 7 [*Rapaniscus crassipes* (Hansen, 1916), *Rapaniscus dewdneyi* Siebenaller & Hessler, 1981] or the operculum (*Rapaniscus multisetosus* Brandt, 2002).

Further differences exist in the presence or absence of the uropodal exopodite among *Nannoniscus* species; most species within the genus possess biramous uropods, while a lack a uropodal exopod is reported for two species (*N. ovatus* and in one new *Nannoniscus* species described below). Presence of uniramous or biramous uropods has been used as a segregating character to define genera within the munnopsid subfamily Ilyarachninae (Merrin, 2007); however, there are several genera (e.g. within Desmosomatidae, Paramunnidae), where both character states occur (Just & Wilson, 2007; Brix & Bruce, 2008; Kaiser & Marner, 2012 and discussion therein). *Nannoniscus* species described below show a gradual reduction of the exopodite (well-developed vs. minute vs. absent), thus, at least in *Nannoniscus*, the presence or absence of the uropodal exopodite represents a valuable

Table 3. Checklist of described *Nannoniscus* species with information on their type locality and depth distribution

Species	Type locality	Depth (m)
N. acanthurus Birstein, 1963	NW Pacific	3941–5495
N. aequiremus Hansen, 1916	S of Jan Mayen, Arctic Ocean	885
N. affinis Hansen, 1916	SW Iceland, N Atlantic	1505
N. analis Hansen, 1916	Davis Strait, Labrador Sea	2258
N. antennaspinis Brandt, 2002	Angola Basin, SE Atlantic	5389–5415
N. arcticus Hansen, 1916	S of Jan Mayen, Arctic Ocean	75–699
N. arctoabyssalis Just, 1980	Eurasian Basin, Arctic Ocean	3970
N. australis Vanhöffen, 1914	E Antarctic	385
N. bidens Vanhöffen, 1914	E Antarctic	385
N. bidens sensu Brandt, 1992	Weddell Sea	191–257
N. brenkei Kaiser, Brix & Jennings	Eastern German licence area, CCZ	4093–4136
N. camayae Menzies, 1962	Caribbean Panama	1714
N. caspius Sars, 1899	Caspian Sea	n.a.
N. cristatus Mezhov, 1986	Gulf of Alaska, NE Pacific	3200
N. detrimentus Menzies & George, 1972	Peru-Chile-Trench, SE Pacific	3909–3970
N. hilario Kaiser & Kihara	Eastern German licence area, CCZ	4093–4259
N. inermis Hansen, 1916	Davis Strait, Labrador Sea	2258
N. laevis Menzies, 1962	SE Atlantic	4885
N. laticeps Hansen, 1916	N Iceland	552
N. magdae Kaiser, Brix & Jennings	French licence area, CCZ	5017–5024
N. menoti Kaiser, Janssen & Mohrbeck	French licence area, CCZ	4076–5024
N. menziesi Mezhov, 1986	Gulf of Alaska, USA	4800
N. meteori (Brandt, 2002)	Angola Basin, SE Atlantic	5389
N. minutus Hansen 1916	Davis Strait, Labrador Sea	1096
N. muscarius Menzies & George, 1972	Peru-Chile-Trench, SE Pacific	3909–3970
N. oblongus Sars, 1870	Lofoten, Iceland	219–5843
N. ovatus Menzies & George, 1972	Peru-Chile-Trench, SE Pacific	6321–6328
N. pedro Kaiser, Brix & Kihara	GSR licence area, CCZ	4093–5024
N. perunis Menzies & George, 1972	Peru-Chile-Trench, SE Pacific	4823–6281
N. plebejus Hansen, 1916	SW Iceland, N Atlantic	1505
N. profundus Svavarsson, 1982	Norwegian See, off Greenland	2475–2502
N. reticulatus Hansen, 1916	N Iceland	80–1020
N. simplex Hansen, 1916	W Iceland	1070–1505
N. spinicornis Hansen, 1916	S of Jan Mayen, Arctic Ocean	2465
N. teres Siebenaller & Hessler, 1981	NE Atlantic	4426–4435

character at the species, but not at the generic level [see also Brix & Bruce (2008) for desmosomatids].

Siebenaller & Hessler (1981) and Brandt (2002) already discussed the likely paraphyly of *Nannoniscus* particularly referring to "odd" species such as *N. muscarius* (with a strongly produced coxal spine) and *N. ovatus* (= uniramous uropods). However, these species are notsingle occurrences but representative for this heterogeneous group. Up to now there has been no rigorous phylogenetic assessment of all *Nannoniscus* species, and it is not the purpose of the present study to address this issue. Nevertheless, as a prelude, the position of *N. coalescus* (Menzies & George, 1972) is discussed. The species had been first described as *Desmosoma coalescum* in the family Desmosomatidae and was later transferred to *Nannoniscus* by Siebenaller & Hessler, 1977 due to the bulbous terminal article of the antennula as well as fusion of pereonites 6 and 7. Our morphological analyses of the holotype alongside line drawings made by Menzies & George (1972: p. 9.48) suggest the species belongs to *Rapaniscus* owing to a broadened pereopod I carpus bearing several long robust setae (Siebenaller & Hessler, 1981). Therefore, *N. coalescus* is herein transferred to *Rapaniscus*.

NANNONISCUS MENZIESI MEZHOV, 1986
(FIG. 6)

Material examined: Holotype female, ZMMU No. 6143.

Diagnosis: Body slender, length about 4.7 × pereonite 1 width; AI article 2 stout, length and width about 0.8 article 1 length and width; Mxp lateral margin devoid of setae; Mxp epipodite reaching upper third of palpal article 3; Md incisor teeth acute; pereonite 2 anterolateral tergites each with robust seta; Op with

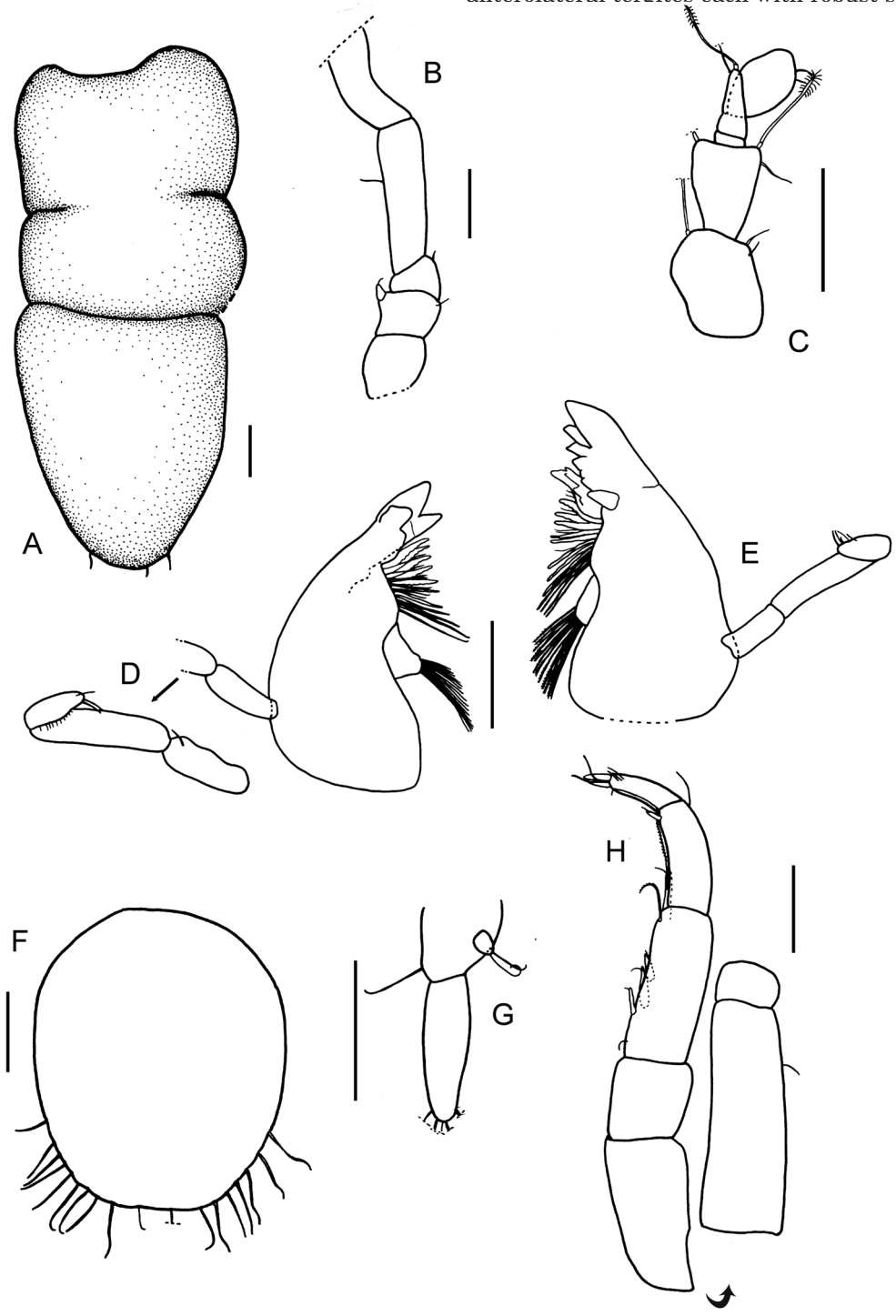

Figure 6. *Nannoniscus menziesi* Mezhov, 1986, holotype female (ZMMU 6143): (A) habitus, posterior somited, dorsal view; (B) AII; (C) AI; (D) rMd; (E) lMd; (F) Op; (G) Urp; (H) PI. Scale bars: A–H = 100 µm.

ventral posteriorly bent spine, posterior margin with numerous (≥ 18) long simple setae; Urp biramous, not projecting beyond Plt posterior margin; Urp exopodite short, length 0.3 protopodite length, endopodite length ≥ 5.4 exopodite length.

Redescription of female holotype: Habitus (Fig. 6A), only pereonites 6 and 7 and the pleotelson are illustrated. Pereonite 6 and 7 medially fused; pereonite 6 and 7 of similar width, pereonite 6 anterior margin strongly concave. Plt width equal to pereonite 6 width, width 0.9 length; posterior margin strongly rounded, anterior margin slightly concave. Urp not projecting beyond Plt posterior margin. AI (Fig. 6C) with five articles. First article circular and broadest, length 1.3 width, with two small simple setae and one broom seta (broken off) distally. Second article length 0.9 article 1 length, length 1.3 width, with two broom setae (one broken off) and one simple seta distally. Article 3 minute, length 0.1 article 1 length, length 0.3 width. Article 4 with long distal projection, article 4 (incl. projection) length 0.7 article 1 length, length 2.2 width, with one long broom seta and one simple seta (broken off) distally. Article 5 length 0.8 article 1 length, length 1.6 width, with one aesthetasc distally. AII (Fig. 6B), only podomere articles 2–5 illustrated. Articles 2–4 short, length of each article (2–4) ≤ 0.4 article 5 length; article 3 with one stout spine and one simple seta distally; article 4 with one small simple seta distally. Article 5 length 2.3 article 2 length, length 3.1 width, with one simple seta laterally. Md (Fig. 6E, F), Md palp of left and right mandible well developed, consisting of three articles almost reaching incisor. Palpal article 2 of lMd length twice article 1 length. Terminal article length about as long as article 1, tapering distally, with several (≥ 5) small setae ventrally. Palp of rMd similar to lMd with several (≥ 10) small setae ventrally, with three somewhat longer setae distally. Incisor process of lMd with seven teeth, incisor of rMd with four teeth. Lacinia mobilis of lMd with four teeth. Spine row of lMd with 12 robust spines of varying size and several slender setae in between; dentation decreasing and site increasing proximally. Spine row of rMd with 11 robust spines and several slender setae in between, dentation decreasing, seta size increasing proximally. Molar of rMd and lMd triangular; molar of rMd with 16, of lMd with 12 long, serrate spines distally. PI (Fig. 6H), damaged between basis and ischium. Basis length 3 width, with one simple seta ventrally. Ischium length 0.6 basis length, length 1.6 width. Merus quadrangular, length 0.6 ischium length, as long as wide. Carpus length 2.1 merus length, length 2.6 width, with three unequally bifid setae and two long simple setae ventrally. Propodus length 0.6 carpus length, length about twice width, with one simple setae dorsally, with numerous small setae, membranously embedded, and two setae (one simple, one unequally bifid) in between ventrally, with one long simple seta distoventrally. Dactylus length 0.6 propodus length, length 3 width, with three slender setae medially. Unguis length 0.4 dactylus length, with two long, slender setae between unguis and ventral claw. Op (Fig. 6F) length 1.2 width. Lateral margin rounded, posterior margin almost straight, with several (≥ 18) simple setae, seta length 0.2 Op length, medial two setae somewhat shorter, length 0.1 Op length. Urp (Fig. 6G) biramous. Protopodite with one long simple seta laterally. Exopodite minute, length 0.3 protopodite length, with two simple setae terminally. Endopodite length 5.4 exopodite length, length 3.2 width, with five setae terminally (all broken off).

Remarks: The anterior part of the specimen was damaged, thus only drawings of the posterior somites were made. These clearly show a lack of articulation between pereonites 6 and 7, which is not obvious in Mezhov's (1986) drawings. Examination of the original slides did not reveal a ventral spine on the operculum, nor damage of the tissue. However, the setation pattern corresponds to Mezhov's illustrations, suggesting that slides did not get mixed up. It remains to be proven that *N. menziesi* possesses a ventral opercular spine.

Nannoniscus ovatus Menzies & George, 1972 (Fig. 7A–F)

Material examined: Holotype, male, USNM Cat. No. 121022; allotype female (Vema.U-15–69), under the same accession number as the holotype.

Diagnosis: Body slender, length about 4.9 × pereonite 1 width; Mxp lateral margin devoid of setae; Mxp epipodite reaching proximal third of palpal article 3; pereonite 2 anterolateral tergites each with robust seta; pereonite 7 lacking ventral spine; Op with ventral posteriorly bent spine, posterior margin with ≤ nine simple setae; Urp uniramous, not projecting beyond Plt posterior margin; male PlpI with three hook-like projections distally.

Redescription of male holotype: Habitus (Fig. 7D–F), body length 4.9 × pereonite 1 width. Coxae not visible in dorsal view. Cephalothorax (Fig. 7D) length 0.9 width. Anterior and lateral margins straight, posterior margin slightly rounded. Antennae inserting frontolaterally in deep fold. Pereonites 1 and 2 of equal width, pereonites 2–7 decreasing in width; pereonite 1 length 0.3 width. Pereonite 2 length 1.4 pereonite 1 length, length 0.5 width. Pereonites 2 and 3 of similar length; pereonite 4 length 1.5 pereonite 1 length. Pereonites 1–4 anterior

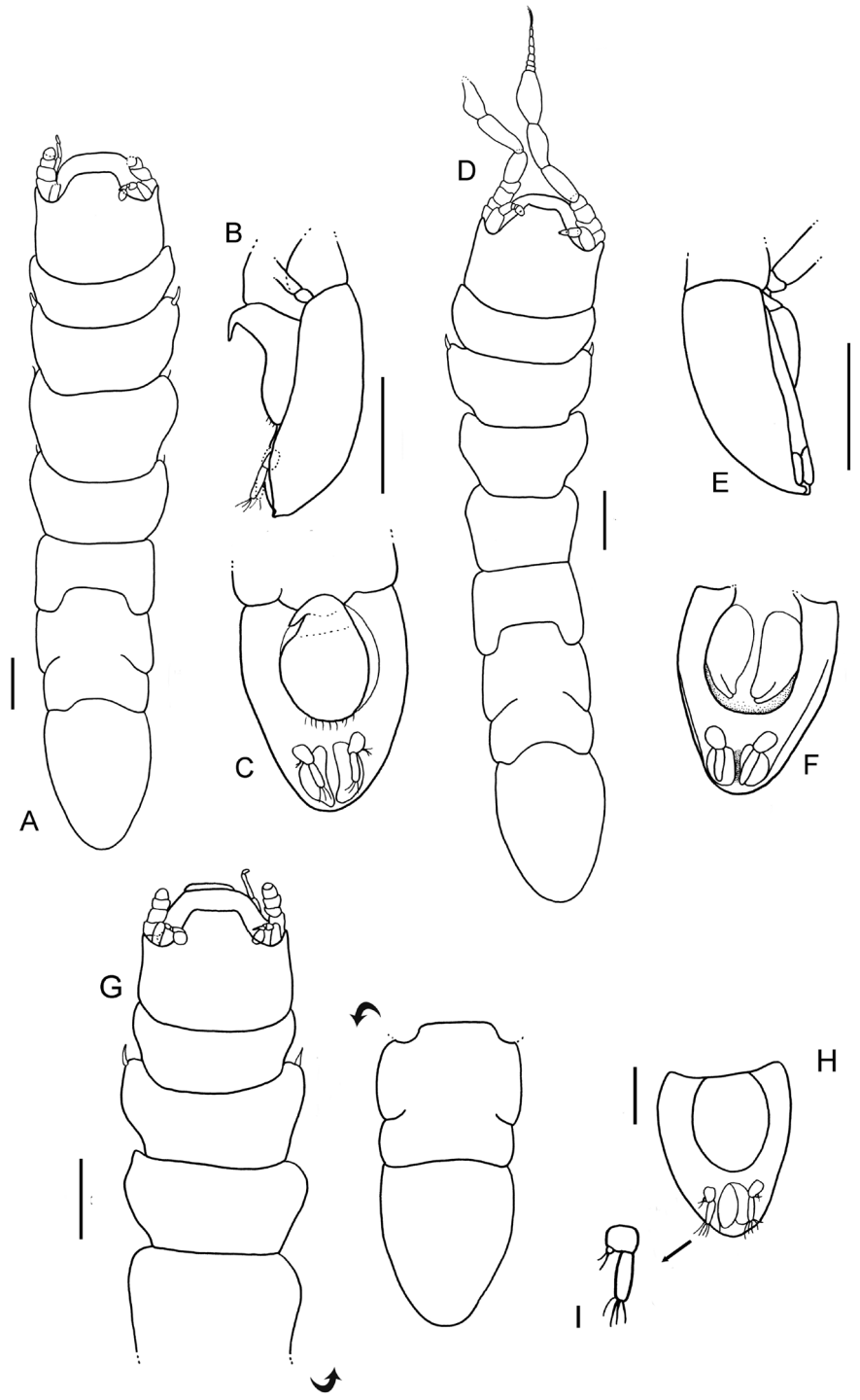

Figure 7. A–C, *Nannoniscus ovatus* Menzies & George, 1972, allotype female (USNM 121022); (D–F) holotype male (USNM 121022); (G–I) *N. perunis* Menzies & George, 1972, holotype female (USNM 121017–121018): (A) habitus, dorsal view; (B) Plt and Op, lateral view; (C) Plt and Op, ventral view; (D) habitus, dorsal view; (E) Plt, lateral view; (F) Plt, ventral view incl. Urp.; (G) habitus, dorsal view; (H) Plt, ventral view; (I) Urp. Scale bars: A, G–I = 100 µm; B–F = 200 µm.

margins frontally directed, rounded; anterolateral tergites of pereonite 2 each tipped with robust seta. Pereonite 5 length 1.2 pereonite 1 length, anterior margin straight. Pereonites 6 and 7 dorsomedially fused, pereonite 6 anterior margin strongly convex. Plt length 0.2 body length, length 1.4 width, width 0.8 pereonite

1 width; posterior margin strongly rounded; anterior margin convex. Urp (Fig. 7F) drawn *in situ*. Uniramous, length 0.3 Plt length, not projecting beyond posterior margin. Protopodite length 1.4 width. Endopodite length 1.4 protopodite length, length 4.4 width.

Description of female paratype: Habitus (Fig. 7A–C), body length 4.7 × pereonite 1 width. Coxae not visible in dorsal view. Cephalothorax (Fig. 7A) length 0.9 width. Anterior and lateral margins straight, posterior margin slightly rounded. Antennae inserting frontolaterally in deep fold. Op (Fig. 7B, C) length 1.4 width, with strong ventral spine, posteriorly bent. Lateral and posterior margins rounded, posterior margin with several (≤ 9) short simple setae. Pereonites 2–7 decreasing in width; pereonite 1 and 2 widest, pereonite 1 length 0.3 width, pereonite 2 length 0.4 width, length 1.5 pereonite 1 length. Pereonite 3 longest, length 2.1 pereonite 1 length. Pereonites 2, 4, 6 and 1, 5 and 7 of similar length. Pereonites 1–4 anterior margins frontally directed, rounded, anterolateral tergites of pereonite 2 each tipped with robust seta, tergites of pereonites 3 and 4 each with small simple seta. Pereonite 5 width 0.8 pereonite 1 width, its anterior margin slightly concave, pereonite 6 anterior margin strongly convex. Pereonites 6 and 7 fused. Plt length 0.2 body length, length 1.4 width, width 0.7 pereonite 1 width tapering towards distal end; posterior margin strongly rounded, anterior margin convex. Urp (Fig. 7C) drawn *in situ*. Uniramous, length 0.2 Plt length, not projecting beyond Plt posterior margin. Protopodite length 1.4 width, with three simple setae laterally. Endopodite length 1.1 protopodite length, length 4.5 width, with few simple setae terminally.

Remarks: Menzies & George (1972) did not provide a description of the female of *N. ovatus*. Yet, owing to gender-related dimorphism also known from nannoniscids (Wilson, 2008), both sexes are required for morphological comparison.

NANNONISCUS PERUNIS MENZIES & GEORGE, 1972

(FIG. 7G–I)

Material examined: Holotype, female, USNM 121017–121018.

Diagnosis: Body slender, length about 4.7 pereonite × 1 width; pereonite 2 anterolateral tergites each with robust seta; pereonites 3–4 anterolateral tergites without setae; pereonite 7 lacking ventral spine; Op with ventral posteriorly bent spine, Urp biramous, not projecting beyond Plt posterior margin; Urp exopodite minute, endopodite length ≥ 7.8 exopodite length.

Redescription female holotype: Habitus (Fig. 7G, H), body length 4.7 × pereonite 1 width. Coxae not visible in dorsal view. Cephalothorax (Fig. 7G) length 0.8 width. Anterior margin slightly concave, lateral margins straight, posterior margin slightly rounded. Antennae inserting frontolaterally in deep fold. Pereonites 2–7 decreasing in width; pereonite 2 widest, length 0.4 width, width 1.1 pereonite 1 width. Pereonites 2 and 3 of similar length, length 1.3 pereonite 1 length; pereonite 4 length 1.9 pereonite 1 length. Pereonites 1–4 anterior margins frontally directed, anterolateral tergites of pereonite 2 each tipped with robust seta. Pereonite 5 not illustrated. Pereonites 6 and 7 dorsolmedially fused, pereonite 6 anterior margin strongly convex. Plt length 2.7 pereonite 1 length, length 1.3 width; posterior margin strongly rounded, anterior margin slightly convex. Urp (Fig. 7H, I) drawn *in situ*. Biramous, length 0.2 Plt length, not projecting beyond Plt posterior margin. Protopodite length 1.3 width. Exopodite minute, length 0.2 protopodite length. Endopodite length 7.8 exopodite length, length 4 width, with few long setae terminally.

Remarks: Illustrations of the holotype of *N. perunis* made by Menzies & George (1972) show a coxal seta on pereonite 2, a character state atypical for nannoniscids. However, examination of type material could instead confirm robust setae on the anterolateral tergites of pereonite 2.

NANNONISCUS HILARIO KAISER & KIHARA, **SP. NOV.**

(FIGS 8–10)

Zoobank registration: urn:lsid:zoobank.org:act:02A15862-0D93-40B4-BD9A-0F41E6D70CA6.

Type fixation: Holotype, preparatory female, ZMH K-55342, 3.6 mm, designated here.

Material examined: Holotype: female (preparatory, Na23), 3.6 mm, CCZ, equatorial NE Pacific, JPIO SO239 expedition, RV Sonne, EBS, station 24 (start: 11°51’19”N, 117°1’30”W, 4093 m; end: 11°51’31”N, 116°58’0”W, 4093 m), date: 22/03/2015, ZMH K-55342.

Paratypes: Preparatory female (Na25), same location as holotype, ZMH K-55381; preparatory female (NB12_Iso020), CCZ, equatorial NE Pacific, BIONOD expedition, RV L’Atalante, EBS, station 06 (start: 11°46’13”N, 116°41’8”W, 4259 m; end: 11°46’13”N, 116°41’7”W, 4259 m), date: 02/04/2012, ZMH K-55341.

Etymology: The new species (noun in apposition) is named after Ana Hilario for her support and enthusiasm to join the SO239 ‘Berta’ team (in this case down to 4259 m).

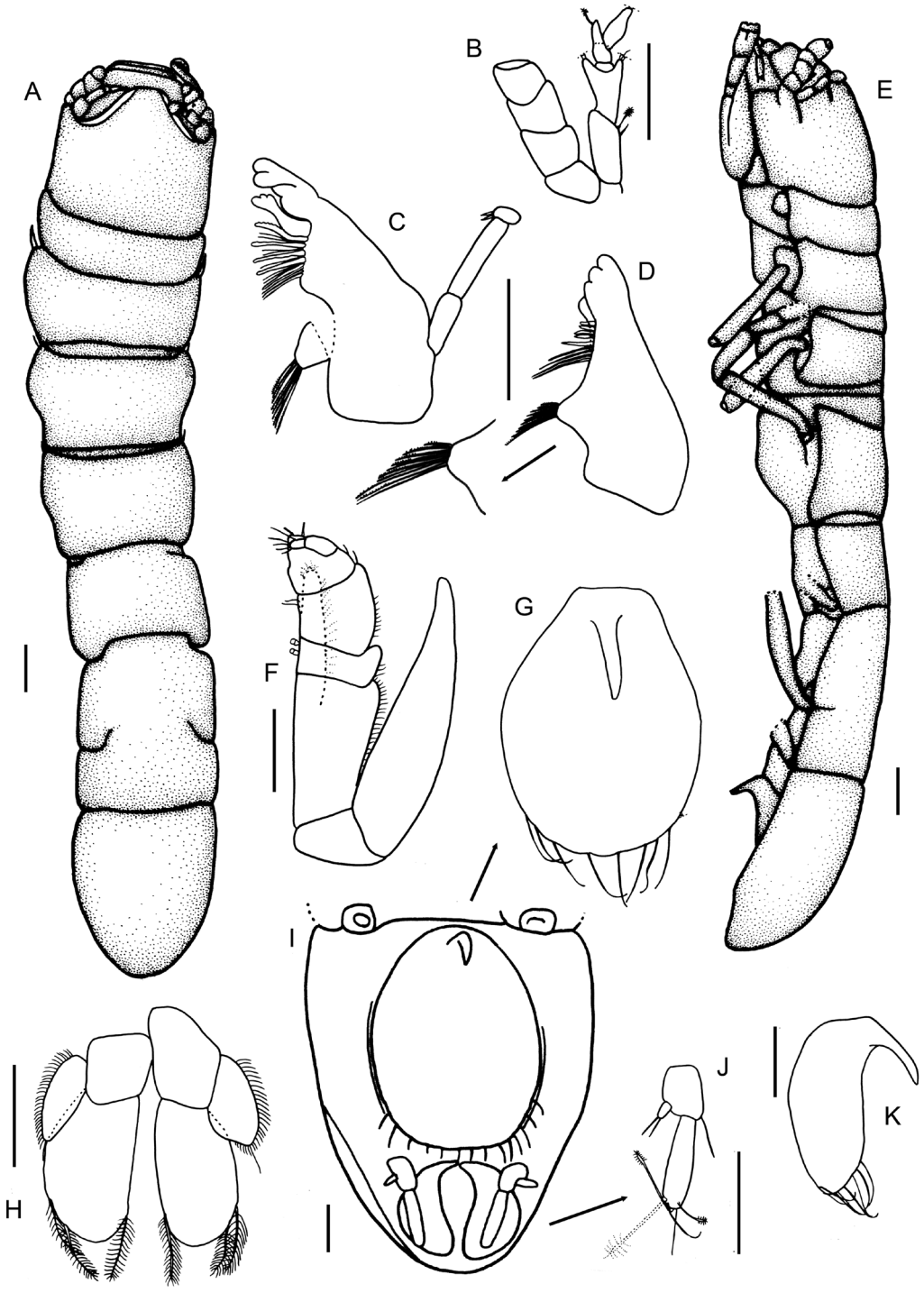

Figure 8. *Nannoniscus hilario*, (A, E, I) holotype female (ZMH K-55342, Na23); (B–D, F–H, J–K) paratype female (ZMH K-55341, NB12_Iso020): (A) habitus, dorsal view; (B) AI, peduncular articles 1–4 AII; (C) lMd; (D) rMd; (E) habitus, lateral view; (F) Mxp; (G) Op, ventral view; (H) PlpIII; (I) Plt, ventral view; (J) Urp; (K) Op, lateral view. Scale bars: A, E, I = 200 µm; B–D, F–H, J–K = 100 µm.

Distribution: Only known from the type locality (German licence area, eastern CCZ), between 4093 and 4259 m depth.

Diagnosis: Body slender, length about 5.5 × pereonite 1 width; Mxp lateral margin with numerous small setae; Mxp epipodite reaching distal third of palpal

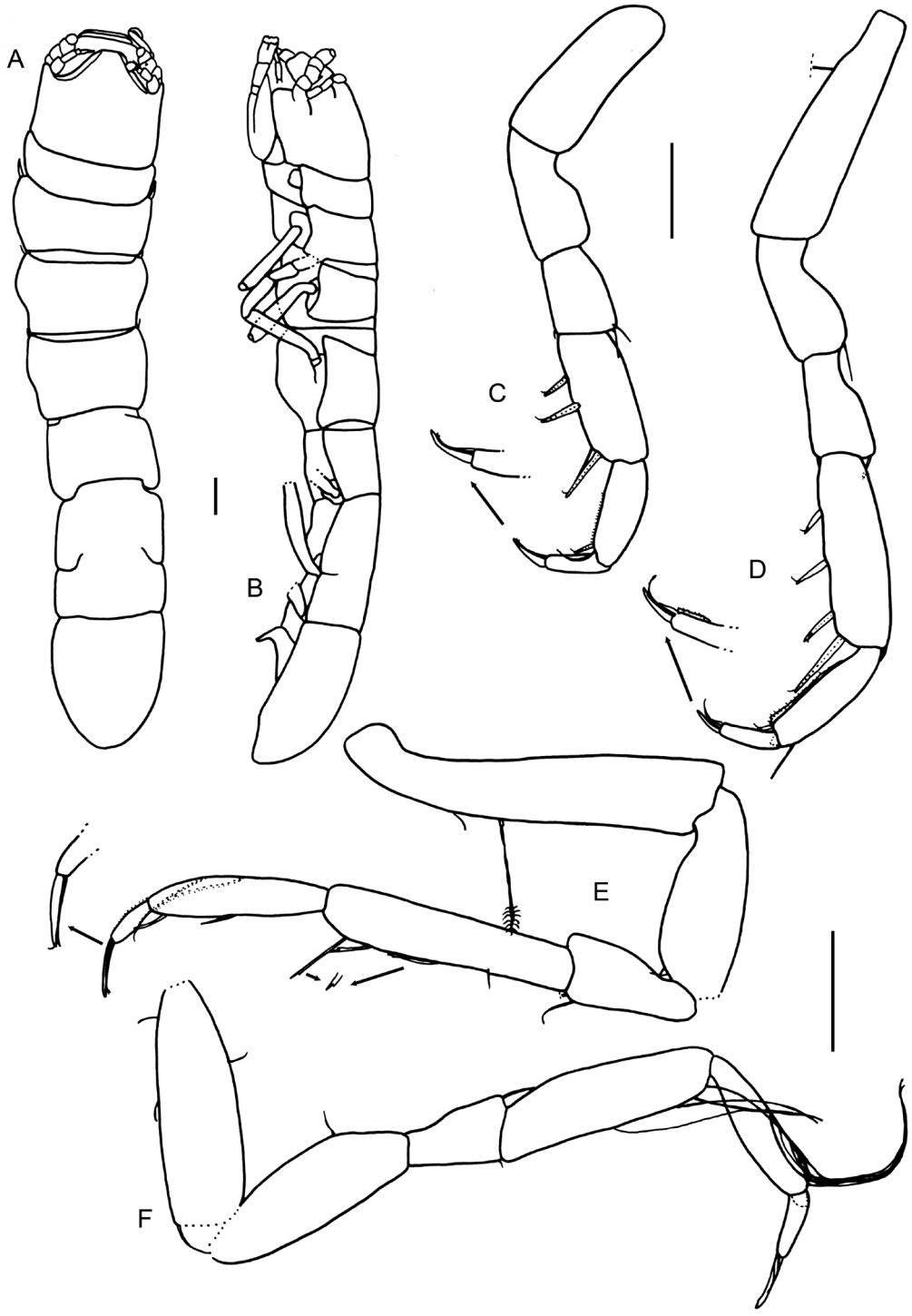

Figure 9. *Nannoniscus hilario*, (A–B) holotype female (ZMH K-55342, Na23); (C–F) paratype female (ZMH K-55341, NB12_Iso020): (A) habitus, dorsal view; (B) habitus, lateral view; (C) PI; (D) PII; (E) PIV; (F) PV. Scale bars: A–B = 200 μm, C–F = 100 μm.

article 2; molar process of both Md with ≥ nine distal spines each; Md incisor teeth rounded; pereonite 2 anterolateral tergites each with robust seta; pereonite 7 without ventral spine; Op with ventral posteriorly bent spine, posterior margin with several (≤ nine) long simple setae; Urp biramous, not projecting beyond Plt posterior margin; Urp exopodite minute, endopodite length ≥ 6.3 exopodite length.

Figure 10. *Nannoniscus hilario*, holotype female (ZMH K-55342, Na23). Confocal laser scanning microscopy images: (A) habitus, dorsal view; (B) habitus, lateral view; (C) habitus, ventral view; (D) mouthparts, ventral view; (E) cephalothorax, lateral view; (F) Plt, ventral view. Scale bars: A–C = 200 µm; D–F = 100 µm.

Description of holotype and paratype female: Habitus (Figs 8A, E, 10), body length 5.5 pereonite 1 width. Coxae not visible in dorsal view. Cephalothorax (Figs 8A, E, 10D–E) almost as long as wide. Anterior and lateral margins straight, posterior margin slightly rounded. Antennae inserting frontolaterally in

deep fold. Pereonites 1–4 of similar height, abruptly flattening from pereonite 4 to 5. Pereonites 1 and 2 of similar width, gradually decreasing in width from 2 to 7; pereonite 1 length 0.3 width. Pereonite 2 length 1.3 pereonite 1 length, length 0.4 width. Pereonite 3 length 1.8 pereonite 1 length; pereonite 4 length 1.7 pereonite 1 length. Pereonites 1–4 anterior margins frontally directed, anterolateral tergites of pereonite 2 each tipped with robust seta, anterolateral tergites of pereonites 3–4 each tipped with simple seta. Pereonite 5 longest, length 1.9 pereonite 1 length, anterior margin straight. Pereonites 6–7 dorsomedially fused; pereonite 6 anterior margin convex. Plt length 0.2 body length, length 1.2 width, width 0.9 pereonite 1 width; posterior margin strongly rounded; anterior margin slightly concave. Urp length 0.3 Plt length, not projecting beyond posterior margin. AI (Fig. 8B) length 0.1 body length, with five articles. First article length 2.3 width, with one small broom seta and one simple seta distally. Second article length 0.7 article 1 length, length 1.4 width, with two broom setae (broken off) and one simple seta distally. Article 3 minute, length 0.1 article 1 length, length 0.3 width. Article 4 length 0.2 article 1 length, with long distal projection reaching mid of article 5, with one small broom seta distally. Article 5 slightly damaged, length 0.7 article 1 length, length 2.5 width, with one aestetasc (?, broken off) terminally. AII (Fig. 8B) broken off, only podomere articles 1–4 present; articles quadrangular of similar length and width. Md (Fig. 8C, D), palp of left mandible well developed (in rMd broken off), consisting of three articles almost reaching incisor. LMd palpal article 2 length 1.5 article 1 length. Terminal article length 0.3 article 2 length, tapering distally, with two setae distally. Incisor process of rMd with four rounded teeth, incisor of lMd with two rounded teeth. Lacinia mobilis of lMd with three teeth. Spine row of rMd with nine robust spines increasing in size proximally. Spine row of lMd with eight robust spines and several slender setae in between, dentation decreasing, seta size increasing proximally. Molar of rMd and lMd triangular; molar of rMd with 10, of lMd with nine serrate spines distally. Mxp (Fig. 8F), left and right Mxp connected by two retinacula. Epipodite smooth, triangular, slender, length 4 width, reaching distal third of palpal article 2. Palpal article 1 short, width 0.3 length, with several small setae laterally. Article 2 length 3 article 1 length, width 1.1 length, with several small setae laterally, with one simple seta distally. Article 3 length 3 article 1 length, width 0.9 length, with two robust sensory setae distally with one simple seta laterally. Article 4 length 1.1 article 1 length, width 0.5 length. Article 5 length 0.6 article 1 length, width 0.5 length, with five slender setae of varying size terminally. Endite distal margin with some robust setae and several fine setae laterally. Basis triangular, length 0.9 width. PI (Fig. 9C) basis length 2.7 width. Ischium 0.6 basis length, length about twice width. Merus length 0.7 ischium length, length 1.5 width, with two long simple setae distodorsally, with one small simple seta distoventrally. Carpus length 1.7 merus length, length 2.5 width, with three unequally bifid setae, increasing in size distally, and one simple seta ventrally. Propodus length 0.7 carpus length, length 2.3 width, with numerous small setae, membranously embedded ventrally, and one robust unequally bifid seta and one simple seta distoventrally. Dactylus length about half propodus length, length 2.9 width. Unguis length 0.9 dactylus length, with two long, slender setae underneath unguis. PII (Fig. 9D) basis length 3.5 width, with one seta (broken off) ventrally. Ischium length about half basis length, length twice width, one long simple seta distodorsally. Merus length 0.9 ischium length, length 1.6 width, with one robust simple seta distodorsally, with one slender simple seta distoventrally. Carpus length 1.9 merus length, length 3.6 width, with one simple seta distodorsally, with row of four unequally bifid setae ventrally, increasing in size distally. Propodus length 0.7 carpus length, length 4 width, with one long simple seta distodorsally, with numerous small setae, membranously embedded ventrally, with one small unequally bifid seta distoventrally. Dactylus length 0.4 propodus length, length 3 width, with numerous small setae, membranously embedded ventrally. Unguis length about half dactylus length, with one slender seta between unguis and ventral claw. PIV (Fig. 9E) slightly damaged between ischium and merus. Basis length 4.8 width, with one short simple seta and one long broom seta dorsally. Ischium length half basis length, length 2.5 width, with two small simple setae dorsally. Merus length 0.6 ischium length, length 1.9 width, with one simple seta distodorsally, with two simple setae (one long, one broken off) distoventrally. Carpus length 2.2 merus length, length 4.7, with one unequally bifid setae (one broken off) ventrally. Propodus length 0.7 carpus length, length 4.8 width, with three long simple setae dorsally, with one slender simple and one stout unequally bifid setae ventrally. Dactylus length 0.3 propodus length, length 2.3 width. Unguis length 1.1 dactylus length, with two slender setae underneath unguis. PV (Fig. 9F) slightly damaged between basis and ischium. Basis length 3.3 width, with one simple seta dorsally, with two simple setae ventrally, with one long simple seta distoventrally. Ischium length 0.9 basis length, length 3 width, with one simple seta dorsally. Merus length 0.4 ischium length, length 1.6 width, with one long simple seta distodorsally, with one long simple seta ventrally, with one seta (broken off) distoventrally. Carpus length 2.3 merus length, length 3.5 width, with four long slender setae ventrally. Propodus length 0.7 carpus length, length 4

width, with five long simple setae dorsally. Dactylus length 0.4 propodus length, length 3.2 width. Unguis length 0.8 dactylus length, with two slender setae underneath unguis. Op (Fig. 8G) length 1.3 width, with strong ventral spine, posteriorly bent. Lateral margin and posterior margins rounded, with several (≤ nine) simple setae, setal length 0.2 Plt length. PlpIII (Fig. 8H), protopodite almost as long as wide, length about half endopodite length. Exopodite half endopodite length, length 2.3 width, tapering in width distally, with numerous short simple setae laterally and one somewhat longer seta distally. Endopodite length 1.6 width, with three long plumose setae distally, distal margin rounded. Urp (Fig. 8J) biramous, length 0.25 Plt length, not projecting beyond Plt posterior margin. Protopodite trapezoid, length 1.3 width, with one long simple seta laterally. Exopodite length 0.3 protopodite length, length twice width, with two simple setae terminally. Endopodite length 6.3 exopodite length, length 3.8 width, with two long simple setae and two long broom setae terminally.

Remarks: *Nannoniscus hilario* is most similar to species with a slender body (length ≥ 4.5 pereonite 1 width), biramous uropods and a ventral opercular spine, *viz*.: *N. menziesi*, *N. meteori* and *N. perunis*.

The new species can be distinguished from *N. menziesi* by the following characters: Mxp lateral margin with numerous small simple setae (vs. setae lacking in *N. menziesi*); Op posterior margin with ≤ nine simple setae (vs. 18 setae); incisor teeth of left and right Md more rounded (vs. acute). *Nannoniscus hilario* also resembles *N. meteori*, but can be differentiated as follows: Mxp lateral margin with numerous small simple setae (vs. setae lacking in *N. meteori*); Mxp endopodite reaching distal third of palpal article 2 (vs. mid of palpal article 3); Op posterior margin with ≤ nine simple setae (vs. 15 setae); Urp endopodite length 6.3 exopodite length (vs. 3.9). The new species can be furthermore differentiated from *N. perunis* by the following features: body length ≥ 5.5 pereonite 1 width (vs. ≤ 4.7 in *N. perunis*); Urp endopodite length 6.3 exopodite length (vs. 7.8); pereonites 3–4 tergites each with an anterolateral seta (vs. setae lacking).

NANNONISCUS MAGDAE KAISER, BRIX & JENNINGS, SP. NOV.

(FIGS 11–14)

Zoobank registration: urn:lsid:zoobank.org:act:B36BAA31-FE02-4E33-BB83-CA8444FB91E5.

Type fixation: Holotype, preparatory female, ZMH K-55375, 2.2 mm, designated here.

Material examined: Holotype: preparatory female (Na26), 2.2 mm, CCZ, equatorial NE Pacific, JPIO SO239 expedition, RV Sonne, EBS, station 171 (start: 14°2’41”N, 130°5’57”W, 5024 m; end: 14°3’12”N, 130°4’36”W, 5017 m), date: 17/04/2015, ZMH K-55375.

Paratypes: Preparatory female (Na12), CCZ, equatorial NE Pacific, JPIO SO239 expedition, RV Sonne, EBS, same station as holotype, ZMH K-55374; preparatory female (NB12Iso99), CCZ, equatorial NE Pacific, BIONOD expedition, RV L’Atalante, EBS, station 67 (start: 14°3’4”N, 130°4’36”W, 5021 m; end: 14°3’10”N, 130°4’27”W, 5021 m), date: 19/04/2012, ZMH K-55373; ovigerous female (Na28), CCZ, equatorial NE Pacific, JPIO SO239 expedition, RV Sonne, EBS, same station as holotype, ZMH K-55376; juvenile male (Na49), CCZ, equatorial NE Pacific, JPIO SO239 expedition, RV Sonne, EBS, same station as holotype, ZMH K-55377.

Etymology: The new species (*magdae*, Latin genitive, feminine) is named in honour of Magdalena Błażewicz for her invaluable help onboard the SO239 Ecoresponse voyage, and her contributions to the taxonomy and biodiversity of deep-sea peracarids.

Distribution: Based on the material available (four specimens), this species has a restricted distribution and is only known from the French licence area of the CCZ, between 5017 and 5024 m depth.

Diagnosis: Body slender, length about 4.8 × pereonite 1 width; Mxp lateral margin with numerous small setae; Mxp epipodite reaching mid of palpal article 3; molar process of both Md with ≥ nine distal spines each; Md incisor teeth rounded; pereonite 2 anterolateral tergites devoid of setae; pereonite 7 without ventral spine; Op with ventral posteriorly bent spine, posterior margin with numerous (≥ 17) long simple setae; Urp biramous, not projecting beyond Plt posterior margin; Urp endopodite length about 2.1 exopodite length.

Description of holotype and paratype female: Habitus (Figs 11B, D, 14A–C), body length 4.8 pereonite 1 width. Coxae not visible in dorsal view. Cephalothorax (Figs 11B, 14D–E) as long as wide (measured from lateral view). Anterior margin straight, posterior and lateral margins slightly rounded. Antennae inserting frontolaterally in deep fold. Pereonites 1–4 gradually flattening, then abruptly flattening from pereonite 4 to 5. Pereonites 1–3 of similar width, gradually decreasing in width from 3 to 7; pereonite 1 length 0.4 width. Pereonite 2 width 0.5 pereonite 1 width, length 1.2 pereonite 1 length. Pereonites 2 and 3 of similar length; pereonite 4 length 1.1 pereonite 1 length. Pereonites 1–4 anterior margins frontally directed, without

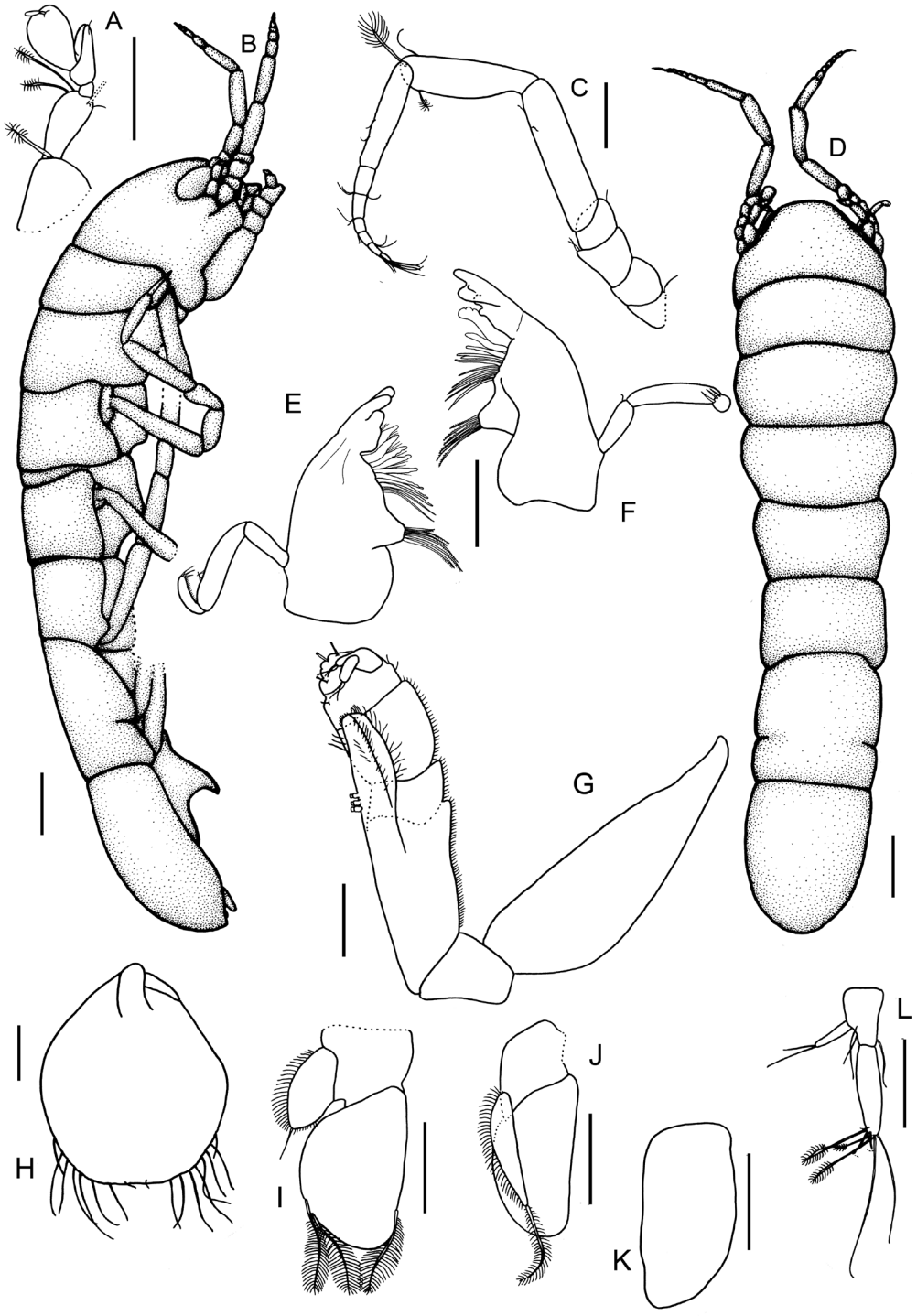

Figure 11. *Nannoniscus magdae*, (A, C, E–G) paratype female (ZMH K-55373, NB12_Iso099); (B, D) holotype female (ZMH K-55375, Na26); (H–L) paratype female (ZMH K-55374, Na12): (A) AI; (B) habitus, dorsal view; (C) AII; (D) habitus, lateral view; (E) rMd; (F) lMd; (G) Mxp; (H) Op; (I) PlpIII; (J) PlpIV; (K) PlpV; (L) Urp. Scale bars: A, C, E–L = 100 µm; B, D = 200 µm.

setation. Pereonite 5 length 1.1 pereonite 1 length, anterior margin straight. Pereonites 6–7 dorsomedially fused, pereonite anterior margin slightly convex. Plt length 0.2 body length, length 1.5 width; width 0.7 pereonite 1 width, posterior margin strongly rounded; anterior margin straight. Urp length 0.3 Plt length,

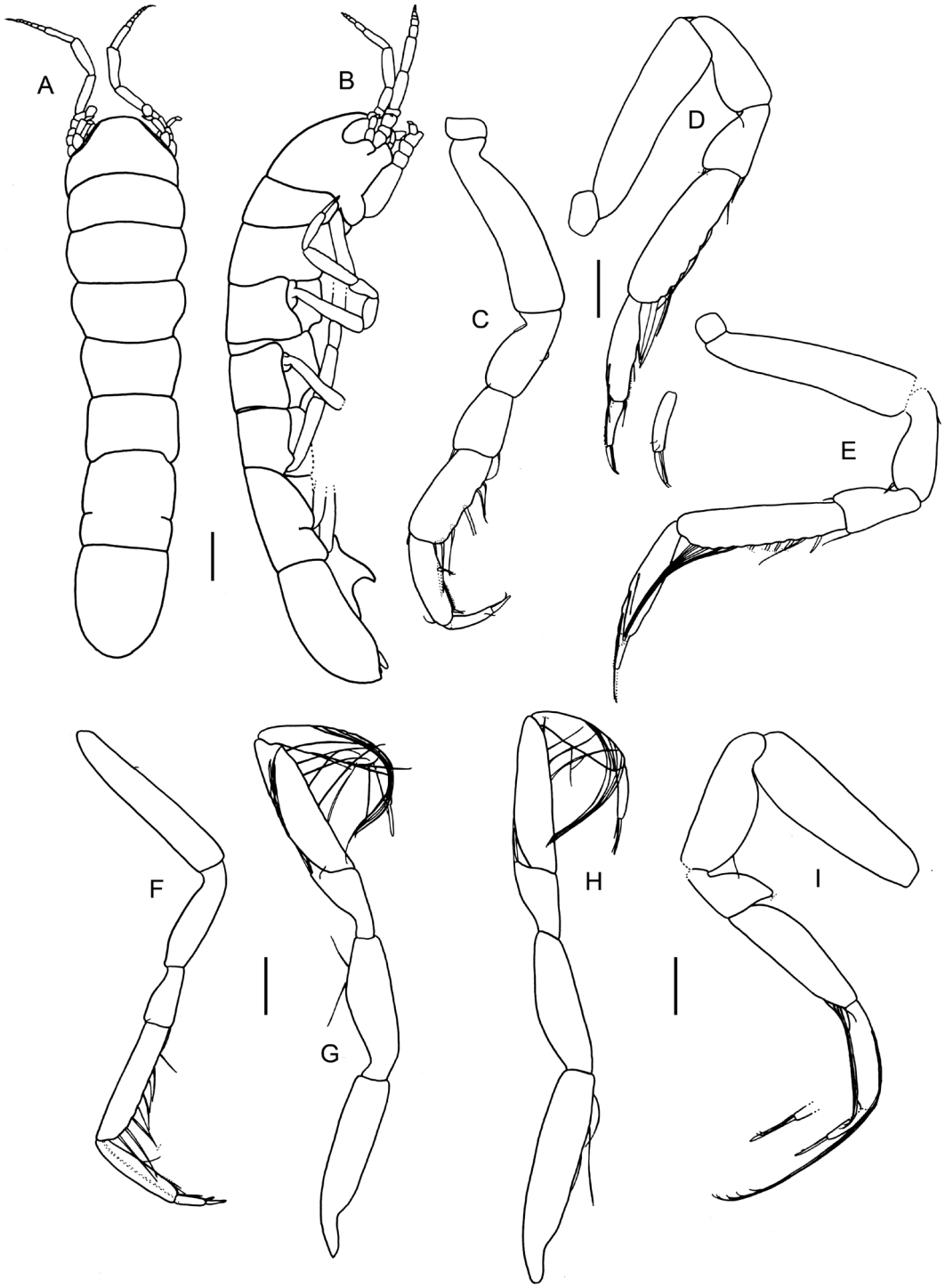

Figure 12. *Nannoniscus magdae*, (A–B) holotype female (ZMH K-55375, Na26); (C–E, I) paratype female (ZMH K-55373, NB12_Iso099); (F–H) paratype female (ZMH K-55374, Na12): (A) habitus, dorsal view; (B) habitus, lateral view; (C–I) PI-PVII. Scale bars: A–B = 200 µm; C–I = 100 µm.

not projecting beyond posterior margin. AI (Fig. 11A) length 0.1 body length, with five articles. First article circular and broadest, with one small broom seta distally. Second article length twice width, with three broom setae (one broken off) and one small simple seta distally. Article 3 minute, length 0.2 article 2 length, as

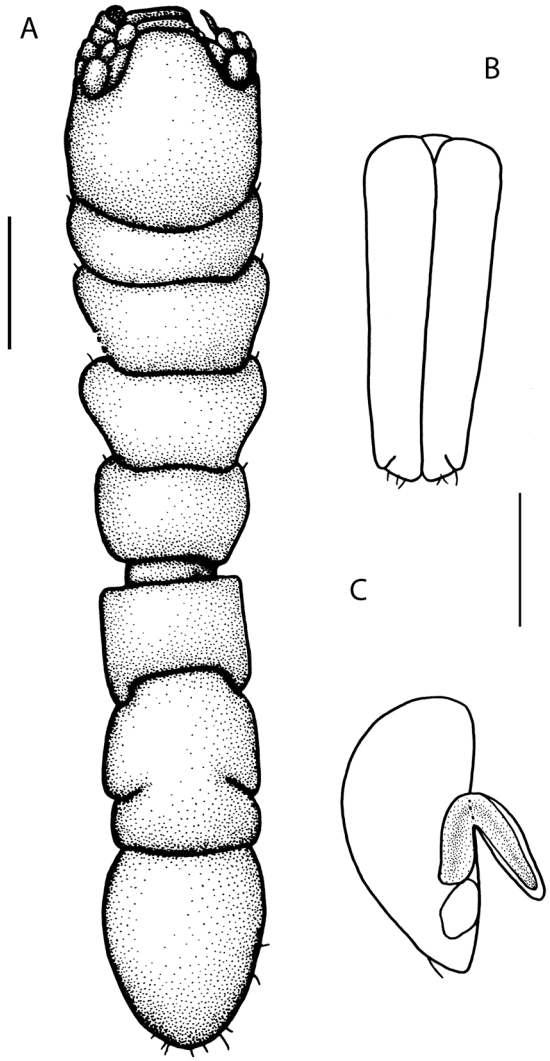

Figure 13. *Nannoniscus magdae*, paratype male (ZMH K-55377, Na49): (A) habitus, dorsal view; (B) PlpI; (C) PlpII. Scale bars: A = 200 µm; B–C = 100 µm.

long as wide. Article 4 length 0.3 article 2 length, with long distal projection reaching mid of article 5, with two simple setae of varying size distally. Article 5 length 0.9 article 2 length, length 1.6 width, with one aestetasc terminally. AII (Fig. 11C) length 0.4 body length, with six podomere and seven flagellar articles. Podomere articles 1–4 short; article 1 with one simple seta distally; article 3 with two simple setae distally, article 4 with one simple seta distally. Article 5 longest, length 1.3 articles 1–4 length, length approximately 4.1 width, with two simple setae laterally. Article 6 length 0.8 article 5 length, length 3.3 width, with two broom setae of varying size and one long simple seta distally. Flagellar article 1 longest, conjoint with two setal positions (fusion of three articles), length 0.9 podomere article 6 length, length 4.6 width, with two simple setae laterally. Flagellar articles 2–7 decreasing in length and width distally; each article with 1–3 short simple setae distally. Article 7 with 5 long slender setae terminally. Md (Fig. 11E, F), palp of left and right mandible well developed, consisting of three articles reaching mid of incisor. Palpal article 2 of rMd length 1.7 article 1 length, with two simple setae laterally. Terminal article length 0.4 article 2 length, tapering distally, with several (≥ nine) small setae ventrally and three somewhat longer setae terminally. Incisor process of rMd with three rounded teeth, incisor of lMd with rounded three teeth. Lacinia mobilis of lMd with three teeth. Spine row of rMd with 10 robust spines and several slender setae in between; dentation decreasing and setal size increasing proximally. Spine row of lMd with ten robust spines and several slender setae in between, dentation decreasing, seta length increasing proximally. Molar of rMd and lMd triangular; molar of rMd and lMd each with nine long, serrate spines distally. Mxp (Fig. 11G), left and right Mxp connected by three retinacula. Epipodite smooth, triangular, slender, length 3.1 width, reaching mid of palpal article 3. Palpal article 1 short, width 1.6 length, with several small setae lateral. Article 2 length 1.9 article 1 length, as long as wide, with several small setae laterally. Article 3 length 1.6 article 1 length, width 0.9 length, with four robust sensory setae distally and two simple setae laterally. Article 4 as long as article 1, width 0.5 length, with distal projection reaching mid of article 5, with three slender setae distally. Article 5 length 0.6 article 1 length, width 0.4 length, with three slender setae terminally. Endite distal margin with some robust, dentate setae and several fine setae laterally. Basis triangular, length 0.7 width. PI (Fig. 12C) basis length 2.7 width. Ischium length about half basis length, length 2.2 width, with two simple setae distodorsally, with one simple seta ventrally. Merus length 0.7 ischium length, length 1.4 width, with two simple seta distodorsally, with one long simple setae distoventrally. Carpus length 1.6 merus length, length 2.4 width, with one simple seta distodorsally, with row of six simple setae ventrally. Propodus length 0.9 carpus length, length 3.8 width, with one simple seta dorsally, with numerous small setae, membranously embedded, and two small unequally bifid setae in between ventrally. Dactylus length about half propodus length, length 4.5 width, with one small simple setae medially. Unguis length half dactylus length, with two long, slender setae underneath unguis. PII (Fig. 12D) basis length 3.7 width, with one simple seta distoventrally. Ischium length about half basis length, length twice width, with five simple setae dorsally, with one simple seta distodorsally. Merus length 0.8 ischium length, length 1.5 width, with one simple seta (broken off)

Figure 14. *Nannoniscus magdae*, holotype female (ZMH K-55375, Na26). Confocal laser scanning microscopy images: (A) habitus, dorsal view; (B) habitus, ventral view; (C) habitus, lateral view; (D) mouthparts, ventral view; (E) cephalothorax, lateral view; (F) Plt, ventral view. Scale bars: A–C = 200 µm; D–F = 100 µm.

distodorsally, with one simple seta distoventrally. Carpus length 2.3 merus length, length 3.9 width, with six long slender simple setae and two long robust setae ventrally. Propodus length 0.6 carpus length, length 3.7 width, with two simple setae dorsally, with numerous small setae, membranously embedded, and

three simple setae in between ventrally. Dactylus length 2.4 propodus length, length 3 width, with two simple setae medially, with numerous small setae ventrally. Unguis length 0.7 dactylus length, with two slender setae underneath unguis. PIII (Fig. 12E) damaged between basis and ischium. Basis length 4.4 width. Ischium length about half basis length, length 2.3 width, with one simple seta distodorsally, with one simple seta ventrally. Merus length 0.8 ischium length, length 1.8 width, with one small seta distodorsally, with one somewhat longer seta distoventrally. Carpus length 2.3 merus length, length 4.5 width, with 11 long slender setae (four broken off) ventrally. Propodus length 0.7 carpus length, length 4.3 width, with three long simple setae dorsally. Dactylus length 0.3 propodus length, length 2.3 width. Unguis damaged, as long as dactylus. PIV (Fig. 12F) basis length 5.9 width, with one simple seta ventrally. Ischium length 0.6 basis length, length 3.8 width. Merus length 0.6 ischium length, length 2.2 width, with one small simple seta distodorsally, with one long simple seta distoventrally. Carpus length 2.2 merus length, length 4.7 width, with nine long slender simple setae ventrally. Propodus length 0.7 carpus length, length 5 width, with numerous small setae and four simple seta ventrally. Dactylus length 0.4 propodus length, length 3.5 width. Unguis length 0.6 dactylus length, ventral claw length 0.3 ungius length. PV (Fig. 12G) basis length 4.9 width. Ischium length 0.8 basis length, length 3.1 width, with two long simple setae dorsally. Merus length about half length, length 1.8 width, with three simple setae (two long, one somewhat shorter) distodorsally. Carpus length twice merus length, length 3.6 width, with four long slender simple setae dorsally, with six long slender simple setae ventrally. Propodus length 0.6 carpus length, length 3.2 width, with four long simple setae dorsally, with five long simple setae ventrally. Dactylus length half propodus length, length 3 width. Unguis length 0.8 dactylus length, ventral claw length 0.6 ungius length. PVI (Fig. 12H) basis length 5.1 width, with three long simple setae ventrally. Ischium length 0.7 basis length, length 3.4 width. Merus length half ischium length, length 1.6 width, with two long simple setae distodorsally. Carpus length 2.4 merus length, length 4.1 width, with four long slender simple setae (one broken off) ventrally. Propodus length 0.6 carpus length, length 3.5 width, with seven long simple setae dorsally, with two simple setae of varying size ventrally. Dactylus length half propodus length, length 2.2 width. Unguis length 0.6 dactylus length, with two slender setae of varying size underneath unguis. PVII (Fig. 12I) slightly damaged between ischium and merus. Basis length 3.2 width. Ischium length 0.8 basis length, length 2.9 width, with one simple seta distodorsally. Merus length 0.4 ischium length, length 1.3 width, with one seta (broken off) distodorsally. Carpus length 2.4 merus length, length 3.1 width, with five slender simple setae (four long, one somewhat shorter) ventrally. Propodus length 0.7 carpus length, length 3.8 width, with seven long simple setae dorsally. Dactylus length 0.4 propodus length, length 4.5 width, with three simple setae medially. Unguis length 0.9 dactylus length, with two slender setae underneath unguis. Op (Fig. 11H) length 1.2 width, with strong ventral spine, posteriorly bent. Lateral margin rounded, posterior margin almost straight, with several (≥ 17) simple setae, setal size 0.3 Plt length. PlpIII (Fig. 11I), protopodite length 0.7 proximal width, length 0.4 endopodite length. Exopodite 0.5 endopodite length, length 1.6 width, width tapering distally, with numerous short simple setae laterally and one somewhat longer distally. Endopodite 1.2 length 1.5 width, with three long plumose setae distally, distal margin strongly rounded. PlpIV (Fig. 11J), protopodite rectangular, as long as wide, length 0.4 endopodite length. Exopodite slender, length 0.7 endopodite length, length 5 width, with several thin setules laterally (outer margin) and one long robust plumose seta distally. Endopodite ovoid-shaped, length twice width. PlpV (Fig. 11K), small oval lobe, without setation. Length twice proximal width, width gradually tapering towards distal end. Urp (Fig. 11L) biramous, length 0.2 Plt length, not projecting beyond Plt posterior margin. Protopodite length 1.5 proximal width, with three long simple setae distally. Exopodite length 0.5 protopodite length, length 4.5 width, with two long simple setae terminally. Endopodite length 2.1 exopodite length, length 3.8 width, with two simple setae (broken off), two long simple setae and two long broom setae terminally.

Description of male paratype: Habitus (Fig. 13). Body length 5.3 pereonite 1 width. Coxae not visible in dorsal view. Cephalothorax (Fig. 13A) length equals width. Anterior, lateral and posterior margins rounded. Antennae inserting frontolaterally in deep fold. Pereonites 3–6 decreasing in width. Pereonite 1 length 0.3 width. Pereonites 1–2 of similar width; pereonite 2 length 1.6 pereonite 1 length. Pereonites 2–3 of similar length. Pereonite 3 width 0.9 pereonite 1 width. Pereonites 2–5 of similar length. Pereonites 1–4 anterior margins frontally directed, anterolateral tergites of perenonite 1–4 each tipped with simple seta. Pereonites 4–7 of similar width, width 0.8 pereonite 1 width. Pereonite 5 anterior margin straight. Pereonites 6–7 dorsomedially fused, pereonite 6 anterior margin straight. Plt 0.2 body length, length 1.2 width, width 0.8 pereonite 1 width; posterior margin strongly rounded, anterior margin slightly concave. Urp not projecting beyond posterior margin. PlpI (Fig. 13B), length 2.5 proximal width. Distal projection width 0.5 proximal

width, lateral margins straight. Lateral lobes rounded. Distal margins almost straight, with three simple setae. PlpII (Fig. 13C), sympod length 2.2 width, outer margin rounded, with one simple seta distally; inner margin straight. Endopod inserting 0.3 from distal tip of sympod. Stylet length 0.7 sympod length, slightly curved, distal end not extending beyond distal tip of sympod. Exopod short and rounded, inserting 0.1 from distal tip of sympod.

Remarks: The new species most closely resembles *N. hilario*, *N. menziesi* and *N. perunis*, but differs from these species by lacking robust setae on the anterolateral tergites of pereonite 2 and a markedly longer uropodal exopodite (Urp endopodite/exopodite length ratio 2.1 vs. ≥ 5.6 in the remaining species). *Nannoniscus magdae* can be furthermore distinguished from *N. hilario* as follows: Mxp endopodite reaching mid of palpal article 3 (vs. distal third of palpal article 2 in *N. hilario*); Op posterior margin with ≥ 17 simple setae (vs. ≤ 9). Additional characters to distinguish the new species from *N. menziesi* are: Mxp lateral margin with numerous small setae (vs. Mxp lateral margin lacking setae in *N. menziesi*); Md incisor teeth rounded (vs. acute). *Nannoniscus magdae* is also similar to *N. meteori*, but can be differentiated as follows: Mxp lateral margin with numerous small setae (vs. Mxp lateral margin lacking setae in *N. meteori*). The description of the male characteristics of *N. magdae* is based on a juvenile specimen, which can differ considerably from the terminal males (Riehl *et al.*, 2012). However, since the specimen is the only male found for the new species, we found it to be a valuable addition to the female description.

NANNONISCUS MENOTI KAISER, JANSSEN & MOHRBECK, **SP. NOV.**

(FIGS 15–19)

Zoobank registration: urn:lsid:zoobank.org:act:8BFC86F5-43FE-41AF-B49B-2793B2E7C3B8.

Type fixation: Holotype, ovigerous female, ZMH K-55354, 3.6 mm, designated here.

Material examined: Holotype: ovigerous female (Na27), 3.6 mm, CCZ, equatorial NE Pacific, JPIO SO239 expedition, RV Sonne, EBS, station 171 (start: 14°2’41”N, 130°5’57”W, 5024 m; end: 14°3’12”N, 130°4’36”W, 5017 m), date: 17/04/2015, ZMH K-55354.

Paratype: Preparatory female (Na18), CCZ, equatorial NE Pacific, JPIO SO239 expedition, RV Sonne, EBS, station 20 (start: 11°50’9”N, 117°58’29”W, 4093 m; end: 11°50’11”N, 116°58’0”W, 4093 m), date: 21/03/2015, ZMH K-55356; preparatory female (Na06), CCZ, equatorial NE Pacific, JPIO SO239 expedition, RV Sonne, EBS, station 117 (start: 13°52’19”N, 123°15’27”W, 4498 m; end: 13°52’37”N, 123°14’16”W, 4521 m), date: 07/04/2015, ZMH K-55352; adult male (MA14_Iso272), CCZ, equatorial NE Pacific, KM14 expedition, RV Kilo Moana, EBS, station 38 (start: 11°47 52”N, 117°30’31”W, 4363 m; end: 11°48’3”N, 117°29’45”W, 4373 m), date: 13/05/2014, ZMH K-55350; preparatory female (Na42/Iso1120), APEI-6, equatorial NE Pacific, ABYSSLINE-2 expedition, RV Thomas G. Thompson, EBS, station APEI-6#1 (start: 19°27’52”N, 120°1’31”W, 4099 m; end: 120°0’58”N, 120°0’58”W, 4076 m), date: 20/03/2015, ZMH K-55355; preparatory female (NB12_Iso068), CCZ, equatorial NE Pacific, BIONOD expedition, RV L’Atalante, EBS, station 33 (start: 11°51’44”N, 117°3’10”W, 4133 m; end: 11°51’54”N, 117°3’8”W, 4133 m), date: 07/04/2012, ZMH K-55353; preparatory female (MA14_Iso352), CCZ, equatorial NE Pacific, MA14 expedition, RV Kilo Moana, EBS, station 39 (start: 11°49’37”N, 117°30’49”W, 4361 m; end: 11°49’47”N, 117°30’5”W, 4343 m), date: 13/05/2014, ZMH K-55351; preparatory female (Na40/Iso1005), CCZ, equatorial NE Pacific, ABYSSLINE-2 expedition, RV Thomas G. Thompson, EBS, station S11 (start: 12°2’43.08”N, 117°25’26”W, 4223 m; end: 12°3’1.44”N, 117°24’17”W, 4235 m), date: 16/03/2015, ZMH K-55349; ovigerous female (MA13_Iso453), CCZ, equatorial NE Pacific, MA13 expedition, RV Kilo Moana, EBS, station 90 (start: 11°49.718’N, 117°30.278’W, 4340 m; end: 11°49.906’N, 117°29.395’W, 4357 m), date: 03/05/2013, ZMH K-55348.

Etymology: The new species (*menoti*, Latin genitive, masculine) is named after Lenaick Menot, leader of the French party of the BIONOD expedition, for joint actions sieving and sorting the mud.

Distribution: This species has a wide distribution across the CCZ, being obtained from the eastern German, OMS, GSR and French (type locality) licence areas, as well as APEI-6 between 4076 and 5024 m depth.

Diagnosis: Body slender, length about 5.1 × pereonite 1 width; Mxp lateral margin with numerous small setae; Mxp epipodite reaching mid of palpal article 3; molar process of left Md with ≥ ten distal spines; Md incisor teeth rounded; pereonite 2 anterolateral tergites each with robust seta; pereonite 2 anterolateral tergites each with robust seta; pereonite 7 without ventral spine; Op with a ventral posteriorly bent spine, posterior margin with numerous (≥ 15) short simple setae; Urp uniramous, not projecting beyond Plt posterior margin; male PlpI without hook-like projections distally.

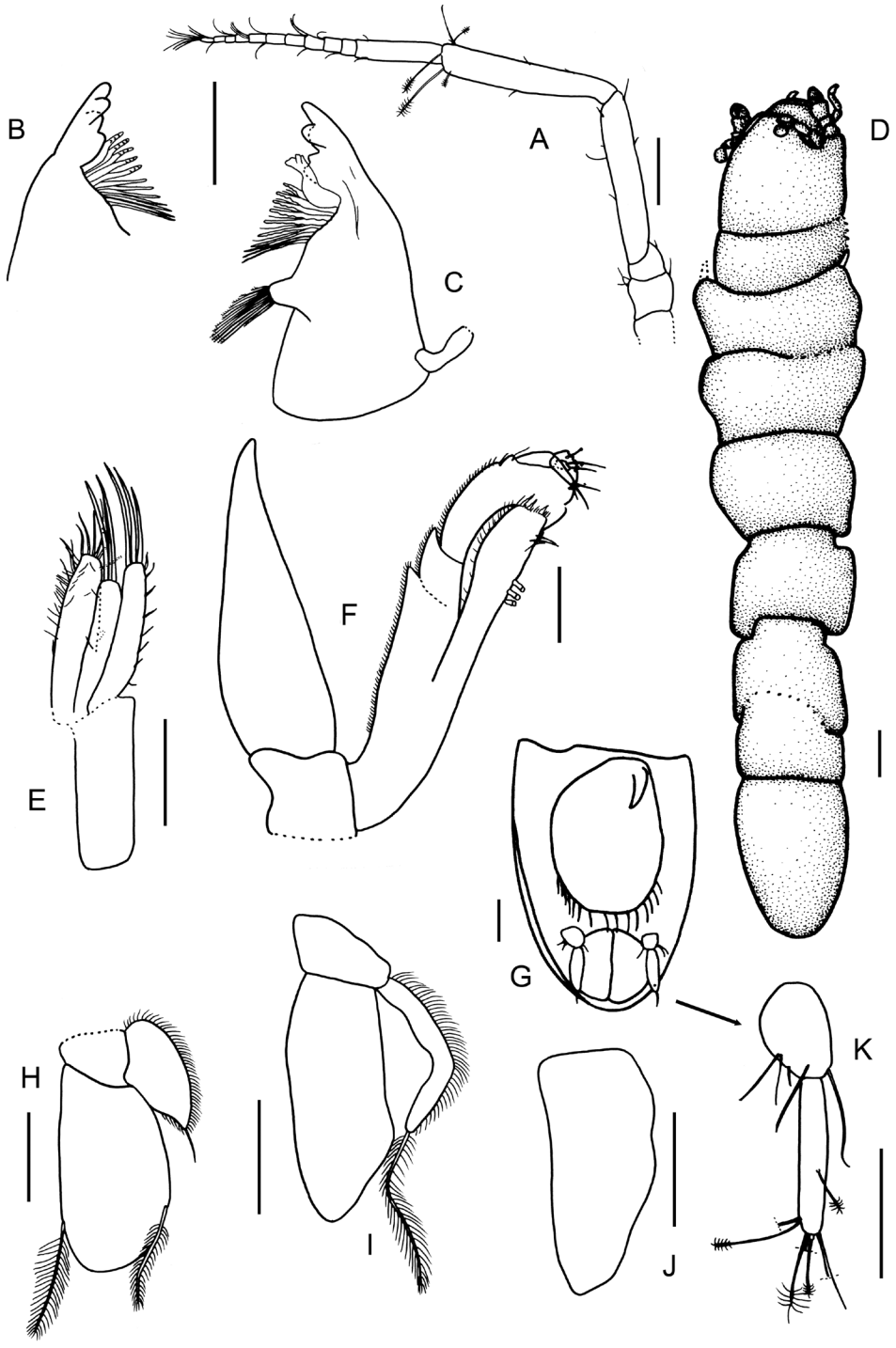

Figure 15. *Nannoniscus menoti*, (A–C, E–F, H–K) paratype female (ZMH K-55356, Na18); (D, G) holotype female (ZMH K-55354, Na27): (A) AII; (B) rMd; (C) lMd; (D) habitus, dorsal view; (E) MxII; (F) Mxp; (G) Plt and Op, ventral view; (H) PlpIII; (I) PlpIV; (J) PlpV; (K) Urp. Scale bars: A–C, E–F, H–K = 100 µm; D, G = 200 µm.

Description of holotype and paratype female: Habitus (Figs 15D, 18), pereonites 2 and 3 damaged. Body length 5.1 pereonite 1 width. Coxae not visible in dorsal view. Cephalothorax (Figs 15D, 18D, E), length 0.9 width. Anterior and lateral margins straight, posterior margin slightly rounded. Antennae inserting

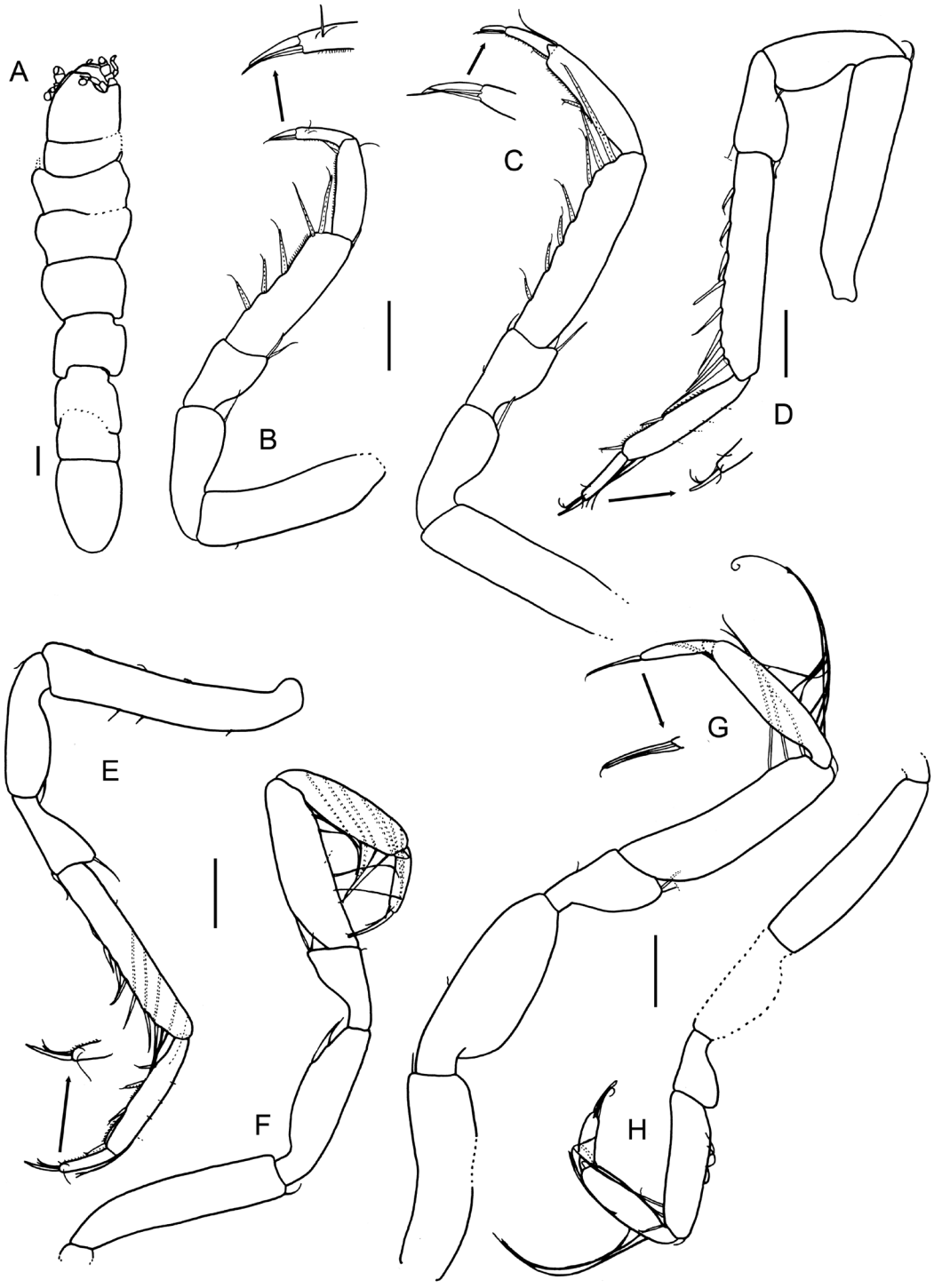

Figure 16. *Nannoniscus menoti*, (A) holotype female (ZMH K-55354, Na27), (B–E, G) paratype female (ZMH K-55356, Na18), (F, H) paratype female (ZMH K-55352, Na6): (A) habitus, dorsal view; (B–H) PI-VII. Scale bars: A = 200 µm; B–H = 100 µm.

frontolaterally in a deep fold. Pereonite 2 widest, pereonites 2–7 decreasing in width. Pereonite 1 width 0.8 pereonite 2 width, length 0.4 width. Pereonites 2 and 3 of similar length and width, length approximately 1.3 pereonite 1 length. Pereonite 4 longest, length 1.7 pereonite 1 length. Pereonites 1–4 anterior margins frontally directed, anterolateral tergites of pereonite 2 each tipped with a robust seta, pereonites 3–4 each

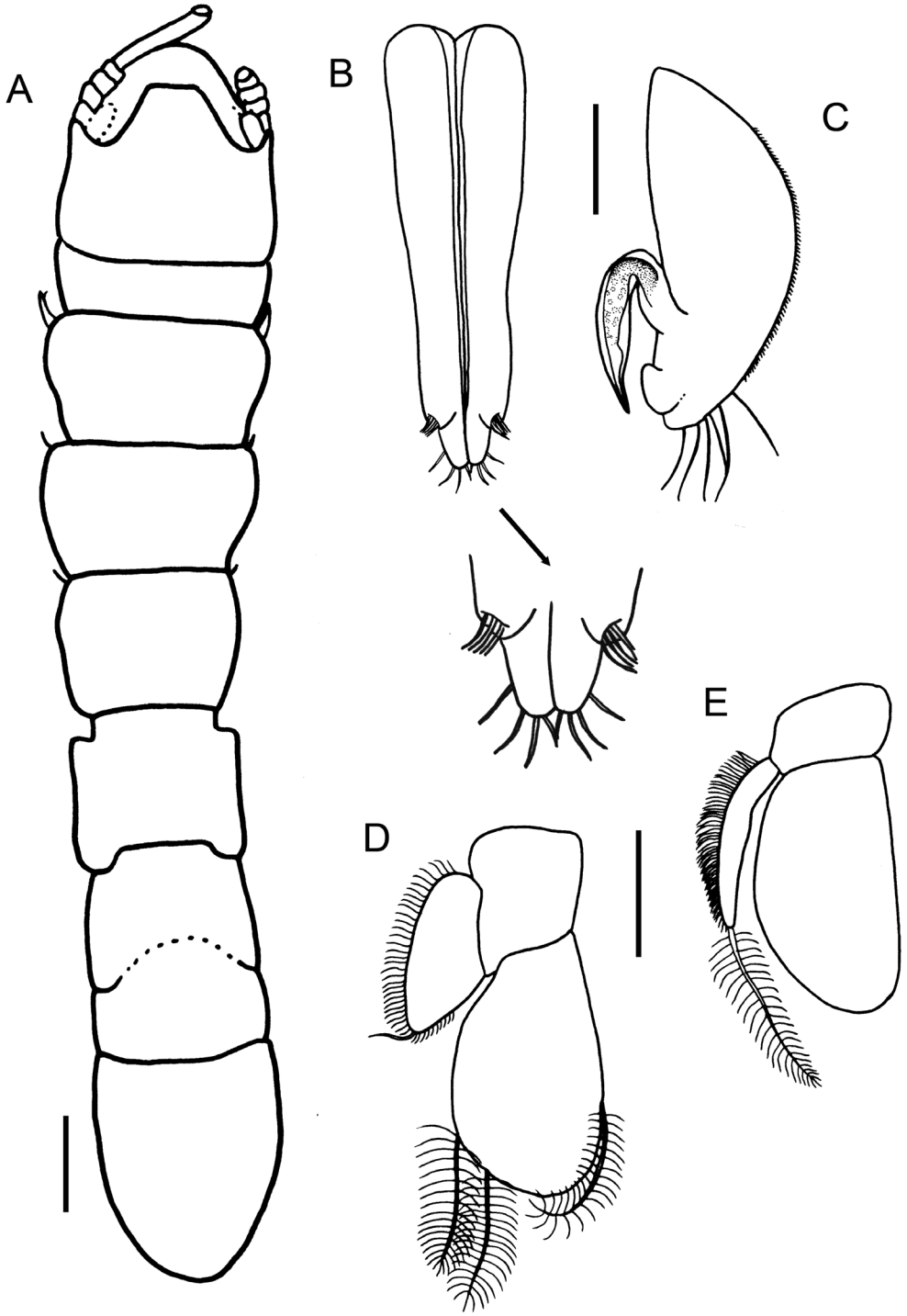

Figure 17. *Nannoniscus menoti*, paratype male (ZMH K-55350, MA14_Iso272): (A) habitus, dorsal view; (B–E) PlpI–IV. Scale bars: A = 250 μm; B–E = 100 μm.

with a slender seta. Pereonite 5 width 0.9 pereonite 1 width, length 1.6 pereonite 1 length; pereonite 5 anterior margin slightly convex. Pereonites 6–7 dorsomedially fused, pereonite 6 anterior margin convex. Plt length 0.2 body length, length 1.4 width; width 0.9 pereonite 1 width, posterior margin strongly rounded; anterior margin straight. Urp length 0.2 Plt length, not projecting beyond posterior margin. AI

Figure 18. *Nannoniscus menoti*, holotype female (ZMH K-55354, Na27). Confocal laser scanning microscopy images: (A) habitus, dorsal view; (B) habitus, ventral view; (C) habitus, lateral view; (D) mouthparts, ventral view; (E) cephalothorax, lateral view; (F) Plt, ventral view. Scale bars: A–C = 200 µm; D–F = 100 µm.

described *in situ* from CLSM (Fig. 18A, E), from CLSM. Length 0.1 body length, with five articles. First article broadest, length twice width, with one broom seta distally. Second article as long as article 1, length 2.4 width, with two broom setae distally. Article 3 minute, length 0.2 article 1 length, as long as wide. Article 4

Figure 19. *Nannoniscus menoti*, paratype male (ZMH K-55350, MA14_Iso272). Confocal laser scanning microscopy images: (A) habitus, dorsal view; (B) habitus, ventral view; (C) habitus, lateral view; (D) mouthparts, ventral view; (E) cephalothorax, lateral view; (F) Plt, ventral view. Scale bars: A–C = 250 µm; D–F = 100 µm.

length 0.3 article 1 length, with a long distal projection reaching mid of article 5. Article 5 length 0.7 article 2 length, length 1.8 width. AII (Fig. 15A) length 0.4 body length, with six podomere and 11 flagellar articles. Podomere article 1 broken off, described from CLSM (Fig. 18A). Articles 1–4 short; article 3 with three

simple setae and one small robust spine distally, article 4 with one simple seta distally. Article 5 length 1.5 articles 1–4 length, length approximately 5.8 width, with six simple setae laterally. Article 6 longest, length 1.1 article 5 length, length 6 width, with three simple setae laterally, with four broom setae of varying size and two long simple setae distally. Flagellar article 1 longest, conjoint with one setal position (fusion of 2 articles), length half podomere article 6 length, length 4.5 width, with two simple setae laterally. Flagellar articles 3–11 decreasing in length and width distally; each article with 1–3 simple setae distally. Article 11 with six long slender setae terminally. Md (Fig. 15B, C), palp of left and right Md broken off. Incisor process of rMd and lMd with four rounded teeth each. Lacinia mobilis of lMd with three teeth. Spine row of rMd with 12 robust spines, dentation decreasing proximally. Spine row of lMd with ten robust spines and several slender setae in between, dentation decreasing, seta size increasing proximally. Molar of lMd triangular, with ten serrate spines of varying size distally. MxII (Fig. 15E), outer margin of mesial endite with several setae of varying length, distal margin with numerous long setae of varying length. Mesial endite as long as lateral endite. Lateral endite and middle endite each with three strong setae distally. Mxp (Fig. 15F), left and right Mxp connected by three retinacula. Epipodite smooth, triangular, slender, length 3.1 width, reaching mid of palpal article 3. Palpal article 1 short, with several small setae laterally. Article 2 length 2.4 article 1 length, width 0.9 length, with several small setae laterally. Article 3 length 1.1 article 1 length, width 1.6 length, with four robust sensory setae (one broken off) and one somewhat longer simple seta distally. Article 4 length 1.4 article 1 length, width 0.3 length, with a distal projection reaching mid of article 5, with two slender setae distally. Article 5 length 0.8 article 1 length, width 0.3 length, with three slender setae of varying size terminally. Endite distal margin with some robust, dentate setae and several fine setae laterally. Basis quadrangular, length 0.9 width. PI (Fig. 16B) basis length 3.4 width, one small simple seta ventrally. Ischium 0.6 basis length, length 2.6 width, with one long simple seta distodorsally. Merus length 0.6 ischium length, length 1.4 width, with two long simple setae distodorsally. Carpus length 2.2 merus length, length 3.7 width, with one simple seta distodorsally, with five unequally bifid setae and numerous small setae ventrally. Propodus length 0.6 carpus length, length 3 width, with one simple seta dorsally, with numerous small setae, membranously embedded, ventrally, with one simple seta distoventrally. Dactylus length about half propodus length, length 3.7 width, with three slender setae medially. Unguis length half dactylus length, with two long, slender setae underneath unguis. PII (Fig. 16C) basis length 3.8 width. Ischium length about half basis length, length 2.3 width, with one long simple seta distodorsally. Merus length 0.7 ischium length, length 1.5 width, with two simple setae of varying length distodorsally, with one simple seta ventrally, and one simple seta distoventrally. Carpus length 2.6 merus length, length 4.3 width, with seven unequally bifid setae ventrally increasing in size distally. Propodus length 0.6 carpus length, length 4 width, with one long simple seta distodorsally, with numerous small setae, membranously embedded, and two small unequally bifid setae ventrally. Dactylus length 0.4 propodus length, length 3.3 width, with numerous small setae, membranously embedded ventrally. Unguis length half dactylus length, with two long, slender setae underneath unguis. PIII (Fig. 16D) basis length 4.7 width, with one long robust simple seta distoventrally. Ischium 0.4 basis length, length 2.1 width, with one simple seta distodorsally. Merus length 0.9 ischium length, length 1.8 width, with one simple seta distodorsally, with one simple seta (broken off) distoventrally. Carpus length 2.5 merus length, length 5.4 width, with eight robust setae (three unequally bifid setae, five simple) ventrally. Propodus length 0.6 carpus length, length 4.8 width, with six long simple setae (four broken off) dorsally, with numerous small setae, membranously embedded, and two small unequally bifid setae ventrally. Dactylus length 0.4 propodus length, length 6 width, with two simple setae medially. Unguis length 0.6 dactylus length, with two long, slender setae underneath unguis. PIV (Fig. 16E) basis length 5.5 width, with three simple setae dorsally, with three simple setae ventrally. Ischium length half basis length, length 2.9 width, with one simple seta distodorsally, with one simple seta ventrally. Merus length 0.6 ischium length, length twice width, with one long simple seta distodorsally, with one long simple seta distoventrally. Carpus length 2.5 merus length, length 6.4 width, with five simple setae (underneath) dorsally, with nine slender simple setae ventrally, increasing in size distally. Propodus length 0.6 carpus length, length 4.8 width, with six simple setae (four broken off) dorsally, with numerous small setae, membranously embedded, and four small unequally bifid setae ventrally. Dactylus length 0.4 propodus length, length 6 width, with two simple setae medially, with numerous small setae ventrally. Unguis length 0.3 dactylus length, with two slender setae underneath unguis. PV (Fig. 16F) basis length 4.5 width, one long simple seta distodorsally. Ischium length 0.8 basis length, length 3.6 width, with two long simple setae dorsally. Merus length half ischium length, length 1.8 width, with two simple setae of varying size distodorsally, with one small simple seta distoventrally. Carpus length 2.1 merus length, length 3.4 width, with six long simple setae (one broken off) ventrally.

Propodus length 0.7 carpus length, length 2.9 width, with seven long simple setae (underneath) dorsally, with four long simple setae ventrally. Dactylus length half propodus length, length 3.5 width. Unguis length 0.7 dactylus length, with two setae of varying size underneath unguis. PVI (Fig. 16G) basis length 3.1 width, with one simple seta distoventrally. Ischium as long as basis, length 2.7 width, with one small simple seta ventrally. Merus length 0.4 ischium length, length 1.5 width, with two simple setae (one broken off) distodorsally, with one small simple seta ventrally. Carpus length 2.4 merus length, length 3.8 width, with one slender setae distodorsally, with three long simple setae ventrally. Propodus length 0.8 carpus length, length 5 width, with eight long setae dorsally, with two long setae distoventrally. Dactylus length half propodus length, length 5.3 width. Unguis length 0.8 dactylus length, with two slender seta underneath unguis. PVII (Fig. 16H) basis length 4.5 width. Ischium damaged, length 0.6 basis length, length 2.4 width. Merus length half ischium length, length 1.3 width. Carpus length 2.4 merus length, length 3.9 width, with eight long slender simple setae dorsally, with three simple setae dorsally, with one simple seta distodorsally, with three setae (two simple, one unequally bifid) of varying size ventrally. Propodus length 0.7 carpus length, length 4 width, with five long simple setae dorsally, with one simple seta ventrally, with one robust simple seta distoventrally. Dactylus length half propodus length, length 3.1 width. Unguis length 0.8 dactylus length, with two slender setae underneath unguis. Op (Fig. 15G), drawn *in situ*. Length 1.4 width, with a strong ventral spine, posteriorly bent. Lateral and posterior margins, with several (≥ 15) simple setae, setal size 0.1 Plt length. PlpIII (Fig. 15H) protopodite length 0.9 width, length 0.3 endopodite length. Exopodite half endopodite length, length 1.8 width, tapering in width distally, with numerous short simple setae laterally and one somewhat longer seta distally. Endopodite length 1.8 width, with two long plumose setae distally, distal margin rounded. PlpIV (Fig. 15I) protopodite rectangular, length 0.6 width, length 0.2 endopodite length. Exopodite slender, length 0.7 endopodite length, length 7.2 width, with several thin setules laterally (outer margin) and one long robust plumose seta distally. Endopodite length 2.6 width, distal end tapering in an acute angle. PlpV (Fig. 15J) small oval lobe, without setation, about as long as pleopod 4 endopodite. Length 2.2 proximal width, width tapering towards distal end. Urp (Fig. 15K) uniramous, length 0.2 Plt length, not projecting beyond Plt posterior margin. Protopodite oval, length 1.4 width, with five simple setae of varying length laterally. Endopodite length 1.6 protopodite length, length 5.3 width, with one broom seta laterally, with three broom setae and four simple setae (three broken off) terminally.

Description of male paratype: Habitus (Figs 17A, 19). Body length 5.7 pereonite 1 width. Coxae not visible in dorsal view. Cephalothorax (Figs 17A, 19D, E), length 1.1 width. Anterior and lateral margins rounded, posterior margin almost straight. Antennae inserting frontolaterally in a deep fold. Pereonites 2–5 decreasing in width. Pereonite 1 length 0.3 width. Pereonite 2 widest, width 1.1 pereonite 1 width, length 2.1 pereonite 1 length. Pereonites 2–3 of similar length. Pereonites 4–7 of similar length, pereonite 4 length 1.9 pereonite 1 length. Pereonites 1–4 anterior margins frontally directed, anterolateral tergites of perenonite 2 each tipped with a robust seta, anterolateral tergites of pereonites 3–4 each with simple seta. Pereonites 5–7 of similar width, width 0.8 pereonite 1 width. Pereonite 5 anterior margin straight. Pereonites 6–7 dorsomedially fused, pereonite 6 anterior margin straight. Plt 0.2 body length, length 1.4 width, width 0.7 pereonite 1 width; posterior margin strongly rounded, anterior margin slightly concave. Anus (Fig. 19B, F) covered by anus valves laterally. Urp inserting closely to the anus valves, length 0.2 Plt length, not projecting beyond posterior margin. PlpI (Figs 17B, 19B, F), length 3.2 proximal width. Distal projection width 0.4 proximal width, lateral margins slightly concave. Lateral lobes rounded, with five small setae inserting distally from each lateral lobe. Distal margins strongly rounded, with four simple setae of varying length each. PlpII (Fig. 17C), sympod length 2.5 width, outer margin rounded, with six long slender simple setae distally, with numerous small setae laterally; inner margin straight. Endopod inserting 0.3 from distal tip of sympod. Stylet length 0.6 sympod length, slightly curved, distal end not extending beyond distal tip of sympod. Exopod short and rounded, inserting 0.1 from distal tip of sympod. PlpIII (Fig. 17D), protopodite length 1.3 width, length half endopodite length. Exopodite half endopodite length, length 1.3 width, tapering in width distally, with numerous short simple setae laterally and one somewhat longer seta distally. Endopodite length 1.6 width, with three long plumose setae distally, distal margin rounded. PlpIV (Fig. 17E), protopodite rectangular, length 0.6 width, length 0.3 endopodite length. Exopodite slender, length 0.7 endopodite length, length 6.8 width, with several thin setules laterally (outer margin) and one long robust plumose seta distally. Endopodite length 1.8 width, distal margin rounded.

Remarks: The new species is distinct from most other species in the genus by possessing uniramous uropods. Besides *N. menoti*, only *N. ovatus* lacks a uropodal

exopodite. The new species can be differentiated from *N. ovatus* as follows: body length 5.1 pereonite 1 width in female (vs. 4.7 in *N. ovatus);* Op posterior margin with ≥ 15 setae (vs. ≤ 9); Mxp lateral margin with numerous small setae (vs. Mxp lateral margin lacking setae); male PlpI without hook-like projections distally (vs. 3).

NANNONISCUS PEDRO KAISER, BRIX & KIHARA, SP. NOV.

(FIGS 20–22)

Zoobank registration: urn:lsid:zoobank.org:act:820608B2-7BAA-43B1-8B40-3A5561937B8B.

Type fixation: Holotype, preparatory female, ZMH K-55358, 3.4 mm, designated here.

Material examined: Holotype: preparatory female (Na08), 3.4 mm, CCZ, equatorial NE Pacific, JPIO SO239 expedition, RV Sonne, EBS, station 133 (start: 13°50‘45”N, 123°15’39”W, 4516 m; end: 13°51’8”N, 123°14’8”W, 4427 m), date: 10/04/2015, ZMH K-55358.

Paratypes: Ovigerous female (Na11), CCZ, equatorial NE Pacific, JPIO SO239 expedition, RV Sonne, EBS, station 171 (start: 14°2’41”N, 130°5’57”W, 5024 m; end: 14°3’12”N, 130°4’36”W, 5017 m), date: 17/04/2015, ZMH K-55362; preparatory female (Na04), CCZ, equatorial NE Pacific, JPIO SO239 expedition, RV Sonne, EBS, station 20 (start: 11°50’9”N, 117°58’29”W, 4093 m; end: 11°50’11”N, 116°58’0”W, 4093 m), date: 21/03/2015, ZMH K-55361; preparatory female (Na05), CCZ, equatorial NE Pacific, JPIO SO239 expedition, RV Sonne, EBS, station 20, ZMH K-55365; preparatory female (Na22), CCZ, equatorial NE Pacific, JPIO SO239 expedition, RV Sonne, EBS, station 24 (start: 11°51’19”N, 117°1’30”W, 4093 m; end: 11°51’31”N, 116°58’0”W, 4093 m), date: 22/03/2015, ZMH K-55363; preparatory female (NB12_Iso_290), CCZ, equatorial NE Pacific, BIONOD expedition, RV L’Atalante, EBS, station 43 (start: 11°48’12”N, 117°32’3”W, 4358 m; end: 11°48’20”N, 117°31’57”W, 4358 m), date: 09/04/2012, ZMH K-55360; preparatory female (NB12_Iso_330), CCZ, equatorial NE Pacific, BIONOD expedition, RV L’Atalante, EBS, station 43, ZMH K-55364; preparatory female (MA13_Iso593), CCZ, equatorial NE Pacific, MA13 expedition, RV Kilo Moana, EBS, station 90 (start: 11°49.718’N, 117°30.278’W, 4340 m; end: 11°49.906’N, 117°29.395’W, 4357 m), date: 03/05/2013, ZMH K-55359; preparatory female (MA13_Iso049), CCZ, equatorial NE Pacific, MA13 expedition, RV Kilo Moana, EBS, station 07 (start: 11°51.503’N, 117°01.205’W, 4131 m; end: 11°51.756’N, 117°00.171’W, 4121 m), date: 12/04/2013, ZMH K-55357; female, badly damaged (MA14_Iso319), CCZ, equatorial NE Pacific, MA14 expedition, RV Kilo Moana, EBS, station 39 (start: 11°49’37”N, 117°30’49”W, 4361 m; end: 11°49’47”N, 117°30’5”W, 4343 m), date: 13/05/2014, ZMH K-55367; male, badly damaged (MA14_Iso242), CCZ, equatorial NE Pacific, MA14 expedition, RV Kilo Moana, EBS, station 39, date: 13/05/2014, ZMH K-55366.

Etymology: The name is a noun in apposition, and dedicated to Pedro Martinez Arbizu, Principal Investigator of the JPIO EcoResponse expedition, for his drive and commitment to the exploration of the abyssal manganese nodule fauna.

Distribution: The species has a broad distribution across the CCZ, being collected from the eastern German, GSR (type locality) and French licence areas between 4093 and 5024 m depth.

Diagnosis: Body slender, length about 5.5 × pereonite 1 width; Mxp epipodite reaching mid of palpal article 3; Mxp lateral margin lacking fringe of setae; molar process of both Md each with only a few (≤ 5) distal spines; Md incisor teeth acute; pereonite 2 anterolateral tergites each with robust seta; pereonite 7 without ventral spine; Op with a ventral posteriorly bent spine, posterior margin with numerous (≥ 21) long simple setae; Urp biramous, not projecting beyond Plt posterior margin; Urp endopodite length ≥ 3.2 exopodite length.

Description of holotype and paratype female: Habitus (Figs 20A, B, 22), body length 5.5 pereonite 1 width. Coxae not visible in dorsal view. Cephalothorax (Figs 20A, 22D–E), length 0.7 width. Anterior and posterior margins straight, lateral margin slightly rounded. Antennae inserting frontolaterally in a deep fold. Body abruptly flattening from pereonite 4 to 5. Pereonites 2–4 decreasing in width, pereonites 4–7 of similar width. Pereonite 1 length 0.3 width. Pereonite 1 and 2 of similar width, pereonite 2 length 1.7 pereonite 1 length. Pereonites 3 and 4 of similar length, length 1.2 pereonite 2. Pereonites 1–4 anterior margins frontally directed, anterolateral tergites of pereonite 2 each tipped with a robust seta, anterolateral tergites of pereonites 3 and 4 each with a simple seta. Pereonite 5 length 1.8 pereonite 1 length, anterior margin straight. Pereonites 6 and 7 dorsomedially fused, anterior margin of pereonite 6 convex. Plt length 0.2 body length, length 1.2 width, width 0.9 pereonite 1 width, posterior margin strongly rounded; anterior margin concave. Urp length 0.3 Plt length, not projecting beyond posterior margin. AI (Fig. 20C), terminal article broken off, inferred from CLSM (Fig. 22A, E). Length

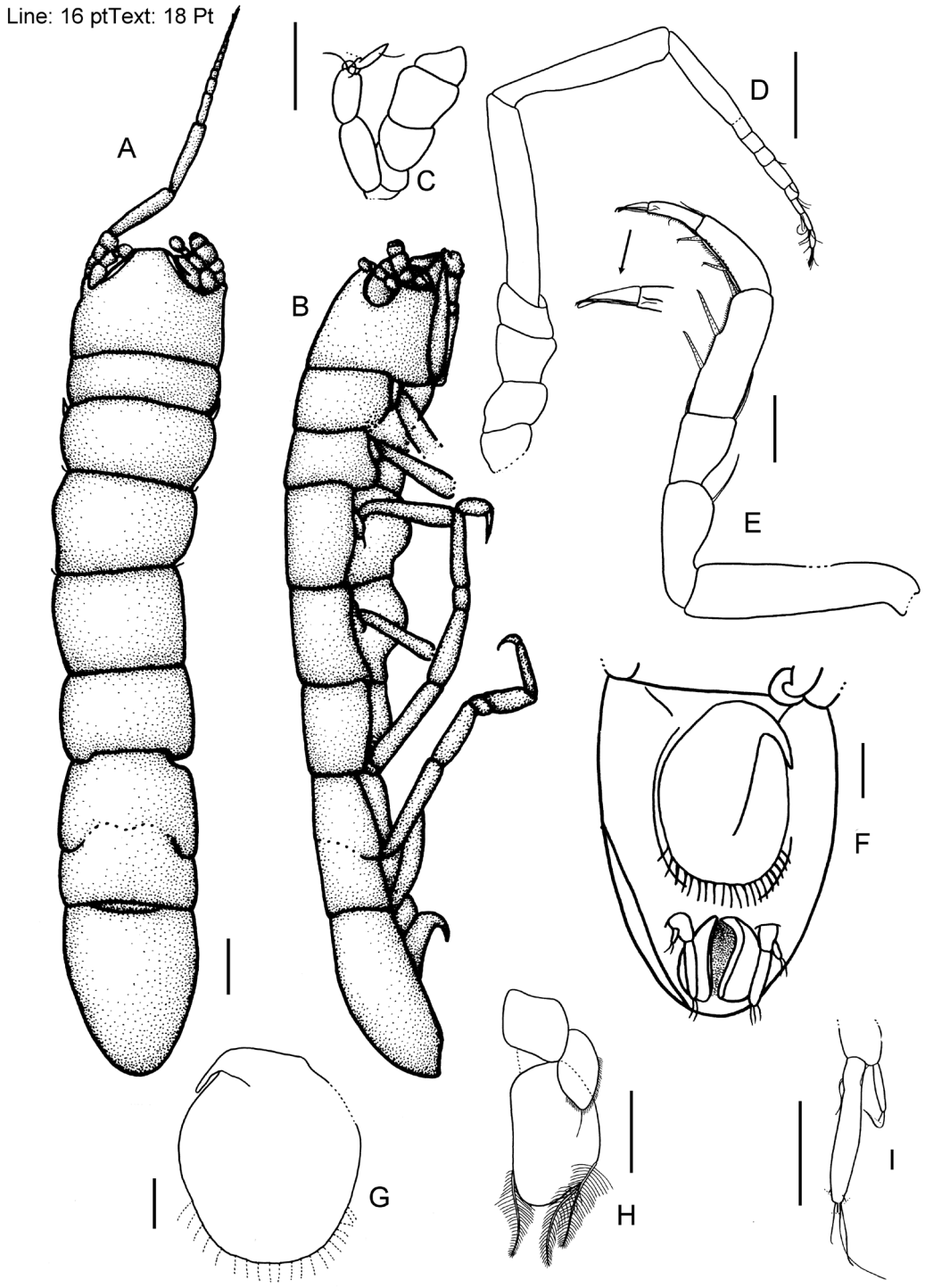

Figure 20. *Nannoniscus pedro,* (A–B, F) holotype female (ZMH K-55358, Na08), (C, E, G–H) paratype female (ZMH K-55361, Na04), (D, I) paratype female (ZMH K-55362, Na11): (A) habitus, dorsal view; (B) habitus, lateral view; (C) AI, AII peduncular article 1–4; (D) AII; (E) PI; (F) Plt, ventral view; (G), Op; (H) PlpIII; (I) Urp. Scale bars: A–B, F = 200 µm; C–E, G–I = 100 µm.

0.1 body length, with five articles. First article circular and broadest, length 2.3 width. Second article length 0.7 article 1 length, length 1.8 width, with two simple setae distally. Article 3 minute, length 0.1 article 1 length, as long as wide. Article 4 length 0.1 article 2 length, with a long distal projection reaching mid of

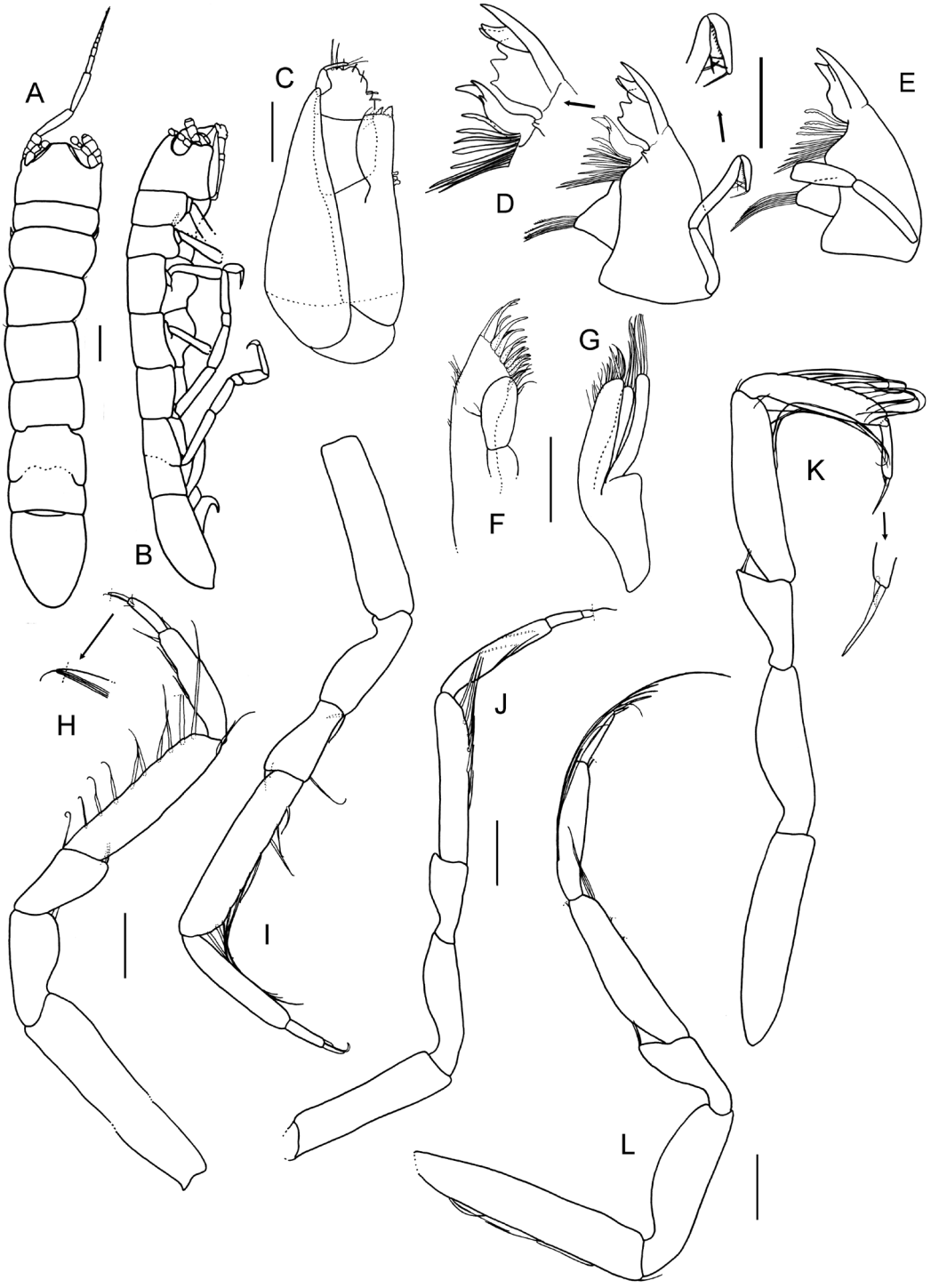

Figure 21. *Nannoniscus pedro,* (A–B) holotype female (ZMH K-55358, Na08), (C–I, K–L) paratype female (ZMH K-55362, Na11), (J) paratype female (ZMH K-55361, Na04): (A) habitus, dorsal view; (B) habitus, lateral view; (C) Mxp; (D) lMd; (E) rMd; (F) MxI; (G) MxII; (H-K) PII–V; (L) PVII. Scale bars: A–B = 200 µm; C–L = 100 µm.

article 5, with one simple seta distally. Article 5 length 0.9 article 2 length, length 1.2 width, with one aestetasc terminally. AII (Fig. 20D) length 0.4 body length, with six podomere and nine flagellar articles. Podomere articles 1–4 short. Article 5 longest, length 1.2 articles 1–4 length, length 5.4 width. Article 6 length 0.9 article

Figure 22. *Nannoniscus pedro*, holotype female (ZMH K-55358, Na08). Confocal laser scanning microscopy images: (A) habitus, dorsal view; (B) habitus, ventral view; (C) habitus, lateral view; (D) mouthparts, ventral view; (E) cephalothorax, lateral view; (F) Plt, ventral view. Scale bars: A–C = 200 μm; D–F = 100 μm.

5 length, length 5.6 width. Flagellar article 1 longest, conjoint (fusion of three articles), length 0.6 podomere article 6 length, length 4.8 width. Flagellar articles 2–4 of similar length, length 0.2 flagellar article 1 length. Flagellar 5 article longest, length 0.3 flagellar article 1 length. Flagellar articles 1–9 decreasing in width

distally, each article with 0–3 simple setae distally. Article 9 with seven long slender setae terminally. Md (Fig. 21D, E), palp of right mandible damaged, of left mandible well developed, consisting of three articles almost reaching mid of incisor. Palpal article 2 of lMd length 1.2 article 1 length, with two simple setae laterally. Terminal article length about half article 2 length, tapering distally, with several small setae ventrally and two somewhat longer setae terminally. Incisor process of rMd with three acute teeth, incisor of lMd with six acute teeth and one subdistal tooth. Lacinia mobilis of lMd with three teeth. Spine row of rMd with ten robust spines of varying size and several slender setae in between; dentation decreasing proximally. Spine row of lMd with eight robust spines and several slender setae in between, dentation decreasing, spine size increasing proximally. Molar of rMd and lMd triangular; molar of rMd with four, of lMd with five long, serrate spines distally. MxI (Fig. 21F) outer endite with 17 robust spine-like setae distally. Outer margin with several slender setae. Inner endite width 0.6 outer endite width, several fine setae distally, with two simple setae laterally. MxII (Fig. 21G), outer margin of mesial endite with several setae of varying length, distal margin with numerous long setae of varying length. Mesial endite almost as long as lateral endite. Lateral endite and middle endite each with three strong setae distally. Mxp (Fig. 21C), left and right Mxp connected by three retinacula. Epipodite smooth, triangular, slender, length 3.1 width, reaching mid of palpal article 3. Palpal article 2 width 0.9 length. Article 3 length 0.7 article 2 length, width 1.2 length, with seven robust sensory setae distally. Article 4 length 0.4 article 2 length, width half length. Article 5 length 0.4 article 2 length, width 0.2 length, with two slender setae terminally. Endite distal margin with some robust, dentate setae and several fine setae laterally. Basis length 1.5 width. PI (Fig. 20E) basis length 4 width. Ischium about half basis length, length 2.3 width, with one long simple seta dorsally. Merus length 0.6 ischium length, length 1.4 width, with one long simple seta distodorsally. Carpus length twice merus length, length 3 width, with numerous small setae, membranously embedded, and three long unequally bifid setae in between ventrally. Propodus length 0.6 carpus length, length 2.7 width, with one slender simple seta distodorsally, with numerous small setae, membranously embedded, and two robust unequally bifid setae in between ventrally, with one simple seta distoventrally. Dactylus length 0.6 propodus length, length 4 width, with two slender setae medially, with numerous small setae, membranously embedded ventally. Unguis length 0.6 dactylus length, with two long, slender setae underneath unguis. PII (Fig. 21H) basis length 4.4 width. Ischium length about half basis length, length 2.1 width, with two simple setae distodorsally. Merus length 0.8 ischium length, length 1.6 width, with three simple setae of varying length distodorsally, with one long simple seta distoventrally. Carpus length 2.1 merus length, length 4.2 width, with nine long slender simple setae (one broken off) ventrally. Propodus length 0.7 carpus length, length 4.3 width, with one simple seta distodorsally, with three simple setae ventrally. Dactylus length 0.4 propodus length, length 5.5 width, with three simple setae medially. Unguis length half dactylus length, with two slender setae underneath unguis. PIII (Fig. 21I) basis length 4 width. Ischium length 0.6 basis length, length 1.7 width, with two simple setae of varying length (one underneath) distoventrally. Merus length 0.7 ischium length, length 1.8 width, with two simple setae of varying length distodorsally, with one long simple seta distoventrally. Carpus length 2.3 merus length, length 4.7 width, with nine long simple setae ventrally. Propodus length 0.7 carpus length. Dactylus length 0.3 propodus length, length 4.5 width. Unguis length 0.6 dactylus length, with two slender setae underneath unguis. PIV (Fig. 21J) basis length 3.8 width. Ischium length 0.8 basis length, length 3.5 width. Merus length 0.6 ischium length, length 2.1 width. Carpus length 1.8 merus length, length 4.4 width, with seven long slender simple setae ventrally. Propodus length 0.9 carpus length, length 6.8 width, with two simple setae (underneath) dorsally, with two simple setae ventrally. Dactylus length 0.3 propodus length, length 3.5 width. Unguis damaged. PV (Fig. 21K) basis length 4.6 width. Ischium length 0.8 basis length, length 3.6 width. Merus length half ischium length, length 1.7 width, with two simple setae distodorsally. Carpus length 2.2 merus length, length 4.6 width, with one small simple seta distodorsally, with one slender simple seta medially, with five long, slender simple setae ventrally. Propodus length 0.7 carpus length, length 4.3 width, with nine long simple setae dorsally. Dactylus length 0.4 propodus length, length 6 width. Unguis length 0.7 dactylus length, ventral claw underneath. PVII (Fig. 21L) basis length 5.2 width, with four long setae simple setae ventrally, with one simple seta distoventrally. Ischium length 0.7 basis length, length 2.9 width. Merus length half ischium length, length 1.7 width, with two simple setae distodorsally. Carpus length twice merus length, length 4.2 width, with one simple seta (one broken off) distodorsally, with four simple setae (two long, two broken off) ventrally. Propodus length 0.8 carpus length, length 5 width, with seven long simple setae dorsally, with one simple seta (broken off) distoventrally. Dactylus length 0.4 propodus length, length 6 width. Unguis length 0.7 dactylus length, ventral claw underneath. Op (Fig. 20G) length 1.2 width, with a strong ventral spine, posteriorly bent. Lateral and posterior margins rounded, with several (≥ 21) simple setae, setal size 0.1 Plt length.

PlpIII (Fig. 20H) protopodite length 0.9 width, length 0.4 endopodite length. Exopodite half endopodite length, length 1.7 width, tapering in width distally, with numerous short simple setae laterally, with one somewhat longer simple seta distally. Endopodite length 1.6 width, with three long plumose setae distally, distal margin strongly rounded. Urp (Fig. 20I), biramous, length 0.25 Plt length, not projecting beyond Plt posterior margin. Protopodite damaged proximally, with one simple seta distally. Exopodite length 7.3 width, with two simple setae (one broken off) terminally. Endopodite length 3.2 exopodite length, length 6.4 width, with one simple seta laterally, with 6 setae (three long simple, three broken off) terminally.

Remarks: *Nannoniscus pedro* is most similar to species that are characterized by a slender body (body length ≥ 4.5 pereonite 1 width) as well as those possessing a uropodal exopodite and a ventral opercular spine. The new species most closely resembles *N. hilario,* but can be differentiated by the following characters: Mxp endopodite reaching mid of palpal article 3 (vs. distal third of palpal article 2 in *N. hilario*); Md incisor teeth acute (vs. rounded); Urp endopodite length 3.2 exopodite length (vs. 6.3); Op posterior margin with ≥ 21 setae (vs. ≤ nine). *Nannoniscus pedro* is also similar to *N. magdae*, but differs from the latter species as follows: robust setae of anterolateral tergites of pereonite 2 present (vs. absent in *N. magdae*); Md incisor teeth acute (vs. rounded). The new species can be distinguished from *N. menziesi* by the following characters: molar process of left and right Md with five and four distal spines, respectively (vs. 12 and 16 spines, respectively, in *N. menziesi*); Urp endopodite length 3.2 exopodite length (vs. 5.4). *Nannoniscus pedro* differs from *N. perunis* as follows: Urp endopodite length 3.2 exopodite length (vs. 7.8). Finally, the new species can be distinguished from *N. meteori* by the following characters: Mxp epipodite length 3.1 width (vs. 6.4 in *N. meteori*); Urp exopodite length 7.3 width (vs. 3.0); Urp endopodite length 6.4 width (vs. 3.2); Op posterior margin with ≥ 21 (vs. ≤ 15).

NANNONISCUS BRENKEI KAISER, BRIX & JENNINGS, SP. NOV.

(FIG. 23)

Zoobank registration: urn:lsid:zoobank.org:act:AF031C17-94B8-4274-A079-D113BC1423BC.

Type fixation: Holotype, preparatory female, ZMH K-55370, 2.5 mm, designated here.

Material examined: Holotype: preparatory female (NB12_Iso070), 2.5 mm, CCZ, equatorial NE Pacific, BIONOD expedition, RV L'Atalante, EBS, station 33 (start: 11°51'44"N, 117°3'10"W, 4133 m; end: 11°51'54"N, 117°3'8"W, 4133 m), date: 07/04/2012, ZMH K-55370.

Paratypes: Preparatory female (Na03), CCZ, equatorial NE Pacific, JPIO SO239 expedition, RV Sonne, EBS, station 20 (start: 11°50'9"N, 117°58'29"W, 4093 m; end: 11°50'11"N, 116°58'0"W, 4093 m), date: 21/03/2015, ZMH K-55369; ovigerous female (Na24), CCZ, equatorial NE Pacific, JPIO SO239 expedition, RV Sonne, EBS, station 24 (start: 11°51'19"N, 117°1'30"W, 4093 m; end: 11°51'31"N, 116°58'0"W, 4093 m), date: 22/03/2015, ZMH K-55371; male (?), badly damaged (MA14_Iso258), CCZ, equatorial NE Pacific, MANGAN 14 expedition, RV Kilo Moana EBS, station 21 (start: 11°49'44.52"N, 117°00'27.06"W, 4132 m; end: 11°49'56.76"N, 116°59'40.62"W, 4136 m), date: 10/05/2014, ZMH K-55368.

Etymology: The name of the new species (*brenkei*, Latin genitive, male) is dedicated to Nils Brenke, builder of the Brenke sledge ("Berta"), in recognition of his passion for deep-sea isopod taxonomy.

Distribution: The species is only known from four stations in the eastern German claim of the CCZ (type locality) between 4093 and 4136 m depth.

Diagnosis: Body slender, length about 5.0 × pereonite 1 width; Mxp epipodite reaching mid of palpal article 3; Mxp lateral margin with a fringe of setae; molar process of both Md each with only a few (≤ 5) distal spines; Md incisor teeth rounded; pereonite 2 anterolateral tergites each with robust seta; pereonite 7 without ventral spine; Op with a ventral posteriorly bent spine, posterior margin with numerous (≥ 14) long simple setae; Urp biramous, not projecting beyond Plt posterior margin; Urp endopodite length ≤ 5.8 exopodite length; Plp 3 exopodite 0.6 endopodite length, length 2.5 width, strongly tapering in width distally.

Description of holotype and paratype female: Habitus (Fig. 23A). Body length 5.5 pereonite 1 width. Coxae not visible in dorsal view. Cephalothorax (Fig. 23A), length 0.8 width. Anterior and posterior slightly rounded, lateral margins straight. Antennae inserting frontolaterally in a deep fold. Pereonites 2–4 decreasing in width, pereonites 4–7 of similar width. Pereonite 1 length 0.3 width. Pereonite 1 and 2 of similar width, pereonite 2 length 1.1 pereonite 1 length. Pereonite 3 length 1.3 pereonite 2 length. Pereonite 4 length 1.2 pereonite 2 length. Pereonites 1–4 anterior margins frontally directed, anterolateral tergites of pereonite 2 each tipped with a robust seta, anterolateral tergites of pereonites 3 and 4 each with a simple seta. Pereonite 5

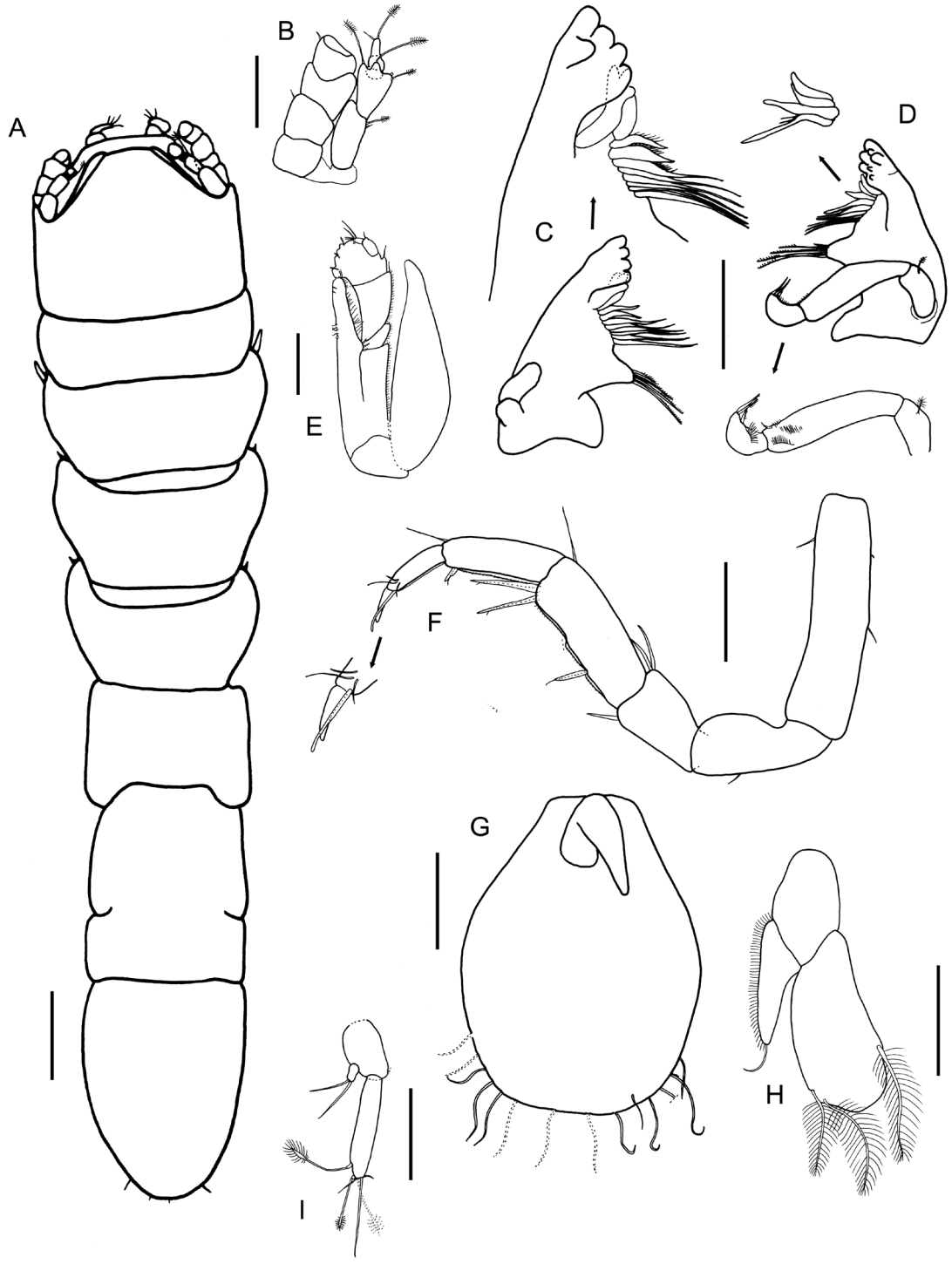

Figure 23. *Nannoniscus brenkei*, (A) holotype female (ZMH K-55370, NB12_Iso070), (B–I) paratype female (ZMH K-55369, Na03): (A) habitus, dorsal view; (B) AI, AII peduncular articles 1–4; (C) lMd, details: incisor, lacinia mobilis and spine row; (D) rMd, details: Md palp, spine row spines 1–4; (E) Mxp; (F) PI; (G) Op; (H) PlpIII; (I) Urp. Scale bars: A = 200 µm; B–I = 100 µm.

length 1.5 pereonite 1 length, anterior margin straight. Pereonites 6 and 7 dorsomedially fused, anterior margin of pereonite 6 convex. Plt length 0.2 body length, length 1.4 width, width 0.8 pereonite 1 width, posterior margin strongly rounded; anterior margin slightly concave. Urp length 0.3 Plt length, not projecting beyond posterior

margin. AI (Fig. 23B), terminal article broken off, inferred from holotype (*in situ*). Length 0.1 body length, with five articles. First article circular and broadest, length 2.1 width, with one small broom seta and one simple seta distally. Second article length 0.9 article 1 length, length 1.6 width, with three long broom setae and one seta (broken off) distally. Article 3 minute, length 0.2 article 1 length, half as long as wide. Article 4 length 0.3 article 2 length, with a long distal projection, with one long broom seta and two simple setae distally. Article 5 length 0.5 article 1 length, as long as wide. AII (Fig. 23B) broken off, only podomere articles 1–4 present; articles quadrangular of similar length and width. Md (Fig. 23C, D), palp of left mandible broken off, of right mandible well developed, consisting of three articles extending beyond distal end of incisor process. Palpal article 2 of rMd length 2.5 article 1 length, with one simple seta and two fringes of small setule laterally. Terminal article length about one-third article 2 length, tapering distally, with several small setae ventrally and three somewhat longer setae terminally. Incisor process of rMd with seven rounded teeth, incisor of lMd with five rounded teeth. Lacinia mobilis of lMd with three teeth. Spine row of rMd with nine robust spines of varying size and several slender setae in between; size increasing proximally. Spine row of lMd with nine robust spines, dentation decreasing, spine size increasing proximally. Molar of rMd and lMd triangular; molar of rMd with five, of lMd with four long, serrate spines distally. Mxp (Fig. 23E), left and right Mxp connected by three retinacula (one broken off). Epipodite smooth, triangular, slender, length 3.6 width, reaching mid of palpal article 3. Palpal article 2 as wide as long. Article 3 length 0.8 article 2 length, width 1.2 length, with four robust sensory setae and two simple setae distally. Article 4 length 0.3 article 2 length, width half length. Article 5 length 0.2 article 2 length, width about half length, with two slender setae terminally. Endite distal margin with some robust, dentate setae and several fine setae laterally. Basis length 0.7 width. PI (Fig. 23F) basis length 4 width, with one simple seta dorsally and two simple setae ventrally. Ischium length 0.6 basis length, length 2.2 width, with one small simple seta ventrally. Merus length 0.6 ischium length, length 1.2 width, with one long simple seta distodorsally and one long simple seta distoventrally. Carpus length twice merus length, length 2.6 width, with one long simple seta distodorsally, with numerous small setae, membranously embedded, and three long unequally bifid setae in between ventrally. Propodus length 0.7 carpus length, length 2.7 width, with one slender simple seta distodorsally, with numerous small setae, membranously embedded, and one small robust unequally bifid seta ventrally. Dactylus length 0.6 propodus length, length 3.1 width, with three slender setae medially, with numerous small setae, membranously embedded ventrally. Unguis length about half dactylus length, with one long, slender seta underneath unguis. Op (Fig. 23G) length 1.3 width, with a strong ventral spine, posteriorly bent. Lateral margins rounded, posterior margin almost straight, with several (≥ 14) simple setae, setal size 0.2 Plt length. PlpIII (Fig. 23H) protopodite length 1.7 width, length 0.7 endopodite length. Exopodite 0.6 endopodite length, length 2.5 width, strongly tapering in width distally, with numerous short simple setae laterally, with one somewhat longer simple seta distally. Endopodite length 2.1 width, with three long plumose setae distally, distal margin strongly rounded. Urp (Fig. 23I), biramous, length 0.3 Plt length, not projecting beyond Plt posterior margin. Protopodite length 1.7 width, with one simple seta distally (broken off). Exopodite length 3.0 width, with two simple setae terminally. Endopodite length 5.8 exopodite length, length 6.0 width, with six setae (three broom setae, three simple of varying length) terminally.

Remarks: The new species is characterized by a slender body, robust spines on the anterolateral tergites of pereonite 2, biramous uropods and a ventral opercular spine, and thus most closely resembles *N. hilario*, *N. menziesi*, *N. meteori*, *N. pedro* and *N. perunis*. *Nannoniscus brenkei* is most similar to *N. hilario*, but can be differentiated from the latter as follows: molar process of left and right mandible with ≤ five spines distally (vs. ≥ nine spines in *N. hilario*); Op distal margin with ≥ 14 simple setae (vs. ≤ nine). *Nannoniscus brenkei* also resembles *N. meteori,* but differs from the latter as follows: Mxp lateral margin with numerous small simple setae (vs. setae lacking in *N. meteori*); Urp endopodite length 5.8 exopodite length (vs. 3.9). The new species can be differentiated from *N. menziesi* by the following characters: Mxp lateral margin with numerous small simple setae (vs. setae lacking in *N. menziesi*); molar process of left and right mandible with ≤ 5 spines distally (vs. ≥ 12). *Nannoniscus brenkei* can be distinguished from *N. pedro* as follows: Md incisor teeth rounded (vs. acute in *N. pedro*); Mxp lateral margin with numerous small simple setae (vs. setae lacking); Urp endopodite length ≥ 5.8 exopodite length (vs. ≤ 3.2). Finally, the new species differs from *N. perunis* by the following features: body length ≥ 5.0 pereonite 1 width (vs. ≤ 4.7 in *N. perunis*); Urp endopodite length 5.8 exopodite length (vs. 7.8); pereonites 3–4 tergites each with an anterolateral seta (vs. setae lacking) (see also the identification key, Table 4).

DISCUSSION

Defining species boundaries

Conservation planning and biodiversity assessment strongly rely on robust species identification to enable

comparison of diversity, endemism and connectivity patterns among taxa and areas. Setting species limits based on morphological criteria alone can be challenging, especially in the food-deprived abyss characterized by low population densities. Collecting enough specimens from enough locations to infer intraspecific variability is just part of the problem. Congeneric species that lack or show only subtle morphological differentiation, but are genetically distinct (so-called cryptic or pseudocryptic species), represent a widespread phenomenon amongst deep-sea invertebrates (Etter *et al.*, 2005; Raupach *et al.*, 2007; Vrijenhoek, 2009; Havermans *et al.*, 2013; Brandt *et al.*, 2014; Brix *et al.*, 2015; Schnurr *et al.*, 2018). Furthermore, pronounced morphological differences between conspecific males and females in some species may lead to false species allocation and, in some cases, with males and females even being described as separate species (Riehl *et al.*, 2012; Błażewicz-Paszkowycz *et al.*, 2014; Bober *et al.*, 2017). Adding a genetic dimension to morphology-based taxonomy has been demonstrated to be a powerful tool to delineate species among deep-sea isopods (Brökeland & Raupach, 2008; Brandt *et al.*, 2014; Brix *et al.*, 2015, 2018; Bober *et al.*, 2017; Kaiser *et al.*, 2018; Schnurr *et al.*, 2018; Riehl & De Smet, 2020). In the present study, a combined morphological and mtDNA approach confirmed our *a priori* morphological presumption of three different species in the study area, but also provided indications of further species within the genus (Fig. 2). Our dataset was based on a relatively large number of specimens compared to many other deep-sea isopod studies (e.g. Brökeland & Raupach, 2008; Brandt *et al.*, 2014; Brix *et al.*, 2015; Kaiser *et al.*, 2018), but it also revealed some notable limitations. Phylogenetic reconstruction based on a single mitochondrial locus can be problematic overall, because of differential evolutionary histories of particular genes and species respectively (Ballard & Whitlock, 2004). In addition, due to their maternal inheritance, mtDNA-derived phylogenies provide only insights into patterns of dispersal and gene flow of the female, which does not inevitably reflect those seen in males (Avise, 1994). Yet, since sexual dimorphism of the *Nannoniscus* species studied here seems to be minimal (where males are known), effects of male-biased dispersal on population structure are likely to be negligible.

In addition, coamplification of nuclear mitochondrial pseudogenes (numts), introgressive hybridization and incomplete lineage sorting may result in false species demarcations and often overestimation

Table 4. Key to Pacific species of *Nannoniscus* G.O. Sars, 1870

KEY TO PACIFIC SPECIES OF *NANNONISCUS* (BASED ON FEMALE CHARACTERS ONLY)	
1. Uropods uniramous	2
– Uropods biramous	3
2. Op posterior margin with ≥ 15 setae	*N. menoti*
– Op posterior margin with ≤ nine setae	*N. ovatus*
3. Op without ventral spine	4
– Op with ventral spine[1]	6
4. Pereonite 2 coxae strongly produced, pereonite 7 with ventral spine	*N. muscarius*
– Pereonite coxae 2 not visible in dorsal view, pereonite 7 without ventral spine	5
5. Body length 3.3 pereonite width, pereonites 5–7 anterolateral tergites with setae	*N. detrimentus*
– Body length 4.5 pereonite width, pereonites 5–7 anterolateral tergites without setae	*N. cristatus*
6. Plt posterior margin acute	*N. acanthurus*
– Plt posterior margin rounded	7
7. Pereonite 2 anterolateral tergite without setae	*N. magdae*
– Pereonite 2 anterolateral tergite with setae	8
8. Urp exopodite well developed, endopodite ≤ 3.2 exopodite length	*N. pedro*
– Urp exopodite minute, endopodite ≥ 5.8 exopodite length	9
9. Pereonites 3–4 anterolateral tergites without setae	*N. perunis*
– Pereonites 3–4 anterolateral tergites with setae	10
10. p posterior margin with ≤ 9 simple setae	*N. hilario*
– Op posterior margin with ≥ 14 simple setae	11
11. Molar process of left and right Md with ≥ 12 spines distally	*N. menziesi*
– Molar process of left and right Md with ≤ five spines each	*N. brenkei*

[1]According to Mezhov (1986), the operculum of *N. menziesi* has a ventral spine, but it was not observed when examining appendages of the type material.

of species richness (Song *et al.*, 2008; Dietz *et al.*, 2015; Ribardière *et al.*, 2017). Although the amino acid translation of obtained *COI* sequences argues against the presence of numts in this dataset. The latter two processes are harder to rule out; one would expect them, however, to have the strongest effect in highly-dispersive and younger species, whereas *Nannoniscus* is a brooding taxon that likely diverged from related genera 50–125 Mya (Brix *et al.*, unpubl. data). Furthermore, in validating the delimitations presented herein, we argue that the combined use of phenotypic and molecular criteria in this study should help to reduce potential deficiencies of each character system (Schwentner *et al.*, 2011; Carstens *et al.*, 2013). Accordingly, species were differentiated, when the majority of SD methods employed (ABGD, sGMYC and mPTP) yielded congruent results (cf. Dellicour & Flot, 2018) and corresponded to the morphological findings. For most species their assignment seemed to be straightforward. Although, Dellicour & Flot (2018) noted that distance-based approaches, such as ABGD, tend to over-lump, whereas tree-based approaches (sGMYC, mPTP) tend to over-split species, which also was evident in our study (clades A and C, Fig. 2).

Applying the ABGD threshold of 5.7% to differentiate between intra- and interspecific variation, it became apparent that incongruities between sGMYC and mPTP occurred when genetic distances between *Nannoniscus* specimens fell into the barcode gap, for example concerning clades C1a+C1b+C2+C3 (Fig. 2), where distances between individuals of these subclades varied between 2.6 and 3.8% (Supporting Information, Table S1). The magnitude of intraspecific vs. congeneric variation in *COI* that we detected for *Nannoniscus* in this study was in the range found in previous studies on deep-sea asellotes; for instance, Brix *et al.* (2011) detected intraspecific distances of < 1.8% (uncorrected p-distances) and interspecific distances of 9–20% within *Haploniscus* Richardson, 1908 (Haploniscidae Hansen, 1916), while Brix *et al.* (2015) reported intraspecific p-distances of below 0.4% compared to 15.6–18.6% between species of *Chelator* Hessler, 1970 (Desmosomatidae G.O. Sars, 1897). For the *Eurycope producta* complex (Munnopsidae Lilljeborg, 1864), Schnurr *et al.* (2018) determined within-species divergences of < 1.9% and 19.1–30.3% among species. Morphological assessment revealed a clear distinction between specimens within C1a and C2 (*N. pedro* and *N. brenkei*, respectively). Unfortunately, it was not possible to resolve all uncertainties in species' boundaries using morphological features as the detailed study of some specimens (e.g. C1b) was hampered by their poor condition. Clade C1b differed from C1a by 3.5% (see Fig. 2 and respective specimens within these clades shown in Supporting Information, Table S1); this value is below the ABGD threshold, and below the interspecific ranges cited above. In the interest of not overestimating species richness in the absence of morphological evidence, we decided on a conservative criterion and considered C1a+C1b to represent one species (*N. pedro*).

Clearly, further sampling is required for more detailed morphological and genetic investigations, also because some clades (A2, A5, C3) are only represented by a single individual (Fig. 2), and thus the extent of intraspecific morphological and genetic variation is unknown. Such molecularly-delimited singleton species were likewise delimited in many of the above-cited studies, and were similarly problematic to address. To adequately measure the true range of divergence, multiple loci, including (fast-evolving) molecular markers should be incorporated in any future analysis (e.g. ITS2, Bober *et al.*, 2018) to resolve discrepancies at the species level. Nevertheless, supported by our morphological and genetic assessment, at least five species out of 47 specimens can be distinguished within CCZ *Nannoniscus* studied.

Drivers of phylogeographic patterns in *Nannoniscus* spp.

Taxa with a limited active dispersal potential, such as brooders, may exhibit a spatial genetic structure corresponding to isolation-by-distance (IBD), when the dispersal ability of species is low relative to their geographical distribution (e.g. Wright, 1943; Hoelzer *et al.*, 2008). In the absence of major topographic barriers throughout the CCZ coupled with a putatively poor dispersal capacity of *Nannoniscus* species, we thus expected geographic distance to be a primary determinant of genetic divergence among specimens. Depth differences between sites may be also an important factor contributing to population and/or species differentiation, as has been previously demonstrated (e.g. Jennings *et al.*, 2018; Schnurr *et al.*, 2018). The ability of Mantel tests to separate the effects of depth vs. distance is especially desirable when depth and distance are themselves correlated as they are in the present study [i.e. the largest distance between the UK-1B and FRA licence area (~1470 km) coincided with the greatest depth difference (~1000 m)]. However, the correlation ($r^2 = 0.3709$) was less strong than in many of the studies cited above. Although partial Mantel tests are expected to be the most sensitive to potential IBD in either dimension, it appears that neither dimension presents a significant barrier to dispersal in these species because no test was significant.

Contrary to our initial assumption, we found wide-ranging species (*N. menoti*, clade A6) with shared mitochondrial haplotypes among distant sites (> 1400 km apart, Fig. 3), which were contrasted by several

divergent clades (e.g. *N. pedro,* A3, C3, C4) occurring in close proximity or even sympatry (i.e. same station, Fig. 2, Table 2). Consistent with these results, evidence of IBD was detected in *N. menoti* but not *N. pedro* (Supporting Information, Tables S2, S3). It should be noted that samples were obtained by means of an EBS, where trawling distances can exceed 3 km at abyssal depth, thus overlapping (sympatric) distributions cannot be clearly established.

Haplotype sharing, low intraspecific divergences (< 1% uncorrected p-distances for *COI*) and few mutation steps (≤ 3, Fig. 3) of *N. menoti* individuals between the GER, OMS and GSR licence areas, as well as between the FRA and APEI-6 might be indicative of a recent genetic exchange between these widely-spaced populations (Janssen *et al.*, 2019 and citations therein). Similarly, no or low genetic distances (< 0.2%) between *N. pedro* specimens of the GER, GSR and FRA licence areas (see Fig. 5 and respective specimens in (Supporting Information, Table S1).

Broad geographic distributions, with species maintaining gene flow between subpopulations over several hundreds to thousands of kms, are not uncommon in deep-sea isopods despite their brooding reproductive mode, which has been partially attributed to their swimming capacity (Bober *et al.*, 2018; Brix *et al.*, 2020). However, enhanced dispersal capability does not necessarily lead to wide geographic range sizes, and vice versa. For example, Schnurr *et al.* (2018) could identify species complexes within two presumed wide-ranging and good-dispersing munnopsid species across the Icelandic shelf and slope. Conversely, there are also examples of putative poor dispersers with a wide geographic spread [e.g. within the Macrostylidae: Riehl & Kaiser (2012); Bober *et al.* (2018); Riehl *et al.* (2018); the Haploniscidae: Brix *et al.* (2011); the Desmosomatidae: Brix *et al.* (2015, 2018), and also within the Nannoniscidae (Brix *et al.*, 2018)]. Janssen *et al.* (2015) analysed patterns of genetic structure in CCZ isopods from the GER and FRA licence areas. Similar to our results, they found few broadly distributed and potentially poorly dispersing isopod species and at the same time indications of divergent cryptic lineages in sympatry.

Overall, geographic distance did not serve as a good predictor of the small-scale occurrence of several divergent *Nannoniscus* lineages in the GER and FRA licence areas. Our findings resemble those of Taboada *et al.* (2018), who examined microsatellite data of a common demosponge species (*Plenaster craigi* Lim & Wiklund, 2017) across the CCZ, including collections from two licence areas (UK-1A/UK-1B and OMS) and one APEI (#6). It is believed that *P. craigi* has a lecithotrophic reproduction mode and thus dispersal should be limited (Taboada *et al.*, 2018). Nevertheless, Taboada and coworkers (2018) found stronger connectivity between populations over large (~800 km) distances, and contrastingly high genetic differentiation of lineages that were only tens of km apart (UK-1B and OMS). Hydrodynamic models predicted a predominant north-westerly current flow that may restrict propagule dispersal into OMS, but enabled closer genetic affinities between UK-1A and APEI-6 (Taboada *et al.*, 2018).

Large-scale ocean current movements in combination with localized oceanographic features can play a central role in structuring marine populations, thereby decoupling organisms' dispersal from geographical distance (White *et al.*, 2010). That is, populations at two nearby sites can show strong genetic structure due to presence of oceanic fronts, while widely separated populations may be well connected by strong bottom currents (Taboada *et al.*, 2018). Near-bottom current velocities in the CCZ are on average low (3.8 ± 2.0 cm/s) especially over flat topography (Volz *et al.*, 2018). However, they can still be considered as strong enough to allow dispersal of propagules (Janssen *et al.*, 2019). Furthermore, current speed across the CCZ exhibits some considerable spatial variation and may be enhanced, for example in the vicinity of seamounts (Mewes *et al.*, 2014). In addition, seafloor currents can be intensified in the course of mesoscale eddies, potentially increasing mean current flow by an order of magnitude over several weeks (Aleynik *et al.*, 2017). Conversely, topographical features, such as depressions, can impede current flow and individuals may become trapped, or current directions might channel gene flow and thus affect genetic exchange (Taboada *et al.*, 2018; Janssen *et al.*, 2019).

Although the prevailing mechanisms are not clear, i.e. allopatric/secondary contact of once geographically isolated populations or incipient sympatric speciation, there are certainly other factors to consider that may have contributed to species/population divergence at different spatial scales, as observed in *Nannoniscus*, including vicariance, range expansion, colonization and adaptation to different environmental settings (Grosberg & Cunningham, 2001); the CCZ is characterized by strong gradients in productivity and depth, a diverse topography (e.g. Horst and Graben structures, seamounts and gullies) and differences in sediment structure (e.g. with regard to nodule size and density) promoting high habitat complexity also at small spatial scales (e.g. Vanreusel *et al.*, 2016; Volz *et al.*, 2018; Simon-Lledó *et al.*, 2019). At longer time scales, palaeoceanographic changes in the central Pacific (e.g. variation in current velocities, sediment redeposition and regional anoxia) may have shaped contemporary phylogeographic patterns (Jacobs & Lindberg, 1998; Rogers, 2000; Dubois & Mitchell, 2012; Volz *et al.*, 2018). The number of divergent *Nannoniscus* lineages found, particularly within the GER and FRA

licence areas, is striking and probably the result of a combination of aforementioned interrelated factors and processes. Bayesian phylogeographic analysis indicate that most genetic lineages sampled herein had likely persisted longest in the GER licence area and dispersed from there throughout the region, reaching even APEI-6 despite the distance between these areas (Fig. 5). It is important to note that these preliminary inferences may be distorted as sampling in the above licence areas was not even, and therefore a more balanced sample is needed to fill in gaps. Similarly, the disjunct distribution of haplotypes we observed (GER – GSR – FRA) is probably not real, and finer-scale sampling in between licence areas may reveal a more continuous distribution (Wilson, 2017).

ACKNOWLEDGEMENTS

We thank the masters, crew and participants of RV Sonne, RV L'Atalante, RV Kilo Moana and RV Thomas G. Thompson for their logistic, scientific and hands-on support to collect the samples. We are grateful to Courtney Wickel, Karen Osborn (USNM), Kirill Minin (Shirshov Institute of Oceanology, Russian Academy of Science, Moscow), Karen Jeskulke (DZMB), Antje Fischer (DZMB) and Kathrin Phillips-Bussau (CeNak) for allocating and curating the type material of relevant *Nannoniscus* species, and to Sven Petersen (Geomar) for making shape files of the CCZ available. Marina Malyutina is thanked for her help with the translation of the Russian literature. Special thanks go to Nicole Gatzemeier and Franziska Iwan (DZMB) for their excellent help in the genetics laboratory. The first author acknowledges a grant from the Narodowa Agencja Wymiany Akademickiej (Poland) under the ULAM program. The research leading to these results has received funding from the German Ministry of Education and Science (BMBF) as a contribution to the European project JPI-Oceans "Ecological Aspects of Deep-Sea Mining" (under contract 03F0707E). The BIONOD expedition was funded in equal shares by the Federal Institute for Geosciences and Natural Resources (BGR) and IFREMER, and the KM 13 and 14 expeditions were funded solely by the BGR. We notably thank Craig Smith for his efforts in coordinating the overall ABYSSLINE project. We also are grateful for the support of this work through a commercial arrangement with UK Seabed Resources Ltd. Finally, we thank the associate editor, Shane Ahyong, and two anonymous reviewers for their comments that helped to improve the final version of the manuscript. This is publication number 53 that uses data from the Senckenberg am Meer Confocal Laser Scanning Microscope Facility and publication number 76 from the Metabarcoding and Molecular Laboratory. The authors declare that they have no conflict of interest.

REFERENCES

Aleynik D, **Inall ME**, **Dale A**, **Vink A. 2017.** Impact of remotely generated eddies on plume dispersion at abyssal mining sites in the Pacific. *Scientific Reports* **7:** 1–14.

Avise JC. 1994. *Molecular markers, natural history and evolution.* New York: Chapman and Hall.

Ballard JWO, **Whitlock MC. 2004.** The incomplete natural history of mitochondria. *Molecular Ecology* **13:** 729–744.

Birstein JA. 1963. Deep-sea isopod crustaceans of the northwestern Pacific Ocean. *Institute of Oceanology of the U.S.S.R., Akademii Nauk: Moscow* [in Russian with English summary]: 213 pp.

Birstein JA. 1971. Fauna of the Kurile-Kamchatka Trench. Additions to the fauna of isopods (Crustacea, Isopoda) of the Kurile-Kamchatka Trench. Part II. Asellota 2. *Trudy Instituta Okeanogiya, Akademiya Nauk SSSR, Moscow* **92:** 162–238.

Błażewicz-Paszkowycz M, **Jennings RM**, **Jeskulke K**, **Brix S. 2014.** Discovery of swimming males of Paratanaoidea (Tanaidacea). *Polish Polar Research* **35:** 415–453.

Bober S, **Brix S**, **Riehl T**, **Schwentner M**, **Brandt A. 2018.** Does the Mid-Atlantic Ridge affect the distribution of abyssal benthic crustaceans across the Atlantic Ocean? *Deep Sea Research Part II: Topical Studies in Oceanography* **148:** 91–104.

Bober S, **Riehl T**, **Henne S**, **Brandt A. 2017.** New Macrostylidae (Isopoda) from the northwest Pacific Basin described by means of integrative taxonomy with reference to geographical barriers in the abyss. *Zoological Journal of the Linnean Society* **182:** 549–603.

Bonifácio P, **Menot L. 2019.** New genera and species from the Equatorial Pacific provide phylogenetic insights into deep-sea Polynoidae (Annelida). *Zoological Journal of the Linnean Society* **185:** 555–635.

Bouckaert R, **Vaughan TG**, **Barido-Sottani J**, **Duchêne S**, **Fourment M**, **Gavryushkina A**, **Heled J**, **Jones G**, **Kühnert D**, **De Maio N**, **Matschiner M. 2019.** BEAST 2.5: an advanced software platform for Bayesian evolutionary analysis. *PLoS Computational Biology* **15:** e1006650.

Boyko CB, **Bruce NL**, **Hadfield KA**, **Merrin KL**, **Ota Y**, **Poore GCB**, **Taiti S**, **Schotte M**, **Wilson GDF**, **eds. 2008.** *World marine, freshwater and terrestrial isopod crustaceans database.* Available at: https://marinespecies.org/aphia.php?p=taxdetails&id=155716. Accessed 3 May 2018.

Brandt A. 2002. New species of Nannoniscidae (Crustacea, Isopoda) and *Saetoniscus* n. gen. from the deep sea of the Angola Basin. *Zootaxa* **88:** 1–36.

Brandt A, **Brix S**, **Held C**, **Kihara TC. 2014.** Molecular differentiation in sympatry despite morphological stasis: deep-sea *Atlantoserolis* Wagele, 1994 and *Glabroserolis* Menzies, 1962 from the south-west Atlantic (Crustacea: Isopoda: Serolidae). *Zoological Journal of the Linnean Society* **172:** 318–359.

Brandt A, **Gooday AJ**, **Brandão SN**, **Brix S**, **Brökeland W**, **Cedhagen T**, **Choudhury M**, **Cornelius N**, **Danis B**, **De Mesel I**, **Diaz RJ**, **Gillan DC**, **Hilbig B**, **Howe J**, **Janussen D**, **Kaiser S**, **Linse K**, **Malyutina M**,

Pawlowski J, **Raupach M**, **Vanreusel A. 2007.** First insights into the biodiversity and biogeography of the Southern Ocean deep sea. *Nature* **447:** 307–311.

Brenke N. 2005. An epibenthic sledge for operations on marine soft bottom and bedrock. *Marine Technology Society Journal* **39:** 10–21.

Brix S, **Bober S**, **Tschesche C**, **Kihara TC**, **Driskell A**, **Jennings RM. 2018.** Molecular species delimitation and its implications for species descriptions using desmosomatid and nannoniscid isopods from the VEMA fracture zone as example taxa. *Deep Sea Research Part II: Topical Studies in Oceanography* **148:** 180–207.

Brix S, **Bruce NL. 2008.** *Prochelator tupuhi* sp. nov., the first record of Desmosomatidae Sars, 1897 (Crustacea: Isopoda) from New Zealand waters. *Zootaxa* **1866:** 482–492.

Brix S, **Leese F**, **Riehl T**, **Kihara TC. 2015.** A new genus and new species of Desmosomatidae Sars, 1897 (Isopoda) from the eastern South Atlantic abyss described by means of integrative taxonomy. *Marine Biodiversity* **45:** 7–61.

Brix S, **Osborn KJ**, **Kaiser S**, **Truskey SB**, **Schnurr SM**, **Brenke N**, **Malyutina M**, **Martinez Arbizu P. 2020.** Adult life strategy affects distribution patterns in abyssal isopods - implications for conservation in Pacific nodule areas. *Biogeosciences* **17:** 6163–6184.

Brix S, **Riehl T**, **Leese F. 2011.** First genetic data for species of the genus *Haploniscus* Richardson, 1908 (Isopoda: Asellota: Haploniscidae) from neighbouring deep-sea basins in the South Atlantic. *Zootaxa* **2838:** 79–84.

Brökeland W, **Raupach MJ. 2008.** A species complex within the isopod genus *Haploniscus* (Crustacea: Malacostraca: Peracarida) from the Southern Ocean deep sea: a morphological and molecular approach. *Zoological Journal of the Linnean Society* **152:** 655–706.

Carstens BC, **Pelletier TA**, **Reid NM**, **Satler JD. 2013.** How to fail at species delimitation. *Molecular Ecology* **22:** 4369–4383.

Clement M, **Snell Q**, **Walker P**, **Posada D**, **Crandall K. 2002.** TCS: estimating gene genealogies. In: *Proceeding 16th International Parallel Distributed Processing Symposium,* **2:** 184.

Cowen RK, **Sponaugle S. 2009.** Larval dispersal and marine population connectivity. *Annual Review of Marine Science* **1:** 443–466.

Danovaro R, **Aguzzi J**, **Fanelli E**, **Billett D**, **Gjerde K**, **Jamieson A**, **Ramirez-Llodra E**, **Smith CR**, **Snelgrove PVR**, **Thomsen L**, **Van Dover CL. 2017.** An ecosystem-based deep-ocean strategy. *Science* **355:** 452–454.

Dellicour S, **Flot JF. 2018.** The hitchhiker's guide to single-locus species delimitation. *Molecular Ecology Resources* **18:** 1234–1246.

Dietz L, **Arango C**, **Dömel JS**, **Halanych K**, **Harder AM**, **Held C**, **Mahon AR**, **Mayer C**, **Melzer RR**, **Rouse GW**, **Weis A**, **Wilson NG**, **Leese F. 2015.** Regional differentiation and extensive hybridization between mitochondrial clades of the Southern Ocean giant sea spider *Colossendeis megalonyx*. *Royal Society Open Science* **2:** 140424.**Dubois N**, **Mitchell NC. 2012.** Large-scale sediment redistribution on the equatorial Pacific seafloor. *Deep Sea Research Part I: Oceanographic Research Papers* **69:** 51–61.

Etter RJ, **Rex MA**, **Chase MR**, **Quattro JM. 2005.** Population differentiation decreases with depth in deep-sea bivalves. *Evolution* **59:** 1479–1491.

Folmer O, **Black M**, **Hoeh W**, **Lutz R**, **Vrijenhoek R. 1994.** DNA primers for amplification of mitochondrial cytochrome *c* oxidase subunit I from diverse metazoan invertebrates. *Molecular Marine Biology and Biotechnology* **3:** 294–299.

Fujisawa T, **Barraclough TG. 2013.** Delimiting species using single-locus data and the Generalized Mixed Yule Coalescent approach: a revised method and evaluation on simulated data sets. *Systematic Biology* **62:** 707–724.

Gjerde KM, **Reeve LLN**, **Harden-Davies H**, **Ardron J**, **Dolan R**, **Durussel C**, **Earke S**, **Jimenez JA**, **Kalas P**, **Laffoley D**, **Oral N**, **Page R**, **Ribeiro MC**, **Rochette J**, **Spadone A**, **Thiele T**, **Thomas HL**, **Wagner D**, **Warner R**, **Wilhelm A**, **Wright G. 2016.** Protecting Earth's last conservation frontier: scientific, management and legal priorities for MPAs beyond national boundaries. *Aquatic Conservation: Marine and Freshwater Ecosystems* **26:** 45–60.

Gollner S, **Kaiser S**, **Menzel L**, **Jones DOB**, **van Oevelen D**, **Menot L**, **Colaço A**, **Brown A**, **Canals M**, **Cuvelier D**, **Durden JM**, **Gebruk A**, **Great Aruoriwok E**, **Haeckel M**, **Mestre NC**, **Mevenkamp L**, **Morato T**, **Pham CK**, **Purser A**, **Sanchez-Vidal A**, **Vanreusel A**, **Vink A**, **Martinez Arbizu P. 2017.** Resilience of benthic deep-sea fauna to mining activities. *Marine Environmental Research* **129:** 76–101.

Grosberg R, **Cunningham CW. 2001.** Genetic structure in the sea: from populations to communities. In: Bertness MD, Hay M, Gaines SD, eds. *Marine community ecology*. Sunderland: Sinauer Associates, 61–84.

Havermans C, **Sonet G**, **d'Acoz CDU**, **Nagy ZT**, **Martin P**, **Brix S**, **Riehl T**, **Agrawal S**, **Held C. 2013.** Genetic and morphological divergences in the cosmopolitan deep-sea amphipod *Eurythenes gryllus* reveal a diverse abyss and a bipolar species. *PLoS One* **8:** e74218.

Hessler RR. 1970. The Desmosomatidae (Isopoda, Asellota) of the Gay Head-Bermuda transect. *Bulletin of the Scripps Institution of Oceanography* **15:** 1–185.

Hessler RR, **Wilson GDF**, **Thistle D. 1979.** The deep-sea isopods: a biogeographic and phylogenetic overview. *Sarsia* **64:** 67–75.

Hoelzer GA, **Drewes R**, **Meier J**, **Doursat R. 2008.** Isolation-by-distance and outbreeding depression are sufficient to drive parapatric speciation in the absence of environmental influences. *PLoS Computational Biology* **4:** e1000126.

Jacobs DK, **Lindberg DR. 1998.** Oxygen and evolutionary patterns in the sea: onshore/offshore trends and recent recruitment of deep-sea faunas. *Proceedings of the National Academy of Sciences of the USA* **95:** 9396–9401.

Janssen A, **Kaiser S**, **Meißner K**, **Brenke N**, **Menot L**, **Martínez Arbizu P. 2015.** A reverse taxonomic approach to assess macrofaunal distribution patterns in abyssal Pacific polymetallic nodule fields. *PLoS One* **10:** e0117790.

Janssen A, **Stuckas H**, **Vink A**, **Martinez Arbizu PM. 2019.** Biogeography and population structure of predominant macrofaunal taxa (Annelida and Isopoda) in abyssal polymetallic nodule fields: implications for conservation and management. *Marine Biodiversity* **49:** 2641–2658.

Jennings RM, **Brix S**, **Bober S**, **Svavarsson J**, **Driskell A. 2018.** More diverse than expected: distributional patterns of *Oecidiobranchus* Hessler, 1970 (Isopoda, Asellota) on the Greenland-Iceland-Faeroe Ridge based on molecular markers. *Marine Biodiversity* **48:** 845–857.

Jones DOB, **Kaiser S**, **Sweetman AK**, **Smith CR**, **Menot L**, **Vink A**, **Trueblood D**, **Greinert J**, **Billett DSM**, **Martinez Arbizu P**, **Radziejewska T**, **Singh R**, **Ingole B**, **Stratmann T**, **Simon-Lledo E**, **Durden JM**, **Clark MR. 2017.** Biological responses to disturbance from simulated deep-sea polymetallic nodule mining. *PLoS One* **12:** e0171750.

Just J, **Wilson GDF. 2007.** Revision of *Austrosignum* Hodgson and *Munnogonium* George & Strömberg (Paramunnidae) with descriptions of eight new genera and two new species (Crustacea: Isopoda: Asellota). *Zootaxa* **1515:** 1–29.

Kaiser S. 2014. New species of *Hebefustis* Siebenaller and Hessler 1977 (Isopoda, Asellota, Nannoniscidae) from the Clarion Clipperton Fracture Zone (equatorial NE Pacific). *Zootaxa* **3784:** 101–119.

Kaiser S, **Barnes DKA**, **Brandt A. 2007.** Slope and deep-sea abundance across scales: Southern Ocean isopods show how complex the deep sea can be. *Deep Sea Research Part II: Topical Studies in Oceanography* **54:** 1776–1789.

Kaiser S, **Brix S**, **Kihara TC**, **Janssen A**, **Jennings RM. 2018.** Integrative species delimitation in the deep-sea genus *Thaumastosoma* Hessler, 1970 (Isopoda, Asellota, Nannoniscidae) reveals a new genus and species from the Atlantic and central Pacific abyss. *Deep Sea Research Part II: Topical Studies in Oceanography* **148:** 151–179.

Kaiser S, **Marner M. 2012.** A new species of *Pentaceration* Just, 2009 (Isopoda, Asellota, Paramunnidae) from the Challenger Plateau, New Zealand (Tasman Sea). *Zoosystematics and Evolution* **88:** 171–184.

Kaiser S, **Smith CR**, **Arbizu PM. 2017.** Biodiversity of the Clarion Clipperton Fracture Zone. *Marine Biodiversity* **47:** 59–264.

Kamenskaya OE, **Gooday AJ**, **Tendal OS**, **Melnik VF. 2017.** Xenophyophores (Rhizaria, Foraminifera) from the Russian license area of the Clarion-Clipperton Zone (eastern equatorial Pacific), with the description of three new species. *Marine Biodiversity* **47:** 299–306.

Kapli P, **Lutteropp S**, **Zhang J**, **Kobert K**, **Pavlidis P**, **Stamatakis A**, **Flouri T. 2017.** Multi-rate Poisson tree processes for single-locus species delimitation under maximum likelihood and Markov chain Monte Carlo. *Bioinformatics* **33:** 1630–1638.

Kato Y, **Fujinaga K**, **Nakamura K**, **Takaya Y**, **Kitamura K**, **Ohta J**, **Toda R**, **Nakashima T**, **Iwamori H. 2011.** Deep-sea mud in the Pacific Ocean as a potential resource for rare-earth elements. *Nature Geoscience* **4:** 535–539.

Katoh K, **Misawa K**, **Kuma KI**, **Miyata T. 2002.** MAFFT: a novel method for rapid multiple sequence alignment based on fast Fourier transform. *Nucleic Acids Research* **30:** 3059–3066.

Kihara TC, **Rocha C. 2009.** *Técnicas para o estudo taxonômico de copépodes harpacticóides da meiofauna marinha*. Porto Alegre: Asterisco.

Larkin MA, **Blackshields G**, **Brown NP**, **Chenna R**, **McGettigan PA**, **McWilliam H**, **Valentin F**, **Wallace IM**, **Wilm A**, **Lopez R**, **Thompson JD**, **Gibson TJ**, **Higgins DG. 2007.** Clustal W and Clustal X version 2.0. *Bioinformatics* **23:** 2947–2948.

Malyutina MV. 2011. Description of two new species of munnopsid isopods (Crustacea: Isopoda: Asellota) from manganese nodules area of the Clarion-Clipperton Fracture Zone, Pacific Ocean. *Zootaxa* **2783:** 1–20.

Malyutina MV, **Kihara TC**, **Brix S. 2020.** A new genus of Munnopsidae Lilljeborg, 1864 (Crustacea, Isopoda), with descriptions of two abyssal new species from the Clarion Clipperton Fracture Zone, north-eastern tropical Pacific. *Marine Biodiversity* **50:** 42.

Menzies RJ, **George RY. 1972.** Isopod Crustacea of the Peru-Chile Trench. *Anton Bruun Report* **9:** 1–124.

Merrin KL. 2007. *New Zealand and south-east Australian Ilyarachninae (Isopoda: Asellota: Munnopsidae) and their worldwide relationships*. Ph. D. Thesis, University of Canterbury.

Mewes K, **Mogollón JM**, **Picard A**, **Rühlemann C**, **Kuhn T**, **Nöthen K**, **Kasten S. 2014.** Impact of depositional and biogeochemical processes on small scale variations in nodule abundance in the Clarion-Clipperton Fracture Zone. *Deep Sea Research Part I: Oceanographic Research Papers* **91:** 125–141.

Mezhov BV. 1986. Bathyal and abyssal Nannoniscidae and Desmosomatidae (Isopoda, Asellota) from Alaska Bay. *Archives of the Zoological Museum* **1986:** 126–167.

Michels J, **Büntzow M. 2010.** Assessment of Congo red as a fluorescence marker for the exoskeleton of small crustaceans and the cuticle of polychaetes. *Journal of Microscopy* **238:** 95–101.

O'Hara T. 2002. Endemism, rarity and vulnerability of marine species along a temperate coastline. *Invertebrate Systematics* **16:** 671–684.

Pons J, **Barraclough TG**, **Gomez-Zurita J**, **Cardoso A**, **Duran DP**, **Hazell S**, **Kamoun S**, **Sumlin WD**, **Vogler AP. 2006.** Sequence-based species delimitation for the DNA taxonomy of undescribed insects. *Systematic Biology* **55:** 595–609.

Puillandre N, **Lambert A**, **Brouillet S**, **Achaz G. 2012.** ABGD, Automatic Barcode Gap Discovery for primary species delimitation. *Molecular Ecology* **21:** 1864–1877.

Rambaut A, **Suchard M**, **Xie D**, **Drummond A. 2014.** *Tracer v.1. 6 (online 2015)*. Available at: http://beast.bio.ed.ac.uk/Tracer.

Ramirez-Llodra E, **Brandt A**, **Danovaro R**, **De Mol B**, **Escobar E**, **German CR**, **Levin LA**, **Arbizu P**, **Menot L**, **Buhl-Mortensen P**, **Narayanaswamy BE**, **Smith CR**, **Tittensor DP**, **Tyler PA**, **Vanreusel A**, **Vecchione M. 2010.** Deep, diverse and definitely different: unique attributes of the world's largest ecosystem. *Biogeosciences* **7:** 2851–2899.

Raupach M, **Malyutina M**, **Brandt A**, **Wagele JW. 2007.** Molecular data reveal a highly diverse species flock within the munnopsoid deep-sea isopod *Betamorpha fusiformis* (Barnard, 1920) (Crustacea: Isopoda: Asellota) in the

Southern Ocean. *Deep Sea Research Part II: Topical Studies in Oceanography* **54:** 1820–1830.

Ribardière A, **Daguin-Thiébaut C**, **Houbi C**, **Coudret J**, **Broudin C**, **Timsit O**, **Broquet T. 2017.** Geographically distinct patterns of reproductive isolation and hybridization in two sympatric species of the *Jaera albifrons* complex (marine isopods). *Ecology and Evolution* **7:** 5352–5365.

Riehl T, **Brandt A. 2010.** Descriptions of two new species in the genus *Macrostylis* Sars, 1864 (Isopoda, Asellota, Macrostylidae) from the Weddell Sea (Southern Ocean), with a synonymisation of the genus *Desmostylis* Brandt, 1992 with *Macrostylis*. *Zookeys* **57:** 9–49.

Riehl T, **Brenke N**, **Brix S**, **Driskell A**, **Kaiser S**, **Brandt A. 2014a.** Field and laboratory methods for DNA studies on deep-sea isopod crustaceans. *Polish Polar Research* **35:** 203–224.

Riehl T, **De Smet B. 2020.** *Macrostylis metallicola* spec. nov.—an isopod with geographically clustered genetic variability from a polymetallic-nodule area in the Clarion-Clipperton Fracture Zone. *PeerJ* **8:** e8621.

Riehl T, **Kaiser S. 2012.** Conquered from the deep sea? A new deep-sea isopod species from the Antarctic shelf shows pattern of recent colonization. *PLoS One* **7:** e49354.

Riehl T, **Wilson GDF**, **Hessler RR. 2012.** New Macrostylidae Hansen, 1916 (Crustacea: Isopoda) from the Gay Head-Bermuda transect with special consideration of sexual dimorphism. *Zootaxa* **3277:** 1–26.

Riehl T, **Wilson GDF**, **Malyutina MV. 2014b.** Urstylidae—a new family of abyssal isopods (Crustacea: Asellota) and its phylogenetic implications. *Zoological Journal of the Linnean Society* **170:** 245–296.

Rogers AD. 2000. The role of the oceanic oxygen minima in generating biodiversity in the deep sea. *Deep Sea Research Part II: Topical Studies in Oceanography* **47:** 119–148.

Rousset F. 1997. Genetic differentiation and estimation of gene flow from F-statistics under isolation by distance. *Genetics* **145:** 1219–1228.

Schnurr S, **Osborn KJ**, **Malyutina M**, **Jennings R**, **Brix S**, **Driskell A**, **Svavarsson J**, **Arbizu PM. 2018.** Hidden diversity in two species complexes of munnopsid isopods (Crustacea) at the transition between the northernmost North Atlantic and the Nordic Seas. *Marine Biodiversity* **48:** 813–843.

Schwentner M, **Timms BV**, **Richter S. 2011.** An integrative approach to species delineation incorporating different species concepts: a case study of *Limnadopsis* (Branchiopoda: Spinicaudata). *Biological Journal of the Linnean Society* **104:** 575–599.

Sewell MA, **Hofmann GE. 2011.** Antarctic echinoids and climate change: a major impact on the brooding forms. *Global Change Biology* **17:** 734–744.

Siebenaller JF, **Hessler RR. 1981.** The genera of the Nannoniscidae (Isopoda, Asellota). *Transactions of the San Diego Society of Natural History* **19:** 227–250.

Siebenaller JF, **Hessler RR. 1977.** The Nannoniscidae (Isopoda, Asellota): *Hebefustis* n. gen. and *Nannoniscoides* Hansen. *Transactions of San Diego Society of Natural History* **19**: 17–44.

Simon-Lledó E, **Bett BJ**, **Huvenne VA**, **Schoening T**, **Benoist NM**, **Jeffreys RM**, **Durden J**, **Jones DOB. 2019.** Megafaunal variation in the abyssal landscape of the Clarion Clipperton Zone. *Progress in Oceanography* **170:** 119–133.

Song H, **Buhay JE**, **Whiting MF**, **Crandall KA. 2008.** Many species in one: DNA barcoding overestimates the number of species when nuclear mitochondrial pseudogenes are coamplified. *Proceedings of the National Academy of Sciences of the USA* **105:** 13486–13491.

Svavarsson J, **Strömberg J-O**, **Brattegard T. 1993.** The deep-sea asellote (Isopoda, Crustacea) fauna of the Northern Seas: species composition, distributional patterns and origin. *Journal of Biogeography* **20:** 537–555.

Taboada S, **Riesgo A**, **Wiklund H**, **Paterson GL**, **Koutsouveli V**, **Santodomingo N**, **Dale AC**, **Smith CR**, **Jones DOB**, **Dahlgren TG**, **Glover AG. 2018.** Implications of population connectivity studies for the design of marine protected areas in the deep sea: an example of a demosponge from the Clarion-Clipperton Zone. *Molecular Ecology* **27:** 4657–4679.

Tsang LM, **Chan BKK**, **Shih FL**, **Chu KH**, **Allen CC. 2009.** Host-associated speciation in the coral barnacle *Wanella milleporae* (Cirripedia: Pyrgomatidae) inhabiting the Millepora coral. *Molecular Ecology* **18:** 1463–1475.

Vanreusel A, **Hilario A**, **Ribeiro PA**, **Menot L**, **Arbizu PM. 2016.** Threatened by mining, polymetallic nodules are required to preserve abyssal epifauna. *Scientific Reports* **6:** 26808.

Volz JB, **Mogollón JM**, **Geibert W**, **Arbizu PM**, **Koschinsky A**, **Kasten S. 2018.** Natural spatial variability of depositional conditions, biogeochemical processes and element fluxes in sediments of the eastern Clarion-Clipperton Zone, Pacific Ocean. *Deep Sea Research Part I: Oceanographic Research Papers* **140:** 159–172.

Vrijenhoek RC. 2009. Cryptic species, phenotypic plasticity, and complex life histories: assessing deep-sea faunal diversity with molecular markers. *Deep Sea Research Part II: Topical Studies in Oceanography* **56:** 1713–1723.

Walsh PS, **Metzger DA**, **Higuchi R. 1991.** Chelex 100 as a medium for simple extraction of DNA for PCR-based typing from forensic material. *Biotechniques* **10:** 506–513.

White C, **Selkoe KA**, **Watson J**, **Siegel DA**, **Zacherl DC**, **Toonen RJ. 2010.** Ocean currents help explain population genetic structure. *Proceedings of the Royal Society B: Biological Sciences* **277:** 1685–1694.

Wilson GDF. 1998. Historical influences on deep-sea isopod diversity in the Atlantic Ocean. *Deep Sea Research Part II: Topical Studies in Oceanography* **45:** 279–301.

Wilson GDF. 2008. A review of taxonomic concepts in the Nannoniscidae (Isopoda, Asellota), with a key to the genera and a description of *Nannoniscus oblongus* Sars. *Zootaxa* **1680:** 1–24.

Wilson GDF. 2017. Macrofauna abundance, species diversity and turnover at three sites in the Clipperton-Clarion Fracture Zone. *Marine Biodiversity* **47:** 323–347.

Wolff T. 1962. *The systematics and biology of bathyal and abyssal Isopoda Asellota*. Copenhagen: Danish Science Press.

Wright S. 1943. Isolation by distance. *Genetics* **28:** 139–156.

SUPPORTING INFORMATION

Additional Supporting Information may be found in the online version of this article at the publisher's web-site:

Figure S1. Genetic divergence (p-distance) in relation to geographic distance in kilometres for *N. pedro*.
Table S1. ABGD *COI* pairwise uncorrected p-distances between *Nannoniscus* specimens.
Table S2. Results of regression analyses on linear and log-transformed datasets for *N. pedro*.
Table S3. Summary of regression analyses on linear and log-transformed datasets for *N. menoti*.